CHALMERS
UNIVERSITY OF TECHNOLOGY

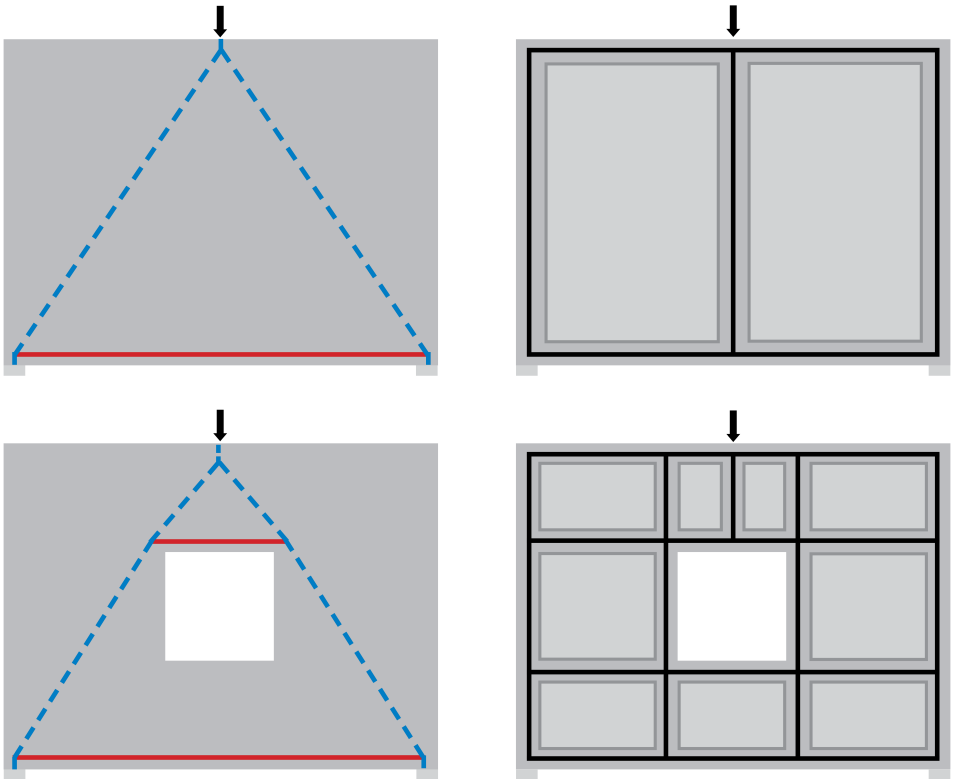

Assessing the Stringer-Panel Method as an Alternative Design Approach for Deep Beams

A Comparative Study with the Strut-and-Tie Method

Master's thesis in Structural Engineering and Building Technology

ALICE HEDENBERG
EMMA HENRYSSON

DEPARTMENT OF ARCHITECTURE AND CIVIL ENGINEERING
CHALMERS UNIVERSITY OF TECHNOLOGY
Gothenburg, Sweden 2025
www.chalmers.se

MASTER'S THESIS 2025

Assessing the Stringer-Panel Method as an Alternative Design Approach for Deep Beams

A Comparative Study with the Strut-and-Tie Method

ALICE HEDENBERG
EMMA HENRYSSON

CHALMERS
UNIVERSITY OF TECHNOLOGY

Department of Architecture and Civil Engineering
Division of Structural Engineering
Concrete Structures
CHALMERS UNIVERSITY OF TECHNOLOGY
Gothenburg, Sweden 2025

Assessing the Stringer-Panel Method as an Alternative Design Approach for Deep Beams
A Comparative Study with the Strut-and-Tie Method
ALICE HEDENBERG
EMMA HENRYSSON

Examiner and supervisor: Senior Lecturer Carlos Gil Berrocal, Department of Architecture and Civil Engineering
Supervisor: Structural Engineer Johannes Lundgren, ELU Konsult AB

Master's Thesis 2025
Department of Architecture and Civil Engineering
Division of Structural Engineering
Concrete Structures
Chalmers University of Technology
SE-412 96 Gothenburg
Telephone +46 31 772 1000

Cover: Four different deep beams, two with and two without a central opening, showing the corresponding strut-and-tie and stringer-panel models.

Typeset in LaTeX
Printed by Chalmers Reproservice
Gothenburg, Sweden 2025

Assessing the Stringer-Panel Method as an Alternative Design Approach for Deep Beams
A Comparative Study with the Strut-and-Tie Method
ALICE HEDENBERG
EMMA HENRYSSON
Department of Architecture and Civil Engineering
Chalmers University of Technology

Abstract

The design of discontinuity regions (D-regions) in reinforced concrete structures presents a challenge due to non-linear stress distributions, which make traditional beam theory insufficient. Two analytical methods for the design of such regions are the Strut-and-Tie Method (STM) and the Stringer-Panel Method (SPM). STM, which is widely used and recommended in most design codes, is suitable for ultimate limit state design but lacks compatibility considerations necessary for serviceability limit state analysis. In contrast, SPM offers the possibility of integrating compatibility conditions and offers potential for both ULS and SLS applications, although it remains less familiar to practising engineers.

This study investigated and compared STM and SPM through parametric analyses on deep beams with varying span-to-depth ratios and varying sizes of a central opening. Reinforcement layouts were designed according to both STM and SPM, and the performance was assessed through analytical calculations and validated via non-linear finite element analysis (FEA) using DIANA. The results from the FEA for STM and SPM were compared to each other, as well as to the analytical calculations. Key parameters evaluated included reinforcement quantity, failure load, crack width, deflection, and reinforcement stress distribution.

The results showed that both methods produce comparable reinforcement quantities and ultimate capacities, with no consistent trend favouring one method over the other. SPM demonstrated better adaptability to geometric variations and allowed direct calculation of deflections, making it more suitable for automation and preliminary design stages. However, limitations in post-cracking predictions highlight the need for stiffness reduction factors to improve the accuracy of SPM in the non-linear range.

It was concluded that SPM is a fully viable alternative to STM for designing D-regions in concrete beams, particularly when serviceability considerations and automation potential are prioritised. Although neither method proved universally superior, the structured approach of SPM suggested valuable opportunities for broader adoption in structural design practice.

Keywords: Strut-and-Tie Method (STM), Stringer-Panel Method (SPM), Discontinuity regions (D-regions), Deep beam, Reinforcement design, Reinforced concrete, Defections, Crack width, Non-linear behaviour, Finite Element Analysis (FEA).

Utvärdering av stringer-panel-metoden som en alternativ metod för utformning av armerade höga balkar i betong
En jämförelse med fackverksmetoden
ALICE HEDENBERG
EMMA HENRYSSON
Institutionen för arkitektur och samhällsbyggnadsteknik
Chalmers tekniska högskola

Sammanfattning

Att utforma diskontinuitetsområden (D-områden) i armerade betongkonstruktioner är en utmaning på grund av icke-linjära spänningsfördelningar, då traditionell balkteori inte är applicerbar. Två analytiska metoder för utformning av sådana områden är fackverksmetoden och stringer-panel-metoden. Fackverksmetoden, som är rekommenderad i de flesta konstruktionsnormer, är lämplig för dimensionering utifrån brottgränstillståndet, men saknar hänsyn till kompatibilitetsvillkor som krävs för analys i bruksgränstillståndet. Stringer-panel-metoden, som är mindre känd bland praktiserande ingenjörer, kan integrera sådana villkor och har potential att användas för både brott- och bruksgränstillstånd.

Studien inkluderade en undersökning mellan fackverksmetoden och stringer-panel-metoden genom parametriska analyser av höga balkar med varierande spännvidder och storlek på en central öppning. Balkarna armerades enligt båda metoderna och analyserades med icke-linjära finita elementanalyser i DIANA. Resultaten jämfördes med varandra samt med analytiska beräkningar. De parametrar som utvärderades inkluderade armeringsmängd, brottlast, sprickbredd, nedböjning och spänningsfördelning i armeringen.

Resultaten visade att båda metoderna genererar jämförbara armeringsmängder och kapaciteter. Stringer-panel-metoden var mer konsekvent vid geometriska variationer och möjliggjorde analytiska nedböjningsberäkningar, vilket gör den lämplig för automatisering och tidiga dimensioneringsskeden. Dock underskattades nedböjningen efter att sprickbildning uppstått, vilket ledde till att styvhetsreduceringsfaktorer utreddes för att förbättra noggrannheten i det icke-linjära området.

Slutsatsen var att stringer-panel-metoden är ett giltigt alternativ till fackverksmetoden för dimensionering av D-områden, särskilt då krav på nedböjning och automatisering prioriteras. Trots att ingen metod var överlägsen i alla avseenden, bedöms stringer-panel-metoden som tillämpbar och utvecklingsbar för bredare användning inom betongkonstruktion.

Nyckelord: Fackverksmetoden, Stringer-panel-metoden (SPM), Diskontinuitetsområden (D-områden), Hög balk, Armeringsdesign, Armerad betong, Nedböjning, Sprickbredd, Icke-linjärt beteende, Finita elementmetoden (FEM).

Acknowledgements

During the spring semester of 2025, we had the privilege of writing our Master's thesis, which explored a method for analysing reinforced concrete deep beams that has not yet been implemented in Sweden. This thesis, accounting for 30 credits, was conducted at the Department of Architecture and Civil Engineering at Chalmers University of Technology. The work was carried out as a collaboration between Chalmers and ELU Konsult AB.

We want to express our sincere gratitude to Carlos Gil Berrocal for generously sharing his knowledge, providing continuous support and valuable feedback, and for encouraging us throughout the entire process. His insights have been essential in advancing our work.

We are also deeply thankful to Johannes Lundgren at ELU for initiating the thesis topic and for offering guidance throughout the writing process. His support has been greatly appreciated. We further thank ELU for providing us with a workspace and for their encouragement throughout the project.

Finally, we would like to thank our peer reviewers, Elin Widén and Malin Larsson, for their helpful feedback and constructive input.

Alice Hedenberg & Emma Henrysson, Gothenburg, June 2025

List of Acronyms

Below is the list of acronyms that have been used throughout this thesis listed in alphabetical order:

DOF	Degree of Freedom
EC2	Eurocode EN 1992-1-1
FEA	Finite Element Analysis
FEM	Finite Element Method
SPM	Stringer-Panel Method
STM	Strut-and-Tie Method

Nomenclature

Below is the nomenclature of parameters and variables that have been used throughout this thesis.

Greek lower case symbols

α_e	Exponent alpha, bond-slip relation
γ	Shear strain in panel
γ_c	Safety factor concrete
γ_s	Safety factor steel
ε	Strain
ε_{cm}	Mean strain in the concrete
ε_{sm}	Mean strain in the reinforcement
ε_{ult}	Strain at ultimate stress
$\varepsilon_{\sigma.max}$	Strain at maximum stress
ν	Effectiveness factor or Poisson ratio
ν_c	Poisson ratio concrete
ν_s	Poisson ratio steel
ρ	Density
ρ	Steel ratio
ρ_{min}	Minimum steel ratio
σ	Stress
σ_c	Concrete stress
σ_s	Steel stress
$\sigma_{Rd,max}$	Stringer strength
τ	Shear stress in panel
τ_p	Uniform shear stress
τ_{max}	Maximum shear stress

τ_f	Ultimate shear stress
ϕ	Diameter of reinforcement bar

Roman lower case symbols

b	Panel width
c_{edge}	Distance from concrete edge, to stringer centre
$c_{supports}$	Distance from concrete edge, to stringer centre, at supports
d_{ef}	Effective distance
d	Deflection
f_c	Concrete compression strength
f_{cd}	Design concrete compression strength
f_{ck}	Characteristic concrete compression strength
f_{cm}	Mean concrete compression strength
f_{ctm}	Mean concrete tensile strength
f_{sy}	Steel yield stress
f_t	Concrete tensile strength
f_u	Ultimate steel stress
f_y	Steel yield stress
f_{yd}	Design steel yield stress
f_{yk}	Characteristic steel yield stress
h_e	Effective height
k_1	Factor for STM calculations
k_2	Factor for STM calculations
k_3	Factor for STM calculations
l_{bd}	Anchorage length
n	Uniformly distributed shear force, Number of bars, or Number of nodes
p	Number of panels
q	Distributed load
s	Number of stringers
s_0	Linearised initial slip section
s_1	Relative slip section
s_2	Relative slip section
s_3	Relative slip section

s_{max}	Maximum spacing between bars
$s_{r,\max}$	Maximum crack spacing
t	Thickness
u	Displacement
w_k	Characteristic crack width
$w_{stringer}$	Stringer width
w_{strut}	Strut width
z	Distance in z-direction

Roman upper case symbols

A	Cross-sectional area
A_{ef}	Effective concrete cross-section area
A_s	Reinforcement area
C	Strut force
E	Youngs modulus
E_s	Youngs modulus steel
E_{cm}	Mean youngs modulus concrete
EA	Extensional stiffness
G	Shear modulus
G_f	Fracture energy
K	Stiffness
L	Length
N	Normal force
P	Panel
P_d	Design load
P_{crack}	Crack load
$P_{failure}$	Failure load
S	Shear force, Strut, or Stringer
T	Tie or Tie force
V	Shear force

Contents

List of Figures

List of Tables

1

Introduction

This chapter introduces the context and motivation for the study, presenting the theoretical and practical background of reinforced concrete design in discontinuity regions (D-regions). It outlines the aims, research questions, and scope of the thesis, and provides an overview of the methodological approach. Together, these elements establish the foundation for the comparative analysis of the Strut-and-Tie Method (STM) and the Stringer-Panel Method (SPM) conducted in the subsequent chapters.

1.1 Background

Structures and structural elements should be designed to ensure adequate strength, serviceability, and durability throughout their intended lifespan (Swedish Standards Institute, 2010). In contemporary structural engineering, the design of reinforced concrete elements subjected to complex loading conditions remains a crucial aspect to ensure both safety and durability. Among the most challenging components to design are regions known as D-regions, where stresses are non-linearly distributed and concentrated. These regions are commonly found in areas such as frame corners, deep beams or dapped end beams, where the assumption that plane cross-sections remain plane cannot be applied (Blaauwendraad, 2018). The complex stress states in these areas necessitate alternative design approaches beyond conventional beam theory to maintain structural integrity and ensure reliable performance under varying loads.

The most widely used method for the design of reinforcement in D-regions is STM (Blaauwendraad, 2018). STM is based on the concept of a truss model, in which the concrete is idealised as compressive struts and the reinforcement as tensile ties. While STM is a powerful tool, especially for Ultimate Limit State (ULS) design based on the lower-bound theorem of plasticity, it demands significant engineering judgement and experience to produce optimal reinforcement layouts in complex cases (Szczecina and Winnicki, 2018). However, STM alone is insufficient for Serviceability Limit State (SLS) assessments, such as deflection and crack width calculations, as it does not inherently account for deformation or compatibility conditions (Blaauwendraad, 2018).

A common way to analyse the SLS behaviour today is by using the Finite Element Method (FEM), which can be done in both a linear-elastic or non-linear manner, depending on

the analysis. A finite element analysis (FEA) can capture different aspects of the structural behaviour, depending on the finite element model. A good approximation of the real structural behaviour can be achieved if the model and mesh are created with care. However, FEA usually requires a lot of input data of the geometries, material, boundary conditions, and other parameters, which may not yet be decided, especially in preliminary dimensioning (Godínez and Restrepo, 2023). Furthermore, modelling complex geometries accurately can be challenging, potentially leading to unreliable or misleading results.

Another less-known method for designing the reinforcement layout of D-regions is SPM (Blaauwendraad, 2018). SPM can, in some ways, be viewed as a combination between STM and FEM, and can be used on all materials where the theory of plasticity is valid, including reinforced concrete structures (Jensen, 2012). The method works by dividing a structure into stringers and panels, where the stringers carry normal forces, like the struts and ties in STM, and the panels transfer membrane shear forces. SPM is currently not included in the international Eurocode, but is recommended in the Danish national annexe to Eurocode EN 1992-1-1 (EC2)(Danish Transport Construction and Housing Authority, 2020).

Unlike STM, SPM can consider compatibility conditions, like FEM, making it possible to calculate displacements analytically (de Mello and de Souza, 2016). The method is also beneficial when designing for cyclic loading, since the same model can be used for different loading directions (Blaauwendraad, 2018). Despite the advantages, SPM faces several challenges, especially concerning the lack of experimental data on concrete D-regions designed using this method (de Mello and de Souza, 2016). Consequently, there is a clear need for further research to assess and refine the method's applicability. By exploring the theoretical foundations of SPM and evaluating its implementation in concrete design, this study aims to refine existing practices and enhance the use of other modelling techniques in structural design.

1.2 Aim and objectives

This master's thesis aims to compare the non-linear behaviour in both Ultimate Limit State (ULS) and Serviceability Limit State (SLS) of deep beams designed using STM and SPM. Furthermore, the study aims to conduct a parametric analysis to investigate how various span-to-depth ratios, as well as the introduction of an opening with varying size, affect the structural response for the different design methods. To compare STM and SPM, the following parameters are to be studied: reinforcement amount, failure load, reinforcement stresses, crack pattern, crack widths, and deflection. The stresses and crack widths obtained analytically for both methods will be evaluated against results from non-linear FEA. Additionally, the study evaluates how well the deflections obtained using SPM correspond to the results from the non-linear FEA.

The following objectives define the purpose:

- Establish reinforcement designs for the deep beams using both STM and SPM.

- Analyse the above-mentioned parameters on the beams designed with SPM and STM when the span-to-depth ratio of the beam varies.
- Analyse the above-mentioned parameters on the beams designed with SPM and STM when an opening is introduced on the beam, and when the size of the opening varies.
- Compare analytically calculated crack widths and reinforcement stresses for the beams designed with SPM and STM with results from the non-linear FEA.
- Investigate how well the deflections predicted by SPM correspond to results from non-linear FEA.
- Identify strengths and limitations of STM and SPM for modelling deep beams and determine their suitability for different design scenarios.

1.3 Research questions

To achieve the objectives and aims, the following research questions have been established.

- How do reinforcement amount, failure load, reinforcement stress, crack pattern, crack width, and deflection differ between deep beams designed with STM and SPM?
- Do the reinforcement stresses and crack widths calculated analytically for both STM and SPM align with the results obtained with FEA?
- Does the deflection calculated analytically with SPM compare well to the deflections of a detailed non-linear finite element model?
- Does the span-to-depth ratio of the deep beam, the introduction of an opening, or the size of the opening affect which of the methods, STM or SPM, is preferred to use for design?

1.4 Scope and limitations

Some limitations were established to restrict and focus the thesis to the purpose. This thesis focuses on comparing STM and SPM for the design and analysis of D-regions in reinforced concrete structures, with a primary emphasis on validating the SPM approach. The study uses non-linear FEA as the main validation tool, with all numerical simulations conducted using the commercial finite element software DIANA.

The D-regions investigated are limited to deep beams of varying span-to-depth ratios, as well as deep beams with an opening of different sizes while keeping the beam height and length fixed. All specimens have the same thickness, concrete strength class, and steel

strength class to ensure consistency between models and make them comparable. The only difference between the STM and SPM models is the amount and layout of the reinforcement. Importantly, both STM and SPM are implemented using the simplest possible modelling assumptions to represent each method. This includes basic and idealised truss layouts for STM and minimal discretisations for SPM, aiming to isolate and compare the core behavioural principles of each method without the influence of advanced optimisation techniques or complex modelling refinements.

The study does not include any physical experiments, making it a purely numerical investigation. Additionally, the research does not explore alternative finite element software, material variations, or other structural analysis methods beyond those specified. The findings are therefore limited to the assumptions and modelling approaches adopted within this study.

1.5 Methodology

The procedure of this master thesis followed a structured methodology to ensure a systematic comparison of STM and SPM as design and analysis methods of deep beams. The methodology consisted of several key phases, including a literature review, selection and design of specimens, analytical calculations, non-linear numerical simulations in DIANA, comparative analyses and conclusions. The workflow of the thesis is summarised in the method chart in Figure 1.1.

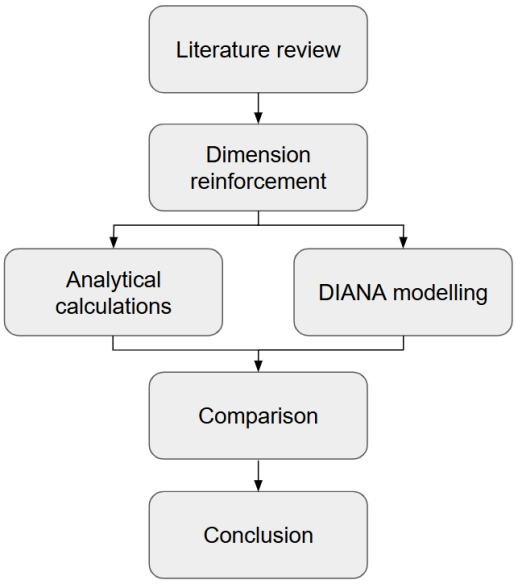

Figure 1.1: Method chart for the thesis work

The research began with a literature review to establish a theoretical foundation on deep beams and the various methods used for their design and analysis. This review included an investigation of the advantages and limitations of STM and SPM. The gathered information was the foundation for the choice of specimens and the appropriate and interesting parameters to vary in the study.

Based on the literature review, representative deep beam geometries were selected to be analysed. The reinforcement of the specimen was designed using both STM and SPM to create two different reinforcement models for the same beam geometry. Variations in key parameters, such as changing the span-to-depth ratio of the beam and varying the size of an opening, were introduced, and for each variation, new reinforcement designs with both STM and SPM were made. For the SPM approach, a Python script was used to automate the design and calculations. For STM, a visual and geometrical tool was used that is based on equations from EC2.

After the design phase, the deep beams were analysed both analytically and through a non-linear analysis in the commercial FEM software DIANA. The STM, SPM, and FEM results were compared based on various parameters, including the amount of reinforcement required, failure load, reinforcement stresses, crack pattern, crack width, and deflection. Special emphasis was placed on evaluating the accuracy of analytical SPM predictions regarding deflections by comparing them with numerical results.

Finally, the results were discussed to determine the accuracy and applicability of SPM for designing deep beams. Based on the comparative analysis together with results from the literature review, the thesis identified the strengths and limitations of both STM and SPM for modelling of deep beams. The findings were used to determine the suitability of each method for different design scenarios.

1.6 Social, ethical and ecological aspects

From a social perspective, constructability and practicality on-site are important considerations in structural design. While SPM can result in simpler reinforcement layouts compared to the sometimes more intricate arrangements derived from STM, certain SPM-based reinforcement patterns, particularly in panels with varying grid reinforcement for different panels, may pose challenges for construction workers. This raises practical concerns regarding labour efficiency and buildability.

Ethically, structural engineers have a responsibility to ensure that design methods are not only safe and code-compliant but also considerate of those involved in the construction process. Design approaches that improve clarity and simplify reinforcement detailing may contribute to reducing errors and improving working conditions on-site.

From an ecological standpoint, the optimisation of reinforcement is of significant importance, as reinforcement steel is a resource- and energy-intensive material. Choosing the most effective design method, which can differ between cases, could contribute to lower material consumption and affect the environmental footprint and long-term ecological goals in the construction industry. This thesis will investigate how the reinforcement amount is affected by the choice of design method, and therefore make it possible to make a well-founded decision from both a structural and ecological perspective.

1.7 AI-disclaimer

Artificial intelligence (AI) tools have been utilised during the work of this master's thesis to enhance the overall quality and efficiency of the work. Specifically, AI has been used for language refinement, including grammar, sentence structure, and paragraph organisation. In addition, AI is used as a supportive tool in the development and debugging of Python scripts. The use of AI is limited to linguistic and programming assistance and does not influence the core technical analysis, methodology, or scientific conclusions. All academic decisions, interpretations, and original contributions are the sole responsibility of the authors.

2

Theory

This chapter presents the theoretical framework of the study, focusing on the background and development of analytical and numerical methods used in the design of discontinuity regions (D-regions) in reinforced concrete structures. It provides a detailed overview of the Strut-and-Tie Method (STM) and the Stringer-Panel Method (SPM), discussing their conceptual foundations, assumptions, and application areas. In addition, the chapter introduces the Finite Element Method (FEM) as a numerical tool for analysing complex stress distributions and verifying structural behaviour in D-regions. By outlining the principles, strengths, and limitations of each approach, this chapter establishes the necessary theoretical basis for the comparative evaluation presented in the following sections.

2.1 D-regions

To analyse beam-like structures, the Euler-Bernoulli beam theory is commonly used, assuming rigid cross-sections that remain plane and perpendicular to the deformed axis (Bauchau and Craig, 2009, p.173). Regions where these assumptions hold are called B-regions. However, reinforced concrete structures often contain discontinuity regions (D-regions), where strain distributions are non-linear and beam theory is invalid (Szczecina and Winnicki, 2018). D-regions arise due to changes in geometry, concentrated loads, or openings. Typical examples include deep beams, frame corners, and dapped ends. A deep beam is defined as a member with a span less than or equal to three times its height (Engström, 2015).

The behaviour of D-regions can be described with Saint-Venant's Principle, where changes due to the geometry of the cross-section or concentrated forces normalise at a distance roughly equal to the largest dimension of the cross-section (de Mello and de Souza, 2016). Regardless of the global level of statical determination, the stresses in D-regions will be statically indeterminate (Engström, 2015). Moreover, since there is no straightforward compatibility condition applicable to D-regions, such as the assumption that plane sections remain plane, it is not possible to directly determine the stresses within the stress field.

In Eurocode EN 1992-1-1 (EC2), the recommended method for designing D-regions is STM (Swedish Standards Institute, 2008), which is explained more in depth in section 2.2. The Eurocode does not specify any design criteria other than that the structural member

should have enough capacity to withstand the worst-case loading scenario under the ultimate limit state (ULS) load combination, the design load.

2.1.1 Structural behaviour

When the concrete remains uncracked, the D-region behaves almost linearly, as reinforcement has limited impact on stress distribution (Engström, 2015). At this stage, stresses depend only on material elasticity and geometry, not load magnitude. A linear elastic analysis is therefore sufficient to obtain a reliable stress field. For statically indeterminate problems, equilibrium, compatibility, and constitutive relations must be satisfied, typically achieved using FEM.

Once cracking occurs, the stiffness of the D-region changes significantly, and linear elastic analysis is no longer valid. Cracked concrete loses much of its load-carrying capacity, and reinforcement begins to carry more load as cracks develop (Engström, 2015). The stress field then depends on the stiffness distribution, which varies with load magnitude, and linear elastic behaviour can therefore no longer be assumed. Different reinforcement layouts result in different stress distributions, even for identical geometries. Although materials still behave elastically, stresses and deformations become non-linear. Accurate analysis of cracked D-regions requires non-linear finite element analysis (FEA), which demands extensive data and a detailed model, which is discussed further in section 2.4.

When either of the materials starts to display non-linear behaviour, the ultimate state of the structural response is reached and will last until the point of ULS (Engström, 2015). The plastic behaviour of the materials at this stage causes the stiffness in the plastic region to decrease, and makes plastic deformations occur. This affects the stress distribution, where plastic redistribution of the stresses takes place from the plastic regions towards the stiffer regions. The stress field can therefore shift substantially during this stage. When the ultimate limit state is reached, a collapse mechanism develops, and the structural member collapses with any further loading.

For solid deep beams without openings, studies have shown that the crack pattern generally follows the same path as the stress distribution predicted in the elastic state (Haque et al., 1986). It has also been concluded that the stress distribution differs only around the openings in the beam compared to an equivalent solid deep beam without openings. Openings impact the critical flexural tensions for shallower deep beams, but become less significant when the beam is deeper (Haque et al., 1986). The placement of the openings greatly affects the magnitude and severity of the diagonal tensile stresses as well as the beam capacity. Diagonal tensions form at the corners of the openings, which are critical for the structure.

Different modes of failure of a deep beam can be identified. These are: splitting of the beam due to diagonal cracks that can be parallel to, or along, the load path, cracking of the concrete between two diagonal cracks, and penetration of a diagonal crack into the compressed zone close to a loading point which leads to crushing of the concrete (Haque et al., 1986). For all three cases, the shear capacity determines the failure. However, flexural cracks will be the first to form in most cases, especially for deep beams with

a smaller depth, but will normally not cause collapse, even though they will propagate. However, this is based on the assumption that the bottom tensile reinforcement is properly anchored.

Parameters such as concrete strength class, geometry, and other aspects can have a large impact on the structural response and ductility of the deep beam, both locally and globally. According to some previous experiments, it was shown that the concrete strength has a relatively low impact on the ultimate strength and rigidity in the case of deep beams with openings (Yang et al., 2006). It was also shown that the size of the opening did not have an impact on the deflections at mid-span before diagonal cracks formed.

2.1.2 Ultimate Limit State (ULS)

The ultimate limit state is when the structural element reaches its failure load, and a collapse mechanism is formed (Engström, 2015). During this stage of the structural response, the materials behave non-linearly, and plastic deformations develop. The majority of the tensile force can be assumed to be carried by the reinforcement, since the concrete can be assumed to be cracked under the ULS load. The reinforcement steel does, in the normal case, yield in some areas at this stage, allowing plastic redistribution of stresses. In some cases, however, a local failure can occur. When this happens, failure is reached before the intended design load for the structural member is reached. The reason why this type of failure occurs is due to the material is not ductile enough. To avoid this, the plastic capacity must be larger than the need for plastic deformations in the stress field assumed in the design.

2.1.3 Serviceability Limit State (SLS)

EC2 requires that structural members be designed to meet serviceability limit state (SLS) conditions, ensuring safety, stability, and minimal maintenance throughout the structure's lifespan (Swedish Standards Institute, 2008). SLS is reached when service criteria, such as function during normal use, experienced comfort, and acceptable deflections or cracking, are no longer fulfilled (Swedish Standards Institute, 2010). Appearance refers to structural performance regarding deflections and cracking, not aesthetics. SLS verification should consider damage to finishes or non-structural elements due to effects like vibrations. While specific SLS limits are set per project, EC2 provides general recommendations for typical cases.

SLS checks are typically simplified by assuming linear elastic behaviour under service loads (Engström, 2015), even though most reinforced concrete elements are cracked at this stage, introducing some non-linearity. Despite this, stress distributions are often approximated as nearly linear elastic. The main serviceability limits for concrete design include stress limitation, crack control, and deflection control (Swedish Standards Institute, 2008). Compressive stresses must be kept low to prevent longitudinal and micro-cracks and excessive creep, while tensile stresses should be limited to avoid plastic strains, intolerable deformations, and creep, ensuring structural performance is not adversely affected.

EC2 states that cracking and deflection are acceptable if tensile reinforcement stresses

remain below $k_3 f_{yk}$ under characteristic load combinations, with $k_3 = 0.8$ recommended (Swedish Standards Institute, 2008). Cracking during service conditions is expected and may result from loading, imposed deformations, long-term effects, chemical reactions, or temperature changes. Acceptable crack widths are defined by durability requirements or functional needs, such as water-tightness. These limits depend on the structure type and environment. EC2 recommends maximum crack widths between 0 and $0.4\,\mathrm{mm}$ for frequent and quasi-permanent load combinations.

The method for calculating the characteristic crack width, as outlined in Section 7.3.4 of EC2, is based on the product of the maximum crack spacing ($s_{r,\max}$) and the difference between the mean strain in the reinforcement (ε_{sm}) and the mean strain in the surrounding concrete (ε_{cm}) as shown in Equation 2.1 (Swedish Standards Institute, 2008). This approach assumes that the crack width is governed by the strain differential between the steel and the adjacent concrete across the estimated crack spacing. In the formulation in EC2, tension stiffening is accounted for in the expression for the reinforcement strain; however, only the strain that develops after cracking is considered. The maximum crack spacing incorporates parameters such as the concrete cover to the tensile reinforcement and the equivalent bar diameter, along with coefficients that reflect bond characteristics, strain distribution, and other relevant correction factors.

$$w_k = s_{r,\max}(\varepsilon_{sm} - \varepsilon_{cm}) \tag{2.1}$$

This approach may be extended to deep beams by treating the bottom tensile reinforcement as part of a conventional reinforced concrete tension member, consisting of the reinforcement and an effective surrounding concrete area (Engström, 2015). The effective depth of this tension zone can be defined as the dimension of the tension tie or stringer, corresponding to twice the distance from the edge of the section to the centroid of the tensile reinforcement, as illustrated in Figure 2.1.

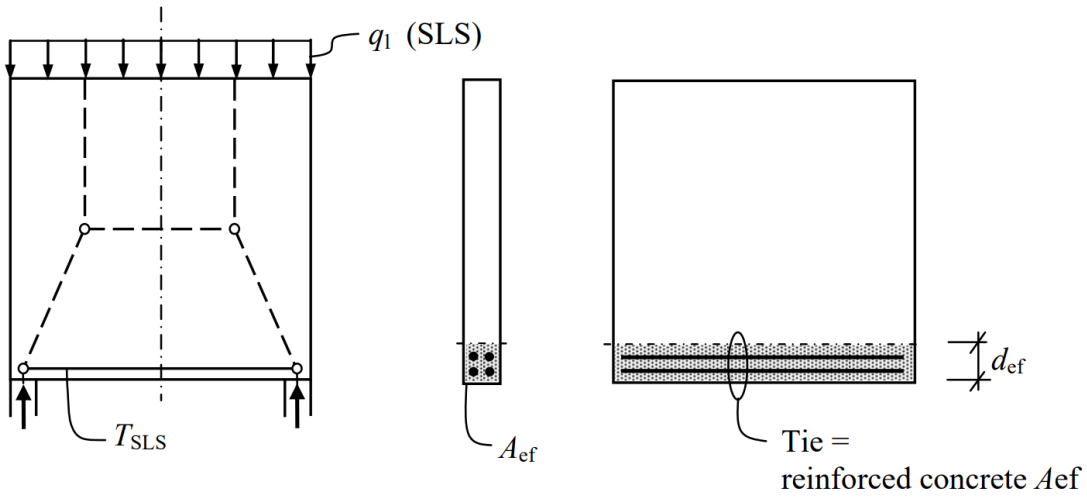

Figure 2.1: Effective area for simplified crack width calculations (Engström, 2015)

The deflections and overall deformations of a structure must remain within acceptable limits to ensure that its functionality is not compromised. The deformation threshold at which structural performance is considered affected varies depending on the type of structure and specific contextual factors. A commonly recommended deflection limit in the SLS is $\frac{L}{250}$, where L is the span length. Additionally, EC2 provides the limit expressions given in Equations (2.2) and (2.3), which define maximum allowable span-to-depth ratios, beyond which detailed deflection calculations can be omitted.

$$\frac{l}{d} = K\left[11 + 1.5\sqrt{f_{ck}}\frac{\rho_0}{\rho} + 3.2\sqrt{f_{ck}}\left(\frac{\rho_0}{\rho} - 1\right)^{\frac{3}{2}}\right], \quad \text{if } \rho \leq \rho_0 \tag{2.2}$$

$$\frac{l}{d} = K\left[11 + 1.5\sqrt{f_{ck}}\frac{\rho_0}{\rho - \rho'} + \frac{1}{12}\sqrt{f_{ck}}\sqrt{\frac{\rho'}{\rho_0}}\right], \quad \text{if } \rho > \rho_0 \tag{2.3}$$

These equations imply that deflection calculations and checks may generally be considered unnecessary for most deep beams, and also for conventional Bernoulli beams with relatively large depths. EC2 does not provide further guidance or recommend specific methods for calculating deflections in deep beams, likely because of this. However, there are situations where deflections in deep structural elements may become relevant, such as cases with very hard requirements on displacements.

2.2 Strut-and-Tie Method (STM)

The most widely used method for designing D-regions and their reinforcement layout is STM, which is the recommended method in EC2 (Swedish Standards Institute, 2008). The concept of STM described in this report is the concept developed by Schlaich and his co-workers in the early 1980s (Dolan and Trey Hamilton, 2019).

2.2.1 Theoretical background and principles

STM is based on the replacement of the concrete element with a truss model, where the struts represent the compressed concrete and the tension ties the reinforcement (Schlaich et al., 1987). The strength of the struts is, for simplicity, a function of the compressive strength of concrete, affected by transverse stressing (Dolan and Trey Hamilton, 2019). Even if the concrete around the tie before cracking carries some tensile force, it is assumed it does not contribute to the strength of the tie. The strength of the tie, therefore, only depends on the reinforcement. The joints where the struts and ties intersect are called nodes, and the nodal zone is the volume of concrete around the node, where the force transfers (Dolan and Trey Hamilton, 2019). The nodal zones are considered to be in compression, and the strength is as for the struts, a function of the compressive strength of concrete.

STM models the stress field in cracked concrete at ULS, just before failure, and after plastic redistribution (Engström, 2015). Based on the lower bound theorem of plasticity, STM permits numerous valid solutions, though only some provide sufficient ductility and

rotational capacity (Amini Najafian and Vollum, 2013). Aligning struts and ties with elastic stress trajectories generally ensures ductility in highly stressed regions, whereas in less stressed areas, alternative layouts may still be adequate (Schlaich et al., 1987). Choosing a model that reflects the actual load case is essential, as the structure adapts to its internal force flow. Even when using elastic stress fields, the behaviour remains non-linear due to both cracking and material plasticity, which will lead to plastic redistribution, even if less than with a plastic stress field (Engström, 2015).

Furthermore, STM is based on the assumptions that materials have an ideal-plastic response with no plastic deformation limitation, and with equilibrium of the stress field and load (Engström, 2015). There is no relation between stress and strain, hence, compatibility cannot be checked or assumed. Since materials, especially concrete, are not ideally plastic and do have limited plastic deformation, and since STM only considers ULS resistance, STM has several limitations.

2.2.2 Design and modelling

Once a structural analysis has been completed, resulting in support reactions, sectional forces, and identification of D- and B-regions, STM can be used to dimension the beam and reinforcement. The selection of an appropriate truss model is critical and can be challenging for complex geometries (Szczecina and Winnicki, 2018). To simplify the representation of the stress field at ULS, two approaches are commonly used (Engström, 2015). Deriving the model from principal stresses via FEA, or applying the load path method, which identifies the most effective load transfer from applied loads to supports (Schlaich et al., 1987). Although handbooks provide schemes and guidelines for truss selection, designers are often required to choose alternative layouts (Szczecina and Winnicki, 2018). To ensure ductility, it is recommended to distribute stresses from concentrated loads with deviation angles below 45°, ideally around 30° (Engström, 2015). Furthermore, angle requirements need to be checked between struts and ties. For a strut between two perpendicular ties, the angle should not be less than 30°, and for a strut meeting a single tie, not less than 45°.

Following truss scheme selection, static equilibrium is used to determine axial forces in struts and ties (Szczecina and Winnicki, 2018). For statically indeterminate models, force calculations become more complex (Blaauwendraad, 2018). Before and during this calculation of internal forces, the angles should be checked so that the requirements are met (Engström, 2015).

Once forces are established, node design is performed. Only concentrated nodes, where concentrated forces act, require verification, as distributed nodes at stress field intersections are generally non-critical (Engström, 2015). Different compressive strength reduction factors can be used depending on the type of node, compression node, tension node, with or without anchored reinforcement, or compression-tension node (Swedish Standards Institute, 2008). EC2 provides recommended national parameters and the effectiveness factor ν, accounting for reduced equivalent plastic strength under constant deformation (Engström, 2015). These stress limits inform loading plate and support sizing, with further node verification details available in EC2 (Swedish Standards Institute, 2008).

Tensile reinforcement is determined from tie forces (Schlaich et al., 1987), with anchorage designed per EC2 guidelines (Swedish Standards Institute, 2008). Strut stresses may be checked against compressive strength per EC2, though if node stress limits are met, strut checks are typically unnecessary as nodes represent critical regions (Engström, 2015). Finally, distributed (secondary) reinforcement is designed, often at minimum levels. While not essential for ULS resistance, since transverse stresses arise from compatibility in uncracked concrete, secondary reinforcement is crucial in serviceability to control cracking and maintain structural integrity.

2.2.3 Behaviour in service state

As outlined above, STM is founded on lower-bound plasticity theory and is thus applicable in ULS. STM primarily addresses strength and does not inherently consider SLS requirements, necessitating adaptations and simplifications (Blaauwendraad, 2018). Generally, the linear elastic stress field provides a reasonable approximation in SLS, even post-cracking, as discussed in subsection 2.1.1. Two approaches exist to assess SLS performance. The first employs a single strut-and-tie model for both SLS and ULS, based on, or closely resembling, the linear elastic stress field (Engström, 2015). Since any equilibrium-compliant stress field is valid within plasticity theory, this model applies to both states. Internal forces and reinforcement stresses can thus be calculated for both service and ultimate loads. However, designing for ULS using a linear elastic stress field may be inefficient and uneconomical, as less reinforcement is required when modelling plastic stress fields. Consequently, the second approach uses a plasticity-informed stress field for ULS design and a linear elastic-based stress field for SLS verification. This ensures ductility requirements are met at ULS, while maintaining appropriate stress assumptions for SLS. An example is illustrated in Figure 2.2, where the reinforcement tie remains constant, but the compression strut layout varies with the stress field.

As illustrated in Figure 2.2, steel tension in SLS can be calculated straightforwardly. However, due to the lack of compatibility considerations, STM does not allow for analytical calculation of deflections and deformations (Engström, 2015). Nonetheless, simplified analytical equations for estimating characteristic crack widths are available for simple geometries, as outlined in subsection 2.1.3 (Schlaich et al., 1987).

2.2.4 Advantages and challenges

Despite more advanced methods, STM remains widely used due to its endorsement in design codes and its simplicity (Zhang et al., 2014). STM offers simplicity and transparency, as the model is easily understood by designers (Blaauwendraad and Hoogenboom, 2002). However, STM has its limitations. It diverges from the elastic stress field, sometimes requiring non-linear FEA to verify ULS (Amini Najafian and Vollum, 2013). Automation is difficult since real structures are continuous, not discrete trusses. Manual reinforcement adjustments are often needed, reducing accuracy and increasing workload. Multiple load cases also require separate STM layouts, making the design process more time-consuming (Blaauwendraad, 2018).

Selecting an appropriate strut-and-tie model is often challenging, particularly in com-

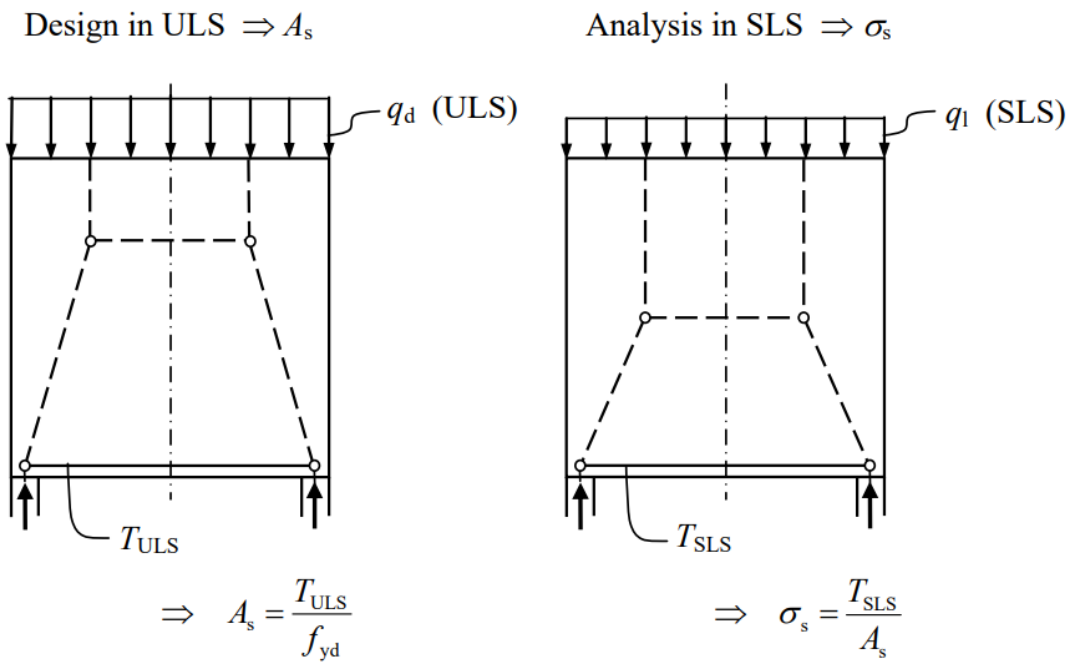

Figure 2.2: Design approach for deep beams, with different stress fields and strut-and-tie models for SLS and ULS (Engström, 2015)

plex D-regions (Blaauwendraad, 2018). Multiple valid models may exist, and the chosen configuration significantly influences the structural behaviour (Engström, 2015). As illustrated in Figure 2.3, the reinforcement required depends on the initial model choice, which can affect both cost and efficiency, giving the designer more influence than is often assumed. Additionally, statically indeterminate strut-and-tie models can be especially difficult to resolve (Blaauwendraad, 2018).

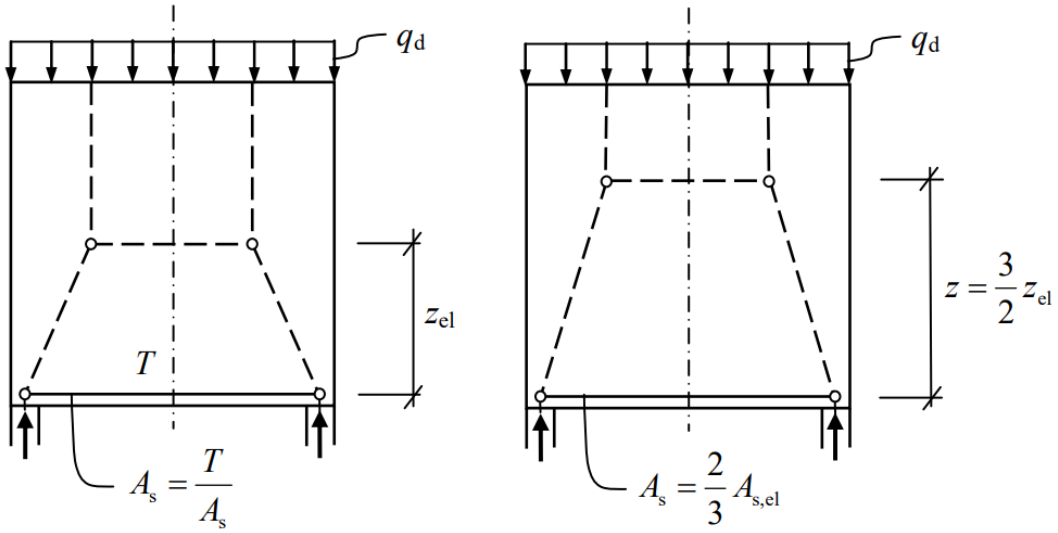

Figure 2.3: Impact on reinforcement amount due to chosen strut-and-tie model (Engström, 2015)

As previously noted, SLS poses a challenge for STM. Since strain compatibility is not considered, deflections are difficult to assess, and crack widths can only be estimated through simplified or iterative methods (Amini Najafian and Vollum, 2013). Consequently, neither deflection nor cracking can be reliably used as design criteria. In STM, linear FEA is often used, neglecting the non-linearity of the material, which is a limitation when having complex structures such as D-regions. Despite these limitations, STM remains a widely used and comprehensible method. However, it is less suitable in two specific cases, SLS assessments and cyclic loading (Blaauwendraad, 2018). In cyclic loading, such as seismic applications, STM is problematic as it requires different models for alternating load directions.

2.3 Stringer-Panel Method (SPM)

An alternative to the more well-known methods for the design of D-regions, like STM, is SPM. SPM can in many ways be seen as a combination of STM and FEM (de Mello and de Souza, 2016). SPM is neither well known nor widely used in any country except for Denmark, which is the only country where this method is recommended in the National Annexe to EC2 (DS/EN 1992-1-1) for in-plane stresses. SPM has many advantages and could be used in areas where STM is not sufficient, or in combination with STM (Blaauwendraad, 2018).

2.3.1 Theoretical background and principles

The SPM was initially developed for aircraft design, particularly to model wing structures requiring both lightness and high stiffness (de Mello and de Souza, 2016). The linear elastic stress field was originally solved using the force method until the introduction of the stiffness method-based FEA (Blaauwendraad, 2018). SPM was first applied to civil engineering in Denmark during the 1960s for wall-type concrete structures, though it applies to any material governed by plasticity theory (Jensen, 2012). Significant developments occurred in the 1990s, but research declined thereafter, with only limited applications pursued (de Mello and de Souza, 2016). Since then, SPM has primarily focused on computational design, including the development of tools like SPanCAD (Blaauwendraad and Hoogenboom, 1997). Despite its potential in early-stage and routine design, manual application of SPM is rarely discussed (de Mello and de Souza, 2016).

When SPM was introduced into structural concrete, as for STM, it was in the context of lower bound plasticity, hence, it also belongs to the stress field methods (Blaauwendraad, 2018). This means that the capacities obtained from SPM will be less than or equal to the actual capacities, and in other words, it provides solutions on the safe side. In addition to focusing on the ULS strength, the applicability in SLS due to linear-elastic analysis also leaves a focus on SLS strength and durability.

SPM can, as mentioned, be described as a combination of STM and FEM (Blaauwendraad and Hoogenboom, 1997). One of the main differences between FEM and SPM is that SPM aims to use the coarsest possible mesh, while FEM typically requires a much finer mesh to ensure convergence (de Mello and de Souza, 2016). Designing a stringer-panel

model with a sufficient mesh, yet as coarse as possible, is a key challenge and skill in applying the method effectively (Blaauwendraad, 2018). In some cases, however, a finer stringer-panel grid may be more appropriate, depending on the situation. This is where engineering judgement and experience become especially important, just as with STM.

SPM is built up by panels that transfer membrane shear forces and stringers that transfer normal forces, a combination of one and two-dimensional elements. The intersection between stringers is called nodes (Danish Transport Construction and Housing Authority, 2020). The normal forces vary linearly in the stringers, and the panels are loaded with uniform shear force. Each panel, a quadrilateral element, should be surrounded by four stringers, most commonly placed in a rectangular shape. It is also possible to have other trapezoidal shapes if needed (de Mello and de Souza, 2016). An explanation of the stringers, stringer segments, panels, and nodes can be seen in Figure 2.4.

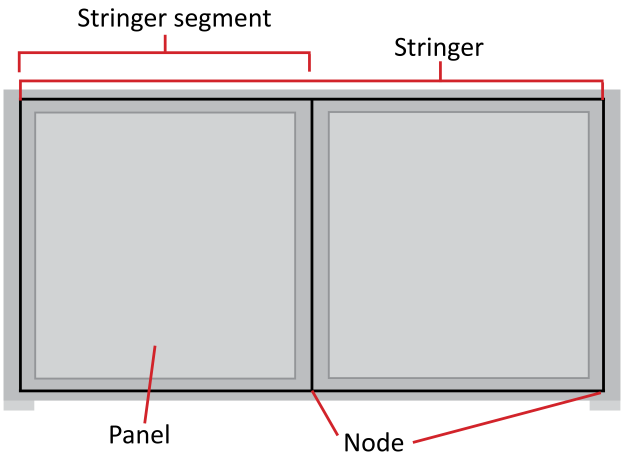

Figure 2.4: Illustration of stringers, stringer segments, panels, and nodes

Similarly to STM, each panel and stringer is in equilibrium, but in contrast to STM, SPM can take compatibility conditions into account (Blaauwendraad and Hoogenboom, 1997). Stringers and panels are connected by grips in nodes. The equilibrium conditions between stringers and panels, both vertical and horizontal equilibrium, are displayed in Figure 2.5. For the case of rectangular panels, the shear resultants on the opposite parallel sides are equally large but in opposite directions to satisfy the equilibrium (Blaauwendraad, 2018).

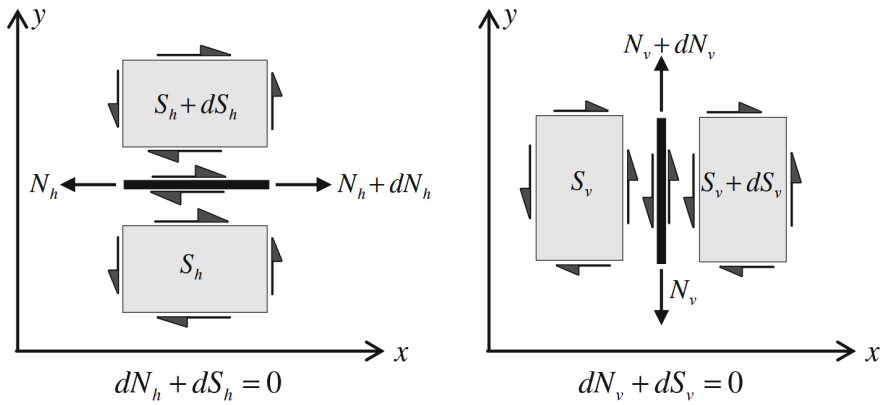

Figure 2.5: Equilibrium conditions and equations for the stringers and panels (Blaauwendraad, 2018)

Due to equilibrium and since the shear force acts in the interface between a panel and the adjacent stringer, the discretisation with SPM of a beam could be visualised as in Figure 2.6. For consistency, the sign convention throughout the thesis for the panels and the stringers will be as displayed in Figure 2.7.

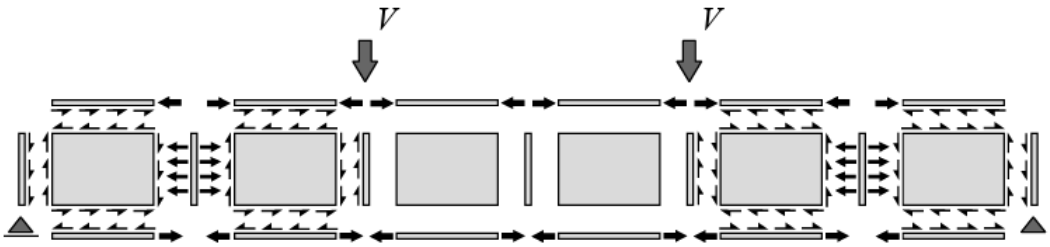

Figure 2.6: Discretised beam with SPM (Blaauwendraad and Hoogenboom, 1997)

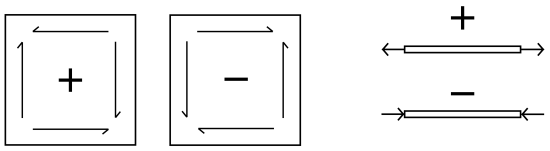

Figure 2.7: Sign convention used throughout the thesis

SPM exists in linear and non-linear forms (de Mello and de Souza, 2016). The non-linear version models material non-linearity and allows panels to absorb normal forces, closely reflecting real structural behaviour. This, however, requires software such as SPanCaD. The linear version assumes linear material in both stringers and panels and can be analysed manually or with simpler scripts for complex geometries.

2.3.2 Design and modelling

Once the D- and B-regions are identified and the internal forces determined, SPM can be applied to design the reinforcement within the D-region. Since SPM shares conceptual similarities with STM, prior experience with STM is beneficial (Blaauwendraad, 2018). The spacing of stringers, placement of tension reinforcement, and calculation of compression members follow STM principles. The following discussion assumes rectangular panels enclosed by four stringers.

2.3.2.1 The model

SPM modelling begins with defining stringer placement, then adding panels between them (Blaauwendraad, 2018). The minimum amount of stringers is achieved by placing stringers along D-region edges, aligned with external loads and supports, and around the edges of eventual openings. Spacing between stringers and beam edges must be selected, typically based on cover requirements and expected widths of bundles and stirrups. As with STM, engineering judgement remains central to these decisions (Blaauwendraad, 2018). Shear panels are placed between stringers, and examples of stringer-panel models are shown in Figure 2.8.

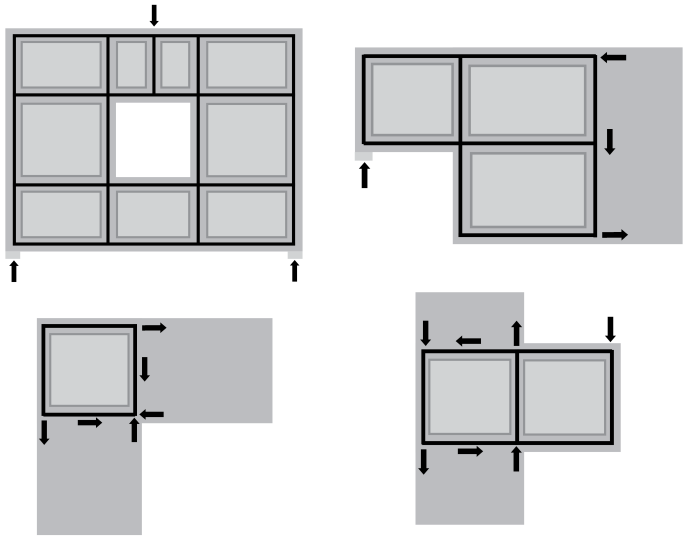

Figure 2.8: Examples of stringer-panel models for different D-regions

The model is statically determinate if Equation (2.4) is satisfied for closed systems, and Equation (2.5) applies when free stringers unconnected to panels are present (Blaauwendraad, 2018). The latter also governs models containing openings. Where n is the number of nodes, p is the number of panels, and s is the number of stringers.

$$2p = n - 2 \tag{2.4}$$

$$3p = s - 1 \tag{2.5}$$

2.3.2.2 Forces in stringers and panels

Forces in stringers and panels are determined depending on whether the model is statically determinate or redundant (Blaauwendraad, 2018). Statically determinate systems can be solved using equilibrium-based analytical methods, and some redundant cases with symmetry may also be addressed manually. Otherwise, iterative shear force estimates or FEA may be used (Jensen, 2012). Redundancy can also be handled by incorporating compatibility, though this increases complexity. This thesis uses the Python script SPM.py, developed by P.C.J. Hoogenboom, which is described in subsection 2.3.3.

2.3.2.3 Reinforcement in tension stringers

Once the internal forces are known, the tensile reinforcement in the stringers can be detailed similarly to the ties in STM (Blaauwendraad, 2018). The required reinforcement area is calculated using Equation (2.6), by EC2 (Swedish Standards Institute, 2008), where f_{yd} is defined by Equation (2.7) using a partial safety factor $\gamma_s = 1.15$. Cover requirements and minimum spacing follow standard EC2 provisions (Jensen, 2012), while anchorage is designed according to Section 8 of EC2 (Swedish Standards Institute, 2010).

$$A_s = \frac{N}{f_{yd}} \tag{2.6}$$

$$f_{yd} = \frac{f_{yk}}{\gamma_s} \tag{2.7}$$

Stringer forces vary linearly between nodes and must be transferred to the reinforcement from the adjacent shear field (Jensen, 2012). The required shear stress which needs to be transferred corresponds to the difference in panel stresses on either side of the stringer. The maximum permitted variation is typically defined as an increase from zero to the design yield force over the anchorage length, as described by Equation (2.8).

$$|\tau_A - \tau_B| = \frac{nA_s f_{yd}}{l_b b} \tag{2.8}$$

Where τ_A and τ_B represent shear stresses in the adjacent panels, b is panel width, n the number of bars, A_s the area per bar, f_{yd} the design yield strength, and l_b the anchorage length. Once l_b is determined, the force transfer between reinforcement and shear field must be verified.

2.3.2.4 Compression stringers

Concrete compression stringers should be checked using principles similar to those for struts in STM (Blaauwendraad, 2018). The compressive stress is calculated as in Equation (2.9) by dividing the axial force by the stringer area, defined as $t * w_{stringer}$. While there is no strict limit on stringer width, it typically does not exceed 20% of the adjacent shear field, with the smallest dimension perpendicular to the stringer (Jensen, 2012).

$$\sigma_c = \frac{N_c}{A_c} \tag{2.9}$$

The compressive stress should then be checked to be lower than the stringer strength, $\sigma_c < \sigma_{Rd,max}$ (Swedish Standards Institute, 2008). Where the stringer strength, $\sigma_{Rd,max}$, could be calculated with Equation (2.10) if the concrete stringer is without transverse tension and Equation (2.11) if the concrete stringer is with transverse tension. This is done with the effectiveness factor ν as Equation (2.12) and f_{cd} as Equation (2.13) with $\gamma_c = 1.5$.

$$\sigma_{Rd,max} = f_{cd} \tag{2.10}$$

$$\sigma_{Rd,max} = 0.6\nu f_{cd} \tag{2.11}$$

$$\nu = 1 - \frac{f_{ck}}{250} \tag{2.12}$$

$$f_{cd} = \frac{0.85 f_{ck}}{\gamma_c} \tag{2.13}$$

The compressive stress in a stringer can initially be set equal to its strength to determine the minimum required width. This width should then be checked against the dimensions of the support and load plates, as well as the selected stringer layout. If the required width is too large, the model must be adjusted or compression reinforcement added. Alternatively, the process may begin with a chosen stringer width, matching the plate size for load- and support-aligned stringers, or twice the distance from the centreline to the edge for edge-adjacent ones. In all cases, the width should not exceed 20% of the panel size (de Mello and de Souza, 2016). The resulting compressive stress is compared to the stringer's capacity, and if exceeded, modifications or reinforcement are required. Any compression reinforcement should be designed according to EC2 (Swedish Standards Institute, 2010).

2.3.2.5 Panels

Distributed mesh reinforcement in the panels is designed based on membrane shear forces. The steel ratio, ρ, is obtained by dividing the uniform shear stress, τ_p, by the steel yield strength, as given in Equation (2.14) (Blaauwendraad, 2018). The shear stress, τ_p, is calculated from the shear force and the panel's cross-sectional area, defined as the thickness, t, times the effective height, h_e, which corresponds to the length of the stringers; see Equation (2.15).

$$\rho f_{sy} = \tau_p \tag{2.14}$$

$$\tau_p = \frac{V}{t * h_e} \tag{2.15}$$

For small shear panels with closely spaced stringers, distributed reinforcement may be unnecessary; all reinforcement can instead be concentrated in the stringers, if appropriate

(Jensen, 2012). Shear stress increases the tensile load in tension stringers and reduces compression in compression stringers, potentially reversing the force direction and requiring tensile reinforcement.

Concrete stresses in the panels must also be checked to avoid premature crushing (de Mello and de Souza, 2016). Assuming equal yield stress and reinforcement ratios in both directions, the resulting concrete struts will get an inclination of a 45° angle, as illustrated in Figure 2.9.

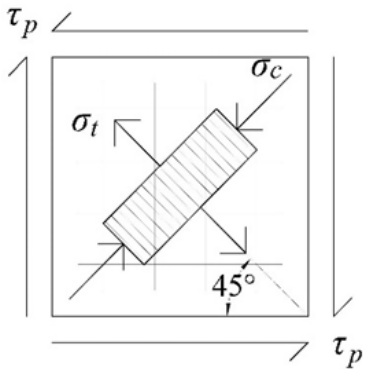

Figure 2.9: Panels with equal yield stress and reinforcement ratios (de Mello and de Souza, 2016)

The assumption of equal yield stress and reinforcement in both directions leads to the relation in Equation (2.16). The resulting compressive stress must not exceed the effective compressive strength of the concrete, as defined in Equation (2.11).

$$\sigma_c = -2|\tau_p| \tag{2.16}$$

If compressive stress is present at the centre of the panel, this method may be overly conservative (Blaauwendraad, 2018). One alternative is to derive the stress from the stringer normal forces, dividing the forces by the stringer area. Regardless of the method, the panel's compressive stress must remain below the effective concrete strength, similar to struts intersected by transverse ties in STM (de Mello and de Souza, 2016). As per Eurocode, this is verified using Equation (2.11), as discussed in subsubsection 2.3.2.4 (Swedish Standards Institute, 2010).

According to EC2, distributed reinforcement in the D-region must meet the minimum reinforcement requirements (Swedish Standards Institute, 2010). If the calculated reinforcement is below this threshold, the EC2 minimum should be applied; otherwise, the calculated amount governs.

2.3.2.6 Summary of design steps

The design steps of SPM could be summarised as follows.

- Develop the stringer-panel model.
- Calculate the forces in the stringers and panels.
- Select appropriate distributed shear reinforcement in panels and bundle reinforcement in stringers. Check the bond and anchoring.
- Evaluate and check dimensions of compression stringers and check concrete stresses in panels.

2.3.3 The Python script SPM.py

As discussed, beams can be designed using SPM either through analytical calculations, assuming shear stresses to resolve indeterminacy, or by including compatibility via stiffness, as in the Python script SPM.py by Hoogenboom (Blaauwendraad, 2018). The script's use is detailed in Blaauwendraad (2018) and further explained in a manual by Hoogenboom (2017).

The script is relatively straightforward. The designer manually defines a stringer-panel grid, where each stringer consists of one or more stringer segments, defined as the portion of a stringer along one panel edge. Each segment has three degrees of freedom (DOFs) in the normal direction, one at each end shared with adjacent segments, and one at the centre, shared with adjacent panels, as shown in Figure 2.10. Panels have four DOFs at the midpoints of their edges, which are shared with the stringers. To define the stiffness, the lengths of stringer segments, panel dimensions, and the concrete's modulus of elasticity are specified. Finally, boundary conditions and forces are assigned to the relevant DOFs, after which the script performs the calculations.

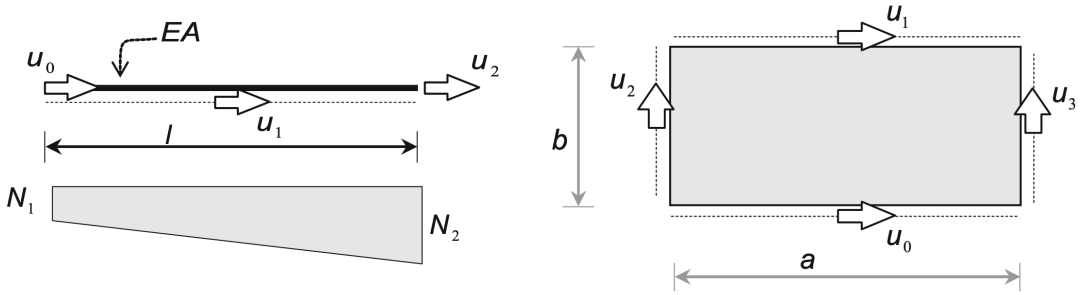

Figure 2.10: DOFs of a stringer segment (left) and a panel (right) (Blaauwendraad, 2018)

The computations in SPM.py resemble numerical FEA, as they incorporate compatibility conditions, allowing analysis of statically indeterminate structures. Each stringer segment is assumed to have a constant cross-sectional area (A) and extensional stiffness (EA). The stringer's constitutive relation is given by Equation (2.17), where N is the normal force

and ε the strain (Hoogenboom, 2017). A uniformly distributed shear force n acts along the stringer segment, described by Equation (2.18).

$$N = EA\varepsilon \tag{2.17}$$

$$n = \frac{N_2 - N_1}{L} \tag{2.18}$$

The kinematic equations of the stringer segments are then described by the equations in (2.19), where u is the displacement in the different DOFs as defined on the left part of Figure 2.10.

$$\varepsilon_1 = \frac{-4u_0 + 6u_1 - 2u_2}{L} \ , \ \varepsilon_2 = \frac{2u_0 - 6u_1 + 4u_2}{L} \tag{2.19}$$

At the edges of the panels, the shear force n acts uniformly distributed, which causes the panel to experience a homogeneous shear stress. The constitutive equation for the panel can be described as in (2.20), where G is the shear modulus of the concrete, t is the thickness of the beam, and γ is the shear strain in the panel.

$$n = Gt\gamma \tag{2.20}$$

The kinematic equation for the panel is described in (2.21), with the DOFs as defined on the right part of Figure 2.10.

$$\gamma = \frac{u_1 - u_0}{b} + \frac{u_3 - u_2}{a} \tag{2.21}$$

The stiffness of the stringers and the panels is assembled into a global stiffness matrix, which is then used together with the external forces to solve for the displacements in each DOF, the support reactions, and the forces in the stringers. These outputs can then be used to determine the amount of reinforcement needed as well as the deflections of the structure. The element stiffness matrix for the 3-DOF stringer segments is defined as in (2.22), and the element stiffness matrix for the 4-DOF panels is defined as in (2.23) (Hoogenboom, 2017).

$$K_{e.stringer} = \frac{EA}{L}\begin{bmatrix} 4 & -6 & 2 \\ -6 & 12 & -6 \\ 2 & -6 & 4 \end{bmatrix} \tag{2.22}$$

$$K_{e.panel} = Gt\begin{bmatrix} \frac{a}{b} & -\frac{a}{b} & 1 & -1 \\ -\frac{a}{b} & \frac{a}{b} & -1 & 1 \\ 1 & -1 & \frac{b}{a} & -\frac{b}{a} \\ -1 & 1 & -\frac{b}{a} & \frac{b}{a} \end{bmatrix} \tag{2.23}$$

2.3.4 Behaviour in service state

Like STM, SPM is based on the lower bound theorem and is therefore applicable in ULS. Unlike STM, however, the same model can be used for both SLS and ULS. Since compatibility is incorporated similarly to FEM, displacements and deflections can be calculated (Blaauwendraad, 2018). For simple models, this can be done by hand, or analytically with the SPM.py script for more complex or indeterminate systems, as shown in subsection 3.2.2. The approach mirrors FEM, using stiffness properties in panels and stringers, and with DOFs linking them together. The mesh derives from the layout of stringers and panels, ideally kept as coarse as feasible. Reinforcement stresses can be calculated directly from internal forces, obtained either through hand calculation or from the SPM.py output (Blaauwendraad, 2018). As for crack widths, they can be calculated approximately as described in subsection 2.1.3.

2.3.5 Advantages, challenges, and comparison with STM

The primary difference between designing a beam using STM versus SPM is that the reinforcement is more concentrated when designed with STM compared to more distributed with SPM (de Mello and de Souza, 2016). Nevertheless, the total reinforcement quantity often remains comparable between the two approaches (Sgambi and Tarquini, 2003). The procedures for determining reinforcement requirements and checking the compressive capacity of concrete are also very similar for both methods (Blaauwendraad, 2018). Furthermore, as discrete methods based on the lower-bound theorem of plasticity, both STM and SPM require engineering judgement, such as defining D-region extents and placing ties or stringers.

One advantage of SPM is its potential simplicity, as the same model can be used for both SLS and ULS under various load combinations and directions (Blaauwendraad, 2018). This is particularly practical for seismic or cyclic loading scenarios. Even in static load cases, SPM is at least as straightforward as STM (de Mello and de Souza, 2016). SPM is also easier to automate, and SLS checks become more manageable due to the relative ease of incorporating compatibility conditions. Moreover, statically indeterminate structures can be solved more easily with SPM, especially with the support of computational tools (Blaauwendraad, 2018).

A notable limitation of SPM is the lack of experimental data on D-regions designed using the method (de Mello and de Souza, 2016). The flexibility in assigning shear stresses in redundant models presents both opportunities and risks (Jensen, 2012). While this allows for potential optimisation, it also introduces the risk of unfavourable stress distributions. As with STM, much of the modelling in SPM relies on the designer's decisions regarding the placement of stringers, panels, and boundary conditions (Blaauwendraad, 2018). However, SPM has proven especially effective for analysing structural elements such as frame corners and panels with openings (Jensen, 2012).

2.4 Finite Element Method (FEM)

The basis of FEM is the subdivision of a larger structure into a finite number of smaller elements, simplifying the representation of a solid structure while still capturing its structural response accurately. FEM is widely used in structural engineering for both linear and non-linear analyses, depending on the purpose. Although large or detailed models can be computationally demanding and require extensive input data, often challenging during early design, FEM enables detailed modelling of complex, non-linear behaviour. This allows for more precise results, including deflections, strains, and stresses (Godínez and Restrepo, 2023; Abdulmajed et al., 2024).

2.4.1 DIANA

DIANA (DIsplacement ANAlyzer) is a commercial FEA software widely used in civil engineering, particularly for reinforced concrete. It offers advanced features such as crack prediction, multiple material models, and detailed modelling of reinforcement–concrete interaction (Chai, 2020). Like other finite element software, DIANA uses iterative methods and provides high precision in non-linear analyses. Its versatility and accuracy are the main reasons it was selected for the analyses in this report.

2.4.2 Non-linear FEA

Non-linear methods use iterative solvers and can account for effects like plasticity, cracking, creep, and other time-dependent or material non-linearities (DIANA FEA BV, 2017). Non-linear analysis is especially valuable for concrete, which behaves non-linearly even under service loads and can yield inaccurate results under linear assumptions in ULS conditions (Plos, 1996).

To solve a non-linear problem, the displacement vector corresponding to force equilibrium must be found through incremental-iterative procedures (DIANA FEA BV, 2024a). Different iterative methods are available to determine the increment size with which the displacement vector should be updated. Among the available methods in DIANA is the Newton-Raphson method. In its regular form, the stiffness matrix is updated each iteration, offering a quadratic convergence characteristic but requiring time-consuming matrix decompositions for every iteration. While efficient when initial predictions are accurate, it may diverge otherwise (DIANA FEA BV, 2024a). The modified Newton-Raphson method evaluates the stiffness matrix only once per increment, improving stability and reducing computational effort per iteration, though typically requiring more iterations overall (DIANA FEA BV, 2024a). The Quasi-Newton (or Secant) method solves non-linear problems by approximating the tangent stiffness matrix using data from previous iterations, avoiding the need to update the matrix each time (DIANA FEA BV, 2024a). Iterations continue until convergence is achieved or predefined criteria, such as force, displacement, energy, or residual norms, are met. The process may also stop if divergence occurs or the iteration limit is reached.

DIANA offers various strategies for selecting step sizes in incremental analysis, including load control, displacement control, and arc-length control (DIANA FEA BV, 2024a).

Load and displacement control apply incremental forces or displacements, respectively. Displacement control is useful for capturing plastic behaviour near failure, where small load increases can cause large displacements. In this method, certain displacements are prescribed, and the remaining values are solved using force-displacement relationships. Load control instead prescribes forces. Arc-length control is suitable for cases with large displacements or near-horizontal load-displacement curves, allowing for step size adjustments to improve convergence and handle snap-back or snap-through responses.

2.4.3 Material definitions

Before non-linear behaviour, materials are typically assumed to behave linearly elastic. After this stage, cracking and plasticity models are used to model the non-linear behaviour and failure mechanism (Plos, 1996). Reinforcing steel is usually considered elastic until yielding, after which plastic deformation occurs. The material models are further described in the following subsections.

2.4.3.1 Concrete

Concrete is a heterogeneous material composed of aggregates, cement, and water, with properties depending on mix proportions, aggregate size, and concrete class (Plos, 1996). For practical applications, however, it is typically modelled as a homogeneous and isotropic material until cracking occurs.

In DIANA, concrete can be defined using various approaches, including different design codes (DIANA FEA BV, 2024b). EC2, commonly used in Sweden, and the fib Model Code for Concrete Structures are two of the options. EC2 defines stress-strain relations for normal-weight concrete classes (C12/15 to C80/95) and lightweight classes (LC12/13 to LC80/88) as in Figure 2.11. Concrete materials in DIANA can also be defined manually, without using design codes, allowing the user to specify various parameters and material models (DIANA FEA BV, 2024b).

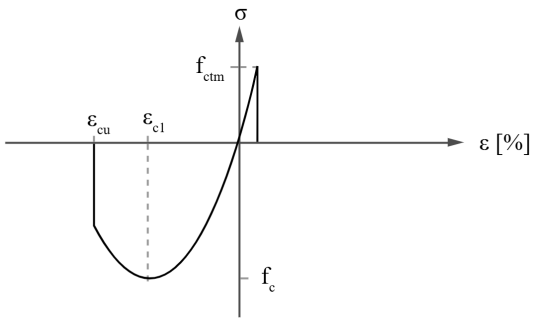

Figure 2.11: Stress-strain diagram according to EC2 (DIANA FEA BV, 2024b)

DIANA commonly employs the total strain crack model, which uses a smeared cracking approach and non-linear stress-strain relationships for both tension (cracking) and compression (crushing) (DIANA FEA BV, 2024a). The model compares principal stresses

and strains with a user-defined stress-strain curve. It supports fixed, rotating, and rotating-to-fixed crack orientations and is compatible with beam, truss (regular and enhanced), plane stress, and plane strain elements (DIANA FEA BV, 2017; DIANA FEA BV, 2024a).

The model accounts for the tensile and compressive stresses according to EC2. The tensile behaviour of the model includes multiple tension softening functions, which are based on fracture energy related to a crack bandwidth, commonly used in smeared crack models. A common model to use is the non-linear softening curve according to Hordijk, as can be seen to the left in Figure 2.12. Compressive behaviour follows EC2, as can be seen to the right in Figure 2.12. The compressive behaviour specifically uses Equation (3.14) in EN 1992-1-1, accounting for increased strength and ductility at higher stress levels. Alternative curves, for both tension and compression, could also be applied in the total strain crack model.

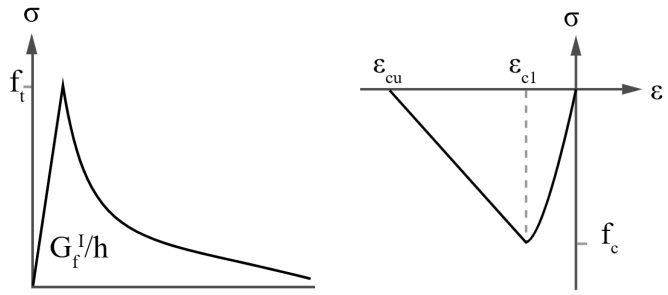

Figure 2.12: Tensile behaviour according to Hordijk (left), compression curve according to EC2 (right) (DIANA FEA BV, 2024b)

Tensile behaviour in the total strain crack model can be defined using a damage-based reduction approach, which accounts for the decrease in Poisson's ratio due to cracking (DIANA FEA BV, 2024a). Lateral confinement and lateral cracking may also be included, except when using purely elastic compression curves. DIANA applies a constant shear stiffness reduction, which is especially relevant in fixed or combined fixed and rotating crack models, where cracking reduces shear stiffness. Various shear retention functions are available to model this behaviour. The model can also incorporate ambient effects and Kelvin chain viscoelasticity, making it suitable for both SLS and ULS analyses, particularly where cracking or crushing dominates (DIANA FEA BV, 2024a). If material properties are defined according to EC2 or another code, DIANA automatically determines compressive, tensile, shear, and lateral effects without requiring further input.

2.4.3.2 Steel and reinforcement

In DIANA, steel can be defined either via user-specified parameters or through design codes (DIANA FEA BV, 2024a). When applying Eurocode EN 1993-1-1, standard construction steels from S235 to S460 can be selected. Users may modify properties such as Young's modulus, Poisson's ratio, thermal expansion coefficient, and density, and may also include damping. Alternatively, steel can be modelled using various linear or plastic material models. Two common plasticity models are Von Mises and Tresca (DIANA FEA BV, 2024b). When plasticity is included, hardening behaviour, kinematic or isotropic, must be defined. One option is total strain hardening, where stresses are related to total

strains. Regardless of the hardening type, a hardening hypothesis, strain or work hardening, must be selected, both requiring the same input parameters. For Von Mises plasticity, the user must also choose between isotropic, kinematic, or combined hardening.

Several material models are available for reinforcement steel in DIANA, including linear elastic models, EC2-based definitions, and plasticity models such as Von Mises (DIANA FEA BV, 2024a). The interaction between reinforcement and concrete is complex and can be modelled with varying levels of detail, for example, using embedded reinforcement or bond-slip relationships. The governing effect on the behaviour of the interaction is secondary cracks in the transverse and longitudinal directions around the reinforcement. The bond-slip relation describes how the concrete and reinforcement interact when moving slightly relative to each other (DIANA FEA BV, 2024a). In DIANA, the mechanical behaviour at the location of the interaction and slip zone is defined by an interface element with no thickness. The constitutive laws are primarily based on total deformation theory, where traction depends on relative displacement. The normal traction–displacement relationship is assumed linear elastic, while the shear traction–slip relationship is non-linear and can follow various predefined curves depending on the chosen theory.

Bond-slip properties significantly affect structural performance, particularly in SLS, where they influence crack widths, spacing, tension stiffening, and curvature (fib, 2010). In ULS, it impacts anchorage strength, lapped joint performance, and rotation capacity of plastic hinges. DIANA includes several bond-slip interface models, each requiring specific slip parameters. The only design-code-based model is the CEB-FIB 2010 function, which differs primarily in its unloading–reloading behaviour compared to other models (DIANA FEA BV, 2024a). Relevant parameters and loading characteristics are defined in the fib Model Code (fib, 2010). Bond-slip failures include pull-out and splitting failures. Anchorage-related failure can also be considered for both linear and non-linear anchors, provided the anchor stiffness is defined (DIANA FEA BV, 2024a).

2.4.4 Crack approaches in finite element modelling

Cracking in DIANA can be modelled using either the discrete or smeared cracking approach (DIANA FEA BV, 2024a). A third option, less commonly available in standard finite element software, is the embedded crack approach, which models cracks as discontinuities within elements. While this method most closely represents real crack behaviour, it requires special elements and is computationally intensive. The discrete crack model simulates cracks as discontinuities between elements and requires predefined crack locations and interface elements, making it ideal for studying specific cracks or crack patterns. In contrast, the smeared crack model distributes cracking over elements, making it suitable when crack locations are unknown and global behaviour is of interest.

The total strain crack model in DIANA uses a smeared crack approach requiring input of crack bandwidth and fracture energy (DIANA FEA BV, 2024b). The crack bandwidth is a length scale parameter used for the softening tensile curves based on the fracture energy. It can either be user-defined or calculated using methods such as Rots' element-based approach, which bases the bandwidth on the finite element size. The mode-I tensile fracture energy is derived from the chosen tension function, for example, Hordijk's curve

(Figure 2.12) (DIANA FEA BV, 2017). In structural analyses, especially for crack predictions when the crack bandwidth is element-based, different behaviours can be seen depending on the mesh size (Alañón et al., 2018). A too fine mesh may overestimate crack width, while a too coarse mesh may underestimate it. Mesh sensitivity is especially an issue as cracks localise and propagate at higher load levels near failure (Modéer, 1979).

The smeared crack approach includes three models: fixed, multi-directional, and rotating cracks (DIANA FEA BV, 2024b). In the fixed crack model, cracks follow the principal stress direction, with shear stresses arising if this direction changes. The multi-directional crack model also has this convention, but new cracks can develop if the direction of the principal stresses changes more than a specific angle. The rotating crack model aligns cracks continuously with the principal stresses, resulting in no shear stresses within cracks.

3

Design and analysis of specimen

A deep beam was analysed through a parametric study, varying one geometric parameter at a time to evaluate the applicability of the Stringer-Panel Method (SPM) and compare it with the Strut-and-Tie Method (STM). For each variation, reinforcement was designed using both methods and analysed through analytical calculations and non-linear finite element analysis (FEA). The beams used C30/37 concrete and reinforcement with a yield stress of $500\,\mathrm{MPa}$, following Eurocode EN 1992-1-1 (EC2). Although higher-strength concrete is common in practice, C30/37 was chosen to better observe cracking and deflections. A cover thickness of $50\,\mathrm{mm}$ was used, and the assumed spacing between reinforcement layers was $20\,\mathrm{mm}$.

For all beams, no safety factors were applied in either the design or the analysis. Since the focus was on investigating structural behaviour rather than achieving code-compliant designs, this approach allowed for a more direct comparison between analytical calculations and non-linear FEA results. Additionally, reinforcement areas and related parameters were not rounded to standard values but kept as calculated. This eliminated rounding errors and ensured consistent, accurate comparisons between different beam models, helping isolate the influence of geometric variations and design methods without the interference of practical detailing adjustments.

3.1 Geometries of specimen

For each specimen, one geometric parameter was varied while keeping the beam height fixed at $3\,\mathrm{m}$ and the thickness at $400\,\mathrm{mm}$. All beams were subjected to a $3000\,\mathrm{kN}$ point load in the negative y-direction, applied at the centre of the top edge via a loading plate, which was considered as the design load for the beams. Simply supported conditions were provided at the ends along the bottom. The loading and support plates measured $400\,\mathrm{mm}$ in width, $100\,\mathrm{mm}$ in height, and matching the beam's thickness. One varied parameter was the span length, increased from $3\,\mathrm{m}$ to $9\,\mathrm{m}$ in $0.5\,\mathrm{m}$ increments. Some examples of beam geometries with varying lengths are shown in Figure 3.1.

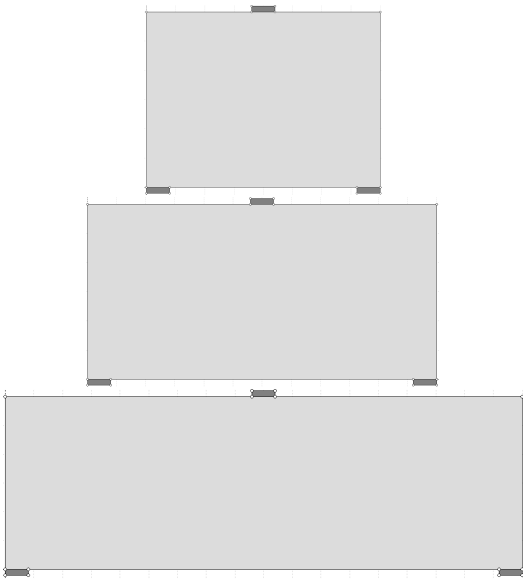

Figure 3.1: Deep beams with a height of $3\,\mathrm{m}$ and a length of $3\,\mathrm{m}$, $6\,\mathrm{m}$, and $9\,\mathrm{m}$

The other parameter studied was a central opening introduced into the beam, which was varied in size. To isolate the influence of the opening, both the beam's height and length were held constant at $4\,\mathrm{m} \times 3\,\mathrm{m}$. The opening was square-shaped, with side lengths ranging from $0.5\,\mathrm{m}$ to $1.5\,\mathrm{m}$, increasing in $0.25\,\mathrm{m}$ increments. This allowed for an analysis of the effect of the opening-to-beam area ratio. Three beams with increasing opening sizes are illustrated in Figure 3.2.

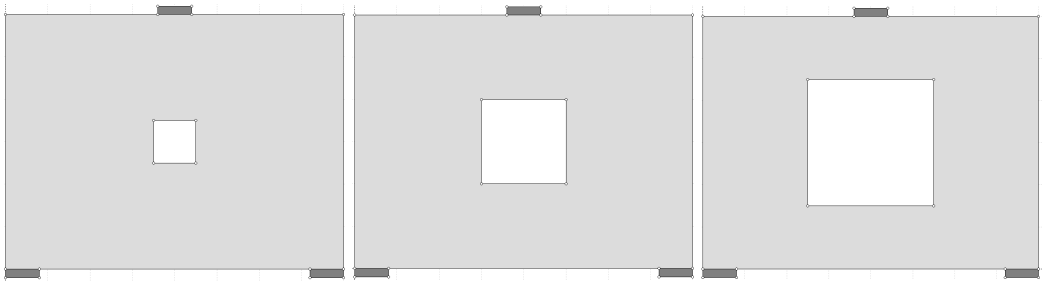

Figure 3.2: Deep beam with dimensions $4\,\mathrm{m} \times 3\,\mathrm{m}$, with varying opening size, $0.5\,\mathrm{m} \times 0.5\,\mathrm{m}$, $1\,\mathrm{m} \times 1\,\mathrm{m}$ and $1.5\,\mathrm{m} \times 1.5\,\mathrm{m}$

3.1.1 Background of choice of geometries

The specimens were designed as deep beams with typical geometries and clear deep beam characteristics. A fixed height of $3\,\mathrm{m}$ was chosen to represent a structural wall element in a building. The span length was varied to study the influence of the span-to-depth ratio and assess whether SPM or STM performs better as the beam becomes deeper or more slender. While this ratio could also be varied by adjusting the height, changing the length was considered more realistic for building applications. Span lengths ranged from $3\,\mathrm{m}$ to $9\,\mathrm{m}$, aligning with the deep beam definition in Engström (2015), which states that a beam

is considered deep when its span does not exceed three times its depth. Shorter beams were avoided, as their behaviour tends to resemble that of columns. Only one geometric parameter was varied at a time to isolate its effect on the structural response and better understand its influence on the suitability of SPM versus STM for reinforcement design in D-regions.

One advantage of SPM is its suitability for beams with openings, due to its rules for stringer placement (Blaauwendraad, 2018). This motivated the choice of an opening with varying size as the second parameter studied. The aim was to assess how openings influence reinforcement layout and method preference. The smallest opening was selected based on when it began noticeably affecting the linear elastic stress field. The largest opening was chosen to ensure the beam still behaved as a deep beam, since larger openings caused it to act more like a frame structure.

3.2 Design of reinforcement

The reinforcement for each specimen with varying geometrical parameters was designed with both STM and SPM. The design process and final reinforcement designs are presented in the following section.

3.2.1 STM

To determine the strut-and-tie layout, a linear elastic analysis was performed in DIANA without reinforcement. The concrete and the loading and support plates were modelled with linear elastic properties, with material parameters listed in Table 3.1. The geometry reflected each beam case, with the variations previously described. Simply supported boundary conditions were applied at the bottom plates, and the design load was applied at the loading plate. A structured mesh with $0.1\,\mathrm{m}$ square elements was used. The analysis produced principal stress plots indicating the linear elastic stress fields. The Python script used for this DIANA analysis is provided in the Appendix in section A.1.

Table 3.1: Linear analysis input parameters

Properties	**Value**
Concrete class	C30/37
f_{cm}	$38\,\mathrm{MPa}$
Aggregate	Quartzite
Cement class	Class N
E_s	$200\,\mathrm{GPa}$
ν_s	0.2
ρ	$7800\,\mathrm{kg/m^3}$

Based on the principal stress fields from the linear analyses, a strut-and-tie model was developed for each beam geometry. Ties placed along the bottom or around openings were offset $80\,\mathrm{mm}$ from the concrete edge, approximating the reinforcement's centre of gravity.

This assumed two layers of $20\,\mathrm{mm}$ bars, $50\,\mathrm{mm}$ cover, and $20\,\mathrm{mm}$ spacing between the layers. The application rules outlined in section 2.2 were followed, and strut angles were verified to meet design criteria. Examples of models for the $4\,\mathrm{m} \times 3\,\mathrm{m}$ beam and the same beam with a $1\,\mathrm{m} \times 1\,\mathrm{m}$ opening are shown in Figure 3.3.

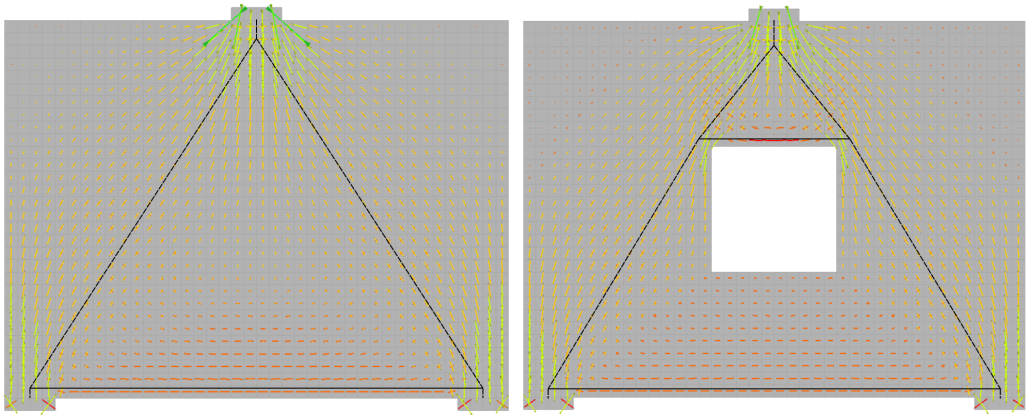

Figure 3.3: Stress field and strut-and-tie model for the beam with dimensions $4\,\mathrm{m} \times 3\,\mathrm{m}$ and the beam with the same dimensions with an opening of $1\,\mathrm{m} \times 1\,\mathrm{m}$

The strut-and-tie models were then analysed in TrussPilot, a software developed by the engineering firm ELU. This program calculates the reinforcement area and the strut widths according to EC2 as explained in section 2.2. The input parameters in Table 3.2 were used in TrussPilot. The results from this analysis and the strut-and-tie models can be found in the Appendix in section A.2.

Table 3.2: TrussPilot input parameters

Properties	**Value**
f_{ck}	$30\,\mathrm{MPa}$
γ_s	1
k_1	1.0
k_2	0.85
k_3	0.75

The distributed reinforcement for all deep beams was calculated according to EC2 for minimum reinforcement to satisfy Equation (3.1) with an area not less than stated in Equation (3.2) (Engström, 2015). The maximum bar spacing was calculated according to Equation (3.3) but not larger than $300\,\mathrm{mm}$. This resulted in a distributed reinforcement of $400\,\mathrm{mm}^2/\mathrm{m}$ with $s_{max} = 300\,\mathrm{mm}$ for all the deep beams designed according to STM.

$$\rho_{min} = 0.001 \tag{3.1}$$

$$A_{min} \geq 150\,\mathrm{mm}^2/\mathrm{m} \tag{3.2}$$

$$s_{max} = 2 * t \tag{3.3}$$

The reinforcement area and length for each tie are presented in Table 3.3 for varying beam lengths and in Table 3.4 for varying opening sizes, where H denotes horizontal and V vertical tensile reinforcement. The tensile reinforcement volume was combined with the distributed reinforcement volume, calculated by multiplying the minimum reinforcement on both sides by the beam's area, to determine the total reinforcement volume for each beam, as summarised in the tables.

Table 3.3: Reinforcement areas and total volume, varying beam length

Beam size [m]	H_1 [mm^2]	L_{H1} [mm]	H_2 [mm^2]	L_{H2} [mm]	V [mm^2]	L_V [mm]	Total Volume [10^{-6} m^3]
3×3	1611	2600	0	0	0	0	18589
3.5×3	1709	3100	0	0	0	0	22098
4×3	1949	3600	0	0	0	0	26216
4.5×3	2180	4100	0	0	0	0	30538
5×3	2446	4600	0	0	0	0	35252
5.5×3	2712	5100	0	0	0	0	40231
6×3	2978	5600	0	0	0	0	45477
6.5×3	3781	3050	1890	2×1525	3000	2×2420	63017
7×3	3928	3300	1964	2×1650	3000	2×2520	68164
7.5×3	4064	3550	2032	2×1775	3000	2×2620	73361
8×3	4191	3800	2095	2×1900	3000	2×2720	78607
8.5×3	4308	4050	2154	2×2025	3000	2×2820	83891
9×3	4574	4300	2287	2×2150	3000	2×2820	89622

Table 3.4: Reinforcement areas and total volume, varying opening size

Dimensions of opening [m]	0.5×0.5	0.75×0.75	1×1	1.25×1.25	1.5×1.5
H_1 [mm^2]	2057	1920	1800	1524	1200
L_{H1} [mm]	3600	3600	3600	3600	3600
H_2 [mm^2]	138	496	700	1471	3992
L_{H2} [mm]	1200	1200	1200	1430	750
H_3 [mm^2]	0	0	0	0	1828
L_{H3} [mm]	0	0	0	0	2×525
V [mm^2]	0	0	0	0	3000
V_V [mm]	0	0	0	0	2×520
Total Volume [10^{-6} m^3]	26371	25807	24920	24290	27953

3.2.1.1 Verification of TrussPilot

To verify the accuracy of the TrussPilot software, an analytical validation was performed using the $4\,\mathrm{m} \times 3\,\mathrm{m}$ beam model. Strut-and-tie forces, strut widths, and reinforcement areas were calculated analytically, as detailed in section A.3 in the Appendix, and compared to the results from TrussPilot. The comparison confirmed that the values matched, validating the software's reliability.

3.2.2 SPM

Analytical calculations were carried out using a Python script to automate designing the reinforcement of the deep beams according to SPM. The Python script SPM.py by Hoogenboom was used as a foundation for these calculations. The explanation of this script can be found in subsection 2.3.3, and more thoroughly in the book by Blaauwendraad (2018).

Hoogenboom's original SPM.py script is not fully automated, as all degrees of freedom (DOFs), lengths, and geometric parameters must be manually defined. This makes the script primarily a tool for checking forces and displacements, requiring the stringer-panel layout to be determined beforehand. To address this limitation, modifications were made to assist with layout design and automate the process. Some other minor changes to the structure of the script were also made, but no changes were made regarding the calculations. The modified script, used in this thesis and available in the Appendix in Appendix B, requires only basic input for geometry and material properties. The input parameters for the geometry of the beam, the material, and the boundary conditions are listed in Table 3.5, Table 3.6, and Table 3.7. These inputs match those used in the STM and FEA. The script automatically generates a stringer-panel grid and performs calculations of forces and displacements as in the original version of the script. Additionally, it includes new features to calculate required reinforcement areas and verify stringer capacities, which were not included in the original script.

Table 3.5: Geometry input parameters for the SPM calculations

Properties	**Value**
Length of beam	(Varies)
Height of beam	$3\,\mathrm{m}$
$c_{supports}$*	$0.2\,\mathrm{m}$
c_{edge}*	$0.08\,\mathrm{m}$
Beam thickness	$0.4\,\mathrm{m}$
Presence of opening	"yes"/"no"
Height of opening	(Varies)
Width of opening	(Varies)

* The distance from the edge of the concrete to the centre of the stringer, when the stringer is aligned with a support or is adjacent to any other edge.

Table 3.6: Material input parameters for the SPM calculations

Properties	**Value**
ν	0.2
E	$32.8\,\mathrm{GPa}$
f_{yk}	$500\,\mathrm{MPa}$

Table 3.7: Input parameters for forces and boundary conditions for the SPM calculations

Properties	**Value**
Number of external forces	1
Dimensioning applied force	$-3000\,\mathrm{kN}$
Applied force	(Varies)
x-coordinate of force*	$\frac{\text{Width of beam}}{2}$
Number of prescribed displacements	3
Prescribed displacements	[0, 0, 0]

The script does not consider non-linear material behaviour and is intended primarily as a convenient tool for automating the layout and analytical calculations for SPM. It supports design and checks for both SLS and ULS loads but is limited in terms of geometry, force placement, and support conditions to those of this thesis. These assumptions ensure consistency between models and allow for generating a mesh as coarse as possible with the minimum number of stringers, as outlined in subsubsection 2.3.2.1. The naming convention for stringers and panels is shown in Figure 3.4 for varying beam lengths and in Figure 3.5 for varying opening sizes.

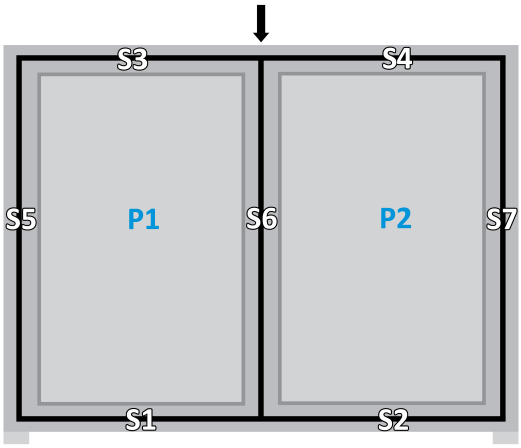

Figure 3.4: Numbering of stringers and panels for a beam without opening

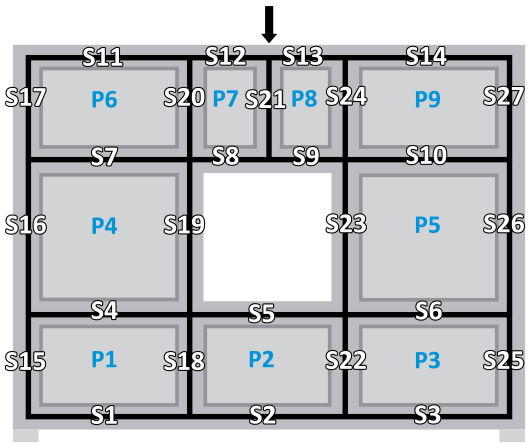

Figure 3.5: Numbering of stringers and panels for a beam with an opening

The reinforcement areas needed for the tension reinforcement in the stringers, as well as for the distributed shear reinforcement in the panels, for the beams with varying span-to-depth ratios are shown in Table 3.8. The reinforcement needed for the deep beams with openings of varying sizes is shown in Table 3.9.

Table 3.8: Reinforcement areas and total volume, varying beam length

Beam size [m]	S1 [mm^2]	S2 [mm^2]	P1 [mm^2/m]	P2 [mm^2/m]	Total Volume [10^{-6} m^3]
3×3	1373.24	1373.24	422.54	422.54	18534
3.5×3	1637.32	1637.32	422.54	422.54	22567
4×3	1901.41	1901.41	422.54	422.54	26864
4.5×3	2165.49	2165.49	422.54	422.54	31426
5×3	2429.58	2429.58	422.54	422.54	36251
5.5×3	2693.66	2693.66	422.54	422.54	41341
6×3	2957.75	2957.75	422.54	422.54	46695
6.5×3	3221.83	3221.83	422.54	422.54	52312
7×3	3485.92	3485.92	422.54	422.54	58194
7.5×3	3750.00	3750.00	422.54	422.54	64340
8×3	4014.08	4014.08	422.54	422.54	70750
8.5×3	4278.17	4278.17	422.54	422.54	77424
9×3	4542.25	4542.25	422.54	422.54	84363

Table 3.9: Reinforcement areas and total volume, varying opening size

Dimensions of opening [m]	0.5×0.5	0.75×0.75	1×1	1.25×1.25	1.5×1.5
S1 [mm^2]	1561	1408	1253	1100	949
S2 [mm^2]	1561	1408	1253	1100	949
S3 [mm^2]	1561	1408	1253	1100	949
S4 [mm^2]	232	315	391	463	531
S5 [mm^2]	232	315	391	463	531
S6 [mm^2]	232	315	391	463	531
S8 [mm^2]	514	842	1261	1810	2559
S9 [mm^2]	514	842	1261	1810	2559
S11 [mm^2]	0	0	0	0	181
S12 [mm^2]	0	0	0	0	181
S13 [mm^2]	0	0	0	0	181
S14 [mm^2]	0	0	0	0	181
S16 [mm^2]	0	0	0	0	110
S17 [mm^2]	0	0	0	0	110
S26 [mm^2]	0	0	0	0	110
S27 [mm^2]	0	0	0	0	110
P1 [mm^2/m]	425	419	411	402	400
P2 [mm^2/m]	400	400	400	400	400
P3 [mm^2/m]	425	419	411	402	400
P4 [mm^2/m]	488	512	539	571	610
P5 [mm^2/m]	488	512	539	571	610
P6 [mm^2/m]	400	400	400	400	400
P7 [mm^2/m]	1101	1244	1429	1678	2034
P8 [mm^2/m]	1101	1244	1429	1678	2034
P9 [mm^2/m]	400	400	400	400	400
Total Volume [10^{-6} m^3]	28551	29461	30592	32088	35373

For stringers S11–S27 in the beam with a $1.5\,\mathrm{m} \times 1.5\,\mathrm{m}$ m opening, the required reinforcement areas are smaller than the distributed reinforcement already present in this area in the beam. As a result, no additional reinforcement is needed in these stringers.

3.2.2.1 Verification of the Python script

The Python script written for and used in this thesis was verified through a comparison with the output for the displacements and forces of the original script written by Hoogenboom for the same stringer-panel layout. The results for the forces given by Hoogenboom's script were then compared to an analytical calculation for a simple statically determined deep beam.

3.3 Analytical calculations

For both STM and SPM, reinforcement stresses and crack widths were analytically calculated and compared to results from the non-linear FEA. Deflections of the SPM-designed beams were computed using the Python script and also compared with FEA results.

To compare the different methods in a relevant way, several load levels were selected, as shown in Table 3.10. The design load for all beams was $3000\,\mathrm{kN}$. Additional checks were made at 0.6 and 0.8 of the ULS load to represent service conditions. These values align with typical load factors in Eurocode, where characteristic service loads often range between 67–80% of ULS (Swedish Standards Institute, 2010). This approach allowed for consistent comparisons across ULS and serviceability states. These load steps were also used when analysing and comparing the results from FEA.

Table 3.10: The magnitudes of the point load applied on the beams, where P_d is the design load

Applied load	**[kN]**
P_d	3000
$0.8P_d$	2400
$0.6P_d$	1800

3.3.1 Stresses in reinforcement

Reinforcement stresses were calculated for beams designed using both STM and SPM. For STM, it was assumed that all tensile reinforcement reaches the yield stress of $500\,\mathrm{MPa}$ at the design load, and required reinforcement areas were determined accordingly, as previously described. Since STM is based on a linear elastic stress field, reinforcement stresses were assumed to scale linearly with the applied load. For example, at 80% of the design load, stresses were taken as 80% of those for the design load. This linear approach provides a reasonable estimate of reinforcement stresses at service load levels based on STM theory.

Reinforcement stresses in the SPM design were calculated similarly, with reinforcement areas based on stringer forces at the design load, assuming steel yielding. As stringer forces vary linearly, the maximum tensile force in each stringer governs the required area. The design load reduced by 80% or 60% were then used, and corresponding forces and stresses were recalculated through the same linear approach as for STM. This approach is valid for estimating service-state stresses, as the stringer-panel model's geometry remains unchanged regardless of load magnitude, aligning with the linear assumptions of the method.

3.3.2 Crack widths

The crack widths were calculated with the approach described in subsection 2.1.3, using the equation given in EC2 and approximating an "effective beam" using the tensile reinforcement at the bottom of the beam along with an effective concrete area surrounding it,

mimicking a regular Bernoulli beam. This was done for both the STM and SPM beams of all geometries.

What was deemed as a crack in this case was if the crack width was larger than 0.11875 mm. This value was equal to the ultimate crack strain according to Hordijk (DIANA FEA BV, 2024a), which defines a fully open crack. This lower limit of the crack size was used for the cracks obtained from both the analytical calculations and the FEA results.

3.3.3 Deflections

The deflections were calculated using the Python script for SPM, as outlined in subsection 2.3.3. These linear-elastic calculations considered stress distribution and stiffness but did not account for non-linear effects. Stiffness for both stringers and panels was required. For reinforcement design, each stringer's stiffness was assumed to be half the width of the adjacent panels, or the distance from the stringer to the beam edge (or opening), multiplied by the beam thickness and Young's Modulus. This assumption follows the examples in the SPM.py user manual by Hoogenboom (2017), ensuring consistency with recommended modelling practices. This approach accounts for the concrete stiffness in both directions for the whole beam.

These values of the stiffness were primarily used throughout all analytical calculations for SPM, which are presented throughout the Results chapter. This approach assumes constant stiffness in the concrete, regardless of load, meaning non-linear effects such as cracking were not considered, limiting the method to linear analysis. To approximate cracking behaviour more realistically, reduced stiffness values were applied in the script by multiplying the total stiffness of stringers and panels by factors of 0.2 and 0.1. This adjustment aimed to mimic stiffness degradation due to cracking. The impact on deflection from this modification is discussed in subsection 5.8.1.

Since the Python script calculations were only valid for linear analysis when stiffness was kept constant, the original script results were also compared to linear FEA results in addition to the non-linear FEA. This comparison was made for beams with lengths of $3\,\mathrm{m}$, $6\,\mathrm{m}$, and $9\,\mathrm{m}$, as well as for beams with openings with the edge measurements $0.5\,\mathrm{m}$, $1\,\mathrm{m}$, and $1.5\,\mathrm{m}$. The analysis was performed for the load steps P_d, $0.8P_d$, and $0.6P_d$, with results presented in section 4.4.

The displacement results from the Python script were provided for each DOF in the model. These deflections were then compared to those obtained from the FEA in DIANA. However, for the deep beams reinforced according to STM, displacements could not be calculated in a similarly straightforward way. Therefore, a comparison of analytically obtained deflections for the STM-designed beams was not conducted.

3.4 Finite element modelling

A FEA was made with the commercial finite element software DIANA. The following section explains how this analysis was carried out. The Python script for the DIANA analysis can be found in the Appendix in section C.1.

3.4.1 Material parameters

Material parameters were, when possible, chosen according to EC2, or the fib Model Code when EC2 was not applicable. The exact material parameters used in this analysis are presented in the following sections for the concrete, steel plates, and reinforcement.

3.4.1.1 Concrete beam

Concrete with predefined material properties according to EC2 was used in the DIANA model, as outlined in subsubsection 2.4.3.1. The values for E_{cm}, ν_c, α_e, ρ, f_{ctm}, and f_{cm} were retrieved for the concrete class C30/37. The aggregate was chosen as quartzite, and the cement as class N.

A total strain-based crack model with a smeared cracking approach was adopted to capture tensile cracking behaviour and compressive plasticity, as crack locations were unknown (DIANA FEA BV, 2024b). Tensile response followed Hordijk's model, while compressive behaviour followed EC2. The crack bandwidth was computed via Rots' element-based method, using the square root of the element area. Mode-I fracture energy, G_F, was derived from the fib Model Code, using Equation (3.4), with $f_{cm0} = 10\,\mathrm{MPa}$ and $G_{F0} = 0.0263\,\mathrm{Nmm/mm^2}$, interpolated for a maximum aggregate size of $10\,\mathrm{mm}$ ('CEB-FIP Model Code 90', 1993).

$$G_F = G_{F0}(f_{cm}/f_{cm0})^{0.7} \tag{3.4}$$

Since Poisson's ratio decreases due to cracking, a damage-based reduction model was used, where the ratio decreases when the damage due to cracking increases (DIANA FEA BV, 2024a). The strain at ultimate stress was adjusted from the EC2 strain of 0.0035 for a $300\,\mathrm{mm}$ cylinder to a strain more appropriate for the element size used to avoid compression failures due to localisation, according to Equation (3.5) (Swedish Standards Institute, 2010). The strain at maximum stress was set to 0.002 for all mesh sizes.

$$\varepsilon_{ult.new} = \frac{300\,\mathrm{mm}}{\text{Mesh element size [mm]}} 0.0035 \tag{3.5}$$

Reductions due to lateral cracking and large tensile strains perpendicular to the principal compressive direction were not considered, since it was not assumed to affect the results of this study. Neither was stress confinement, an increase of compressive strength with increasing stress from lateral confinement, for the same reason. A summary of the concrete material parameters used in the FEA is presented in Table 3.11

Table 3.11: Concrete material properties for DIANA

Compression	**Tension**
$f_{cm} = 38\,\mathrm{MPa}$	$f_{ctm} = 2.89\,\mathrm{MPa}$
ε_{ult} according to (3.5)	$G_F = 66.96\,\mathrm{Nm/m^2}$
$\varepsilon_{\sigma.max} = 0.002$	

3.4.1.2 Loading and support plates

The loading and support plates were modelled as steel with linear material properties, as presented in Table 3.1.

3.4.1.3 Reinforcement

The tensile and distributed reinforcement were assigned identical material properties but defined with different geometries. To realistically simulate cracking behaviour and obtain representative crack patterns and crack widths, the interaction between concrete and reinforcement was modelled using bond-slip relationships. Anchorage effects were excluded, as anchorage failure was not considered a relevant failure mode in this study. Young's modulus, Poisson's ratio, and density were defined following EC2, as shown in Table 3.12.

A non-linear material model with Von Mises plasticity was selected to capture steel yielding, strain hardening, and failure, as well as crack widths and deformations in the service state. While other plasticity models may suit cyclic or complex load cases, this approach was considered most appropriate for the current analysis. The hardening function was defined using a total strain–yield stress diagram shown in Figure 3.6.

The first point represents initial yielding at $f_y = 500\,\mathrm{MPa}$ and $\epsilon = 0.0025$, based on the linear elastic relation $\sigma = E\epsilon$. The second point marks the end of the yield plateau at the same stress, but with $\epsilon = 0.02$. Here, a slight increase in stress to $505\,\mathrm{MPa}$ was applied, due to software limitations prohibiting a perfectly horizontal curve. The third point is the ultimate strength, $f_u = 600\,\mathrm{MPa}$ at $\epsilon = 0.2$ (fib, 2010). The fourth and last point is at the same strain but with a significant drop in stress, indicating failure and a stop to the hardening. The hardening hypothesis was set as strain hardening, and the hardening type as isotropic hardening. No kinematic hardening has been considered.

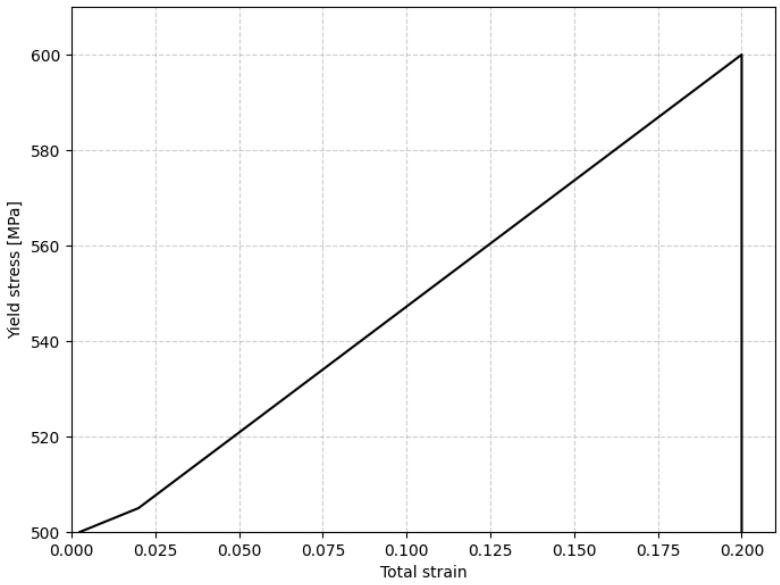

Figure 3.6: Total strain-yield stress diagram used in DIANA

The bond-slip interface parameters were defined based on the fib Model Code 2010. The normal and shear stiffness modules were set to $1 \times 10^{15}\,\mathrm{N/m^3}$ and $1 \times 10^{12}\,\mathrm{N/m^3}$. The bond-slip interface failure model was set as the CEB-FIB 2010 bond-slip function. To prevent numerical errors, the linearised initial slip section was defined as $s_0 = 0.1mm$, which must be greater than zero. Relative slip sections s_1 to s_3 are specified in Table 3.12 and defined for good bond conditions and pull-out failure (fib, 2010). The maximum shear stress was calculated as $\tau_{max} = 2.5 f_{ck}^{0.5}$ with $f_{ck} = 30\,\mathrm{MPa}$. For the same conditions, the ultimate shear stress and the exponent alpha were set as $\tau_f = 0.4\tau_{max}$ and $\alpha = 0.4$. The reinforcement material properties are presented in Table 3.12.

Table 3.12: Reinforcement material properties for DIANA

Properties	Value
E_s	$200\,\mathrm{GPa}$
ν_s	0.2
ρ	$7800\,\mathrm{kg/m^3}$
f_y	$500\,\mathrm{MPa}$
f_u	$600\,\mathrm{MPa}$
Normal stiffness modulus	$1 \times 10^{15}\,\mathrm{N/m^3}$
Shear stiffness modulus	$1 \times 10^{12}\,\mathrm{N/m^3}$
τ_{max}	$13.7\,\mathrm{MPa}$
τ_f	$5.48\,\mathrm{MPa}$
s_0	$0.1\,\mathrm{mm}$
s_1	$1.0\,\mathrm{mm}$
s_2	$2.0\,\mathrm{mm}$
s_3	$5.0\,\mathrm{mm}$
α_e	0.4

3.4.2 Geometry and element properties

The geometries of the concrete deep beams and the steel plates were defined as described in section 3.1. Both were modelled using regular plane stress elements. For the tensile and distributed reinforcement, the shape type was set to reinforcement lines and the element class to bar with the truss bond-slip reinforcement type. This allows reinforcement deformation to differ from the surrounding concrete, which is not possible with embedded bars (fib, 2010). Truss bond-slip was used instead of circular beam bond-slip, as only axial strains and stresses were of interest, excluding shear deformation, curvature, and torsion accounted for by circular beam bond-slip.

For the tensile reinforcement, the cross-section area was set as the entire reinforcement area needed for that specific tie or stringer, not every bar one by one. The number of bars was calculated for bars with a diameter of $20\,\mathrm{mm}$, even if it does not add up to an exact number of bars. For a proper bond-slip interaction, the contact perimeter was defined by multiplying the perimeter of a $20\,\mathrm{mm}$ bar with the exact number of bars, even if it is not an integer. Notably, the cross-sectional area and the circumference do not need to match in this case since they are used for different parts of the analysis.

The geometry of the distributed reinforcement was defined as the minimum reinforcement of $400\,\mathrm{mm^2/m}$ across both sides of the entire beam for all STM and SPM cases. For SPM panels requiring more than the minimum, the additional reinforcement was added locally. An iterative process was used to determine the number, size, and spacing of horizontal and vertical bars to match the required reinforcement without excess. Bar spacing was initially calculated assuming $\phi 12$ mm bars and checked against the maximum spacing limit of $s_{max} = 300\,\mathrm{mm}$. Based on this spacing and the width of the beam or panel, an integer number of bars was determined. A new exact spacing was then recalculated, from which the required bar area and perimeter were derived. These values were applied to both

sides of the reinforcement grid in horizontal and vertical directions. The full calculation process is detailed in the Python script for DIANA in the Appendix in section C.1. The reason for the iterative process and the use of exact values of areas, number of bars and distances was to not let rounding influence the results. It is not possible to optimise like this in reality, but it makes it possible to perform a fair comparison of STM and SPM.

3.4.3 Loads and boundary conditions

The load was applied as a prescribed displacement at the top middle node of the loading plate, rather than as a force, to better capture plastic behaviour and avoid convergence issues from large step increments. The displacement was applied in 100 steps, with the total magnitude adjusted to ensure beam failure occurred near the final step. The loaded node was connected by tyings to the bottom edge of the steel plate to distribute the load evenly to the concrete and prevent local crushing beneath the plate. Support boundary conditions were defined as simply supported, applied at the central nodes on the bottom of each support plate.

3.4.4 Modelling choices, assumptions, and analysis method

The maximum number of iterations per load step was set to 500, which was sufficient for convergence throughout the analysis. A standard Newton-Raphson solution method was used, with energy, displacement, and force as convergence norms. As previously mentioned, displacement control was used in the analyses, as it improves convergence reliability during large deformations, plastic behaviour, and near-failure conditions.

3.4.4.1 Mesh analysis

Just as for the linear DIANA analyses, a mesh with quadrilateral elements was generated for the non-linear analyses. To ensure convergence, a mesh sensitivity study was conducted using the $3\,\mathrm{m} \times 4\,\mathrm{m}$ beam with a $1\,\mathrm{m} \times 1\,\mathrm{m}$ opening. The selected output variable for assessing convergence was the stress in the bottom tensile reinforcement along the left edge of the opening. This output was considered less dependent on mesh size than, for example, crack width or crack location. Load–stress curves were generated for each tested mesh size to visualise convergence, as shown in Figure 3.7.

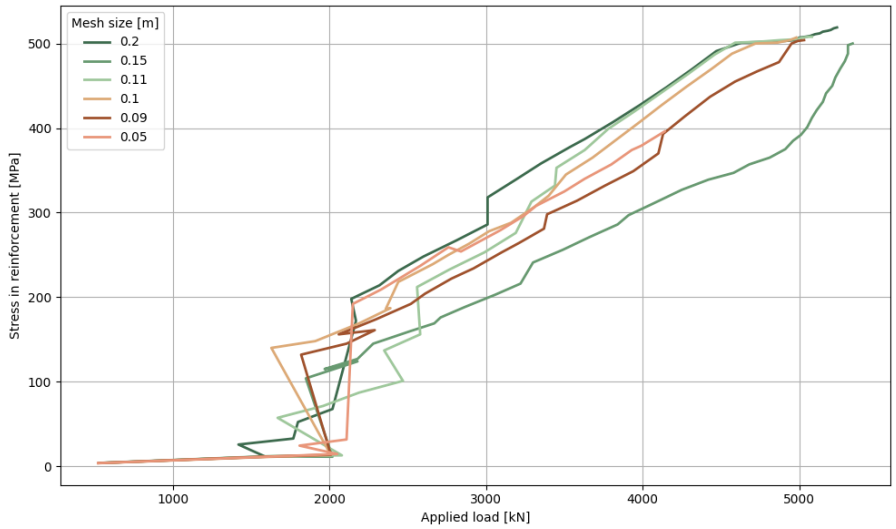

Figure 3.7: Load-stress curves for the different mesh element sizes evaluated in the mesh convergence analysis

The mesh analysis indicated that a mesh size of $0.1\,\mathrm{m}$ was sufficient to achieve convergence for these beams. However, for beams with a $1.5\,\mathrm{m} \times 1.5\,\mathrm{m}$ opening, this mesh size led to singularities beneath the loading plate. To avoid this, a coarser mesh of $0.15\,\mathrm{m}$ was adopted for both the SPM and STM models. Similarly, for beams with lengths ranging from $4.5\,\mathrm{m}$ to $6\,\mathrm{m}$, localised failure occurred directly beneath the loading plate. This was resolved by implementing a zone with a larger mesh of $(0.15\,\mathrm{m})$ beneath the loading plate and above the supports, reducing stress concentrations. For beams exceeding $6.5\,\mathrm{m}$, a uniform $0.15\,\mathrm{m}$ mesh ensured both convergence and numerical stability. In the largest beams, $7\,\mathrm{m}$ to $9\,\mathrm{m}$, a mesh size of $0.2\,\mathrm{m}$ was required under the loading plate to prevent recurring singularities.

3.4.5 Analysis output

The selected output parameters included Cauchy stresses in the reinforcement in the normal direction, vertical displacements, equivalent crack widths, and the reaction force corresponding to the applied displacement. Upon completion of the analysis, these results were extracted from DIANA, compiled, and evaluated, as presented in chapter 4 and discussed in chapter 5. The lower limit of the crack width, defined in subsection 3.3.2, was applied consistently in the FEA, as well as the analytical calculations.

3.4.6 Verification of DIANA model

To assess the accuracy of the DIANA model used in this thesis, its performance was compared with both experimentally tested beams and other published finite element models. The geometry of each reference beam is provided in the Appendix in section C.2. The same modelling assumptions and procedures applied in this thesis were used, with adjustments to material and geometric properties to match the experimental cases. The results

obtained from the DIANA analyses are summarised in Table 3.13, alongside the corresponding experimental and FEA data from the literature, as detailed in section C.2 in the Appendix.

Table 3.13: Results from the verification of the DIANA model

	$\mathbf{P}_{crack}$ [kN]	$\mathbf{P}_{failure}$ [kN]	**d** [mm]	$\mathbf{w}_k$ [mm]
DIANA model 1	117	620	0.27	0.44
Beam 1	225	1030	6.85	1.41
Comparison 1	52%	62%	3.9%	31.2%
DIANA model 2	97.7	360	0.42	-
Beam 2	60	380	8.87	-
Comparison 2	163%	95%	4.7%	-
DIANA model 3	104	260	0.29	0.71
Beam 3	170	256	3.29	1.78
Comparison 3	61%	102%	8.8%	40%
DIANA model 4	-	580	0.15	-
Beam 4	-	300	8.7	-
Comparison 4	-	194%	1.7%	-
DIANA model 5	-	-	0.58	-
Beam 5	-	-	0.67	-
Comparison 5	-	-	87%	-
DIANA model 6	-	548	0.94	-
Beam 6	-	600	4.0	-
Comparison 6	-	91%	24%	-
DIANA model 7	-	900	5.9	-
Beam 7	-	2750	7.1	-
Comparison 7	-	33%	83%	-

In cases where crack parameters were compared, the DIANA model generally underestimated both the cracking loads and crack widths relative to experimental results. This suggests that real beams exhibited larger cracks, but that the model provided a somewhat good estimation of crack load, even if slightly on the low side. The failure loads, however, were often comparable to the experimental values. Notably, the differences in deflection were significant, with the DIANA model typically under-predicting the response, which is discussed and explained further in subsection 5.2.1.

4

Results

In this chapter, the results obtained from the analytical calculations made with the Strut-and-Tie Method (STM) and Stringer-Panel Method (SPM) are presented, followed by the results obtained from the non-linear finite element analyses (FEA). The analytical results and the FEA results are then compared.

The results for the beams with varying span-to-depth ratios and varying opening sizes are presented separately. In the plots showing varying opening size, the result for the beam without an opening with the same outer dimensions as the beams with openings, $3\,\mathrm{m} \times 4\,\mathrm{m}$ m, is shown when relevant.

4.1 Results from analytical calculations

The following presents and compares the results obtained from the analytical calculations using STM and SPM, respectively.

4.1.1 Total reinforcement volume

The total reinforcement volumes for the different beams are shown in Table 4.1 for the beams with varying span length without an opening, and in Table 4.2 for the beams with an opening of varying size. The tables also show the volume of the main tensile reinforcement compared to the volume of the distributed reinforcement. The reinforcement area for each tie or stringer is described in greater detail in section 3.2.

Table 4.1: Total reinforcement volume, comparison for beams with varying span-to-depth ratios

Beam dimensions [m]	Reinforcement volume $[10^{-6}\,\mathrm{m}^3]$					
	Main rein.		**Distr. rein.**		**Tot. reinf. vol.**	
	STM	SPM	STM	SPM	STM	SPM
3×3	4189	3570	14400	14963	18589	18534
3×3.5	5298	5076	16800	17491	22098	22567
3×4	7016	6845	19200	20019	26216	26864
3×4.5	8938	8879	21600	22547	30538	31426
3×5	11252	11176	24000	25075	35252	36251
3×5.5	13831	13738	26400	27603	40231	41341
3×6	16677	16563	28800	30131	45477	46695
3×6.5	31817	19653	31200	32659	63017	52312
3×7	34564	23007	33600	35187	68164	58194
3×7.5	37361	26625	36000	37715	73361	64340
3×8	40207	30507	38400	40243	78607	70750
3×8.5	43091	34653	40800	42771	83891	77424
3×9	46422	39063	43200	45299	89622	84363

Table 4.2: Total reinforcement volume, comparison for beams with varying opening sizes

Opening dimensions [m]	Reinforcement volume $[10^{-6}\,\mathrm{m}^3]$					
	Main rein.		**Distr. rein.**		**Tot. reinf. vol.**	
	STM	SPM	STM	SPM	STM	SPM
0.5×0.5	7571	6795	18800	21756	26371	28551
0.75×0.75	7507	6966	18300	22494	25807	29461
1×1	7320	7381	17600	23211	24920	30592
1.25×1.25	7590	8176	16700	23912	24290	32088
1.5×1.5	12353	10724	15600	24649	27953	35373

The reinforcement volumes for the different beam geometries varied depending on the method, STM or SPM, that was used to design the reinforcement layout. How the total reinforcement volume changed due to varying span lengths and design method is shown in Figure 4.1. It was observed that the reinforcement volumes of the STM beams were slightly smaller than those of SPM, up until the point where the span-to-depth ratio forced the STM layout to change. At this point and onwards, the SPM reinforcement used smaller reinforcement volumes. The two graphs did, however, come closer together as the span length continued to increase.

How the opening size affected the total reinforcement volume for the different methods is shown in Figure 4.2. This plot shows that the beams designed with SPM used a larger amount of reinforcement than the ones with STM. The difference was smaller in the cases of smaller openings, but it increased as the opening got larger. For the largest opening, the reinforcement volume of STM increased significantly, which made the slope resemble the SPM curve more.

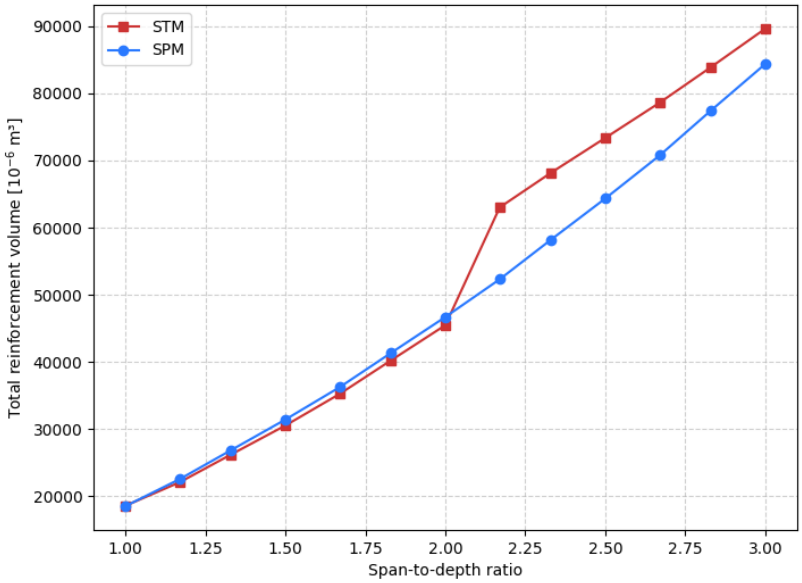

Figure 4.1: Total reinforcement volume for beams with varying span-to-depth ratios, designed with STM and SPM

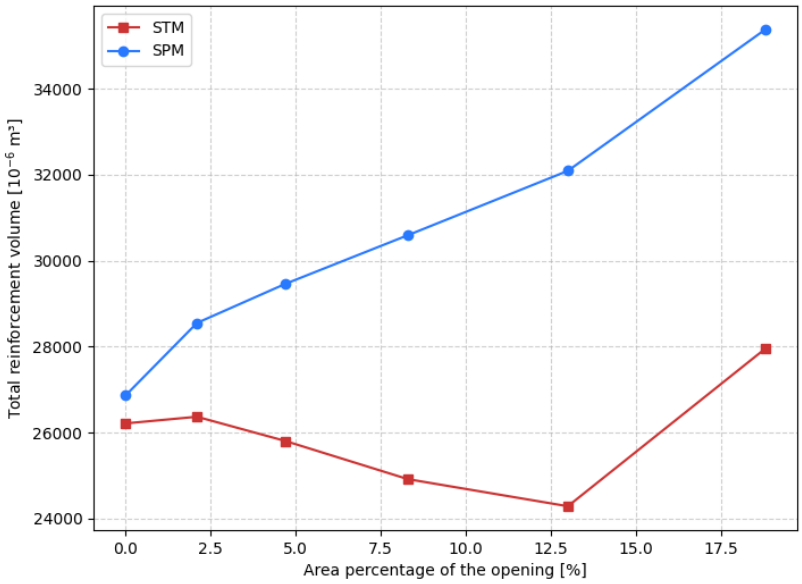

Figure 4.2: Total reinforcement volume for beams with varying opening sizes, designed with STM and SPM

4.1.2 Stresses in reinforcement

The stresses in the main reinforcement were, according to the calculations, assumed to be $500\,\mathrm{MPa}$, which is equal to the yield strength of the steel when the design load was applied. This means that for this load, all tension ties in the strut-and-tie model would experience $500\,\mathrm{MPa}$ (σ_{max}) throughout their entire length, since the normal forces in the ties are constant. However, for the stringer-panel models, this only means that the largest stress in each stringer was $500\,\mathrm{MPa}$. The linear distributions of the stresses along the reinforced stringers are illustrated in Figure 4.3 for the cases without an opening, and in Figure 4.4 for the cases with an opening. These figures only illustrate one example of the geometry. When the span length or opening size was varied, the different lengths of the stringers and segments changed, but the distribution stayed the same.

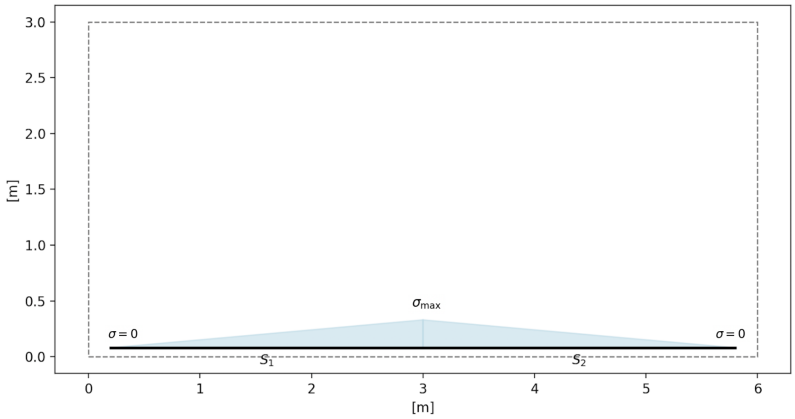

Figure 4.3: The stresses varying linearly in the bottom stringer for a beam without an opening

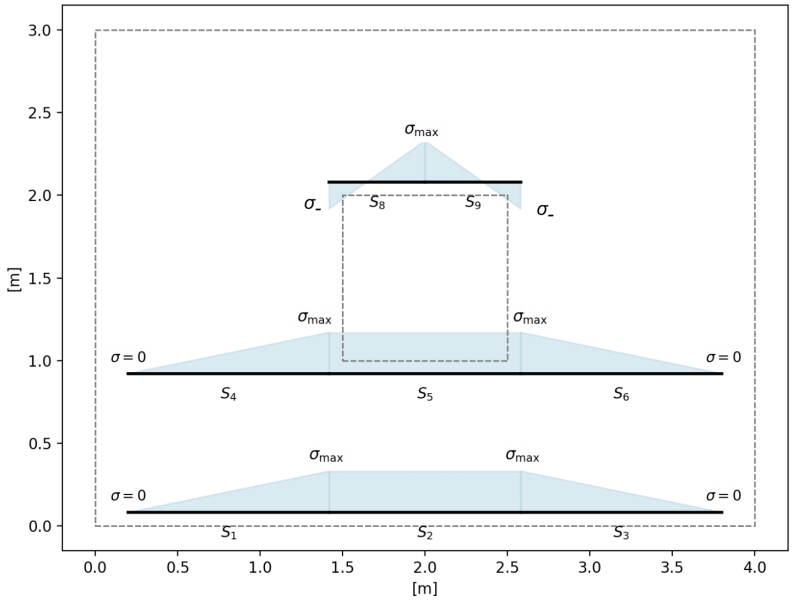

Figure 4.4: The stresses varying linearly in the stringers for a beam with an opening

For the cases with openings in the beams, some parts of the stringer above the opening experienced compressive stresses, but since other segments of the same stringer experienced tensile stress, tensile reinforcement was placed at the stringer. The maximum stresses (σ_{max}) for the three different load magnitudes analysed, as well as the occasional compressive stresses (σ_{-}), are presented in Table 4.3.

Table 4.3: Maximum and negative stresses in the reinforcement of the beams, at different load steps

			$0.6P_d$	$0.8P_d$	P_d
$\sigma_{\max}$ [MPa]			300	400	500
σ_{-} [MPa]	Dimensions [m]	0.5×0.5	-230	-307	-383
		0.75×0.75	-204	-272	-340
		1×1	-193	-257	-321
		1.25×1.25	-190	-254	-317
		1.5×1.5	-195	-260	-325

4.1.3 Crack widths

The characteristic crack widths were calculated according to the simplified method described in subsection 2.1.3. The stresses in the tensile reinforcement along the bottom of the beam were taken from Table 4.3 for each beam geometry. The reinforcement areas for the tensile reinforcement are shown in section 3.2. The calculation was done for each beam under three different magnitudes of the applied point load. The characteristic crack widths for the beams designed with both STM and SPM for varying span lengths are shown in Figure 4.5 and for varying opening sizes in Figure 4.6. The exact values of the characteristic crack widths which are used in the diagrams can also be found in the Appendix in section D.1. As can be seen, the crack widths decreased with increasing span-to-depth ratio, while they increased with increasing opening size. When the length of the beam increased, the crack widths were similar for STM and SPM. For increasing opening size, SPM tended to generate larger crack widths than STM for all load cases.

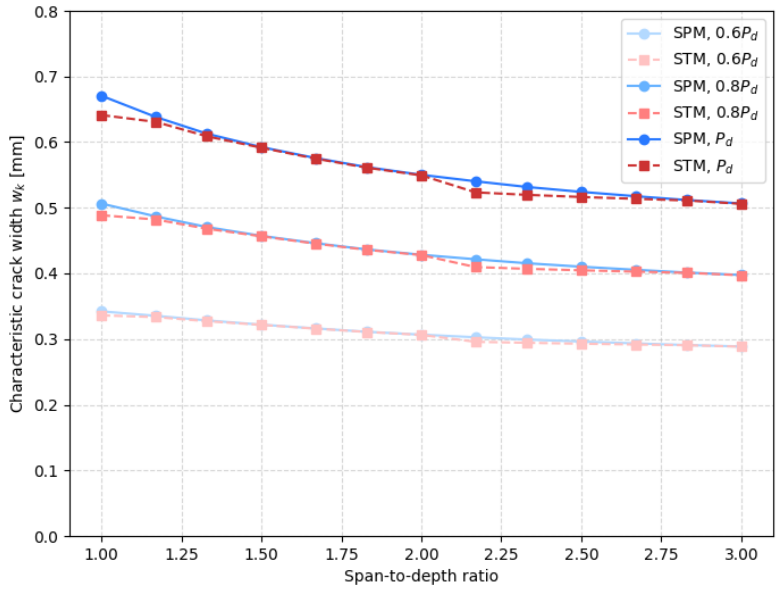

Figure 4.5: Characteristic crack widths for beams with varying span-to-depth ratios, designed with STM and SPM, under different load magnitudes

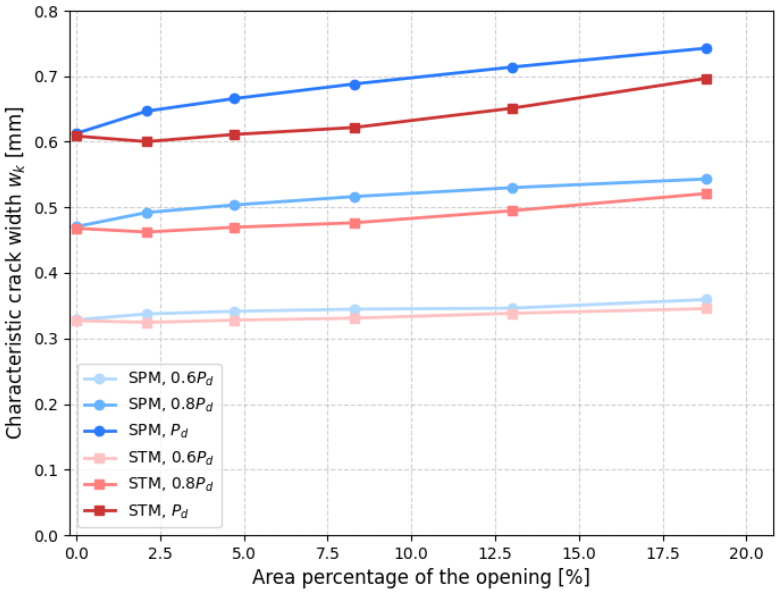

Figure 4.6: Characteristic crack widths for beams with varying opening sizes, designed with STM and SPM, under different load magnitudes

4.1.4 Deflections

The deformations were calculated analytically for the stringer-panel models for each degree of freedom (DOF). In this analysis, the mid-span deflection of every beam was investigated, as well as the deflection above the opening, at the mid-point of the upper edge of the opening, for the beams with openings. How the deflection was affected by varying the span length is shown in Figure 4.7, and how the opening size affected the deflection both at mid-span and above the opening is shown in Figure 4.8 and Figure 4.9 respectively. The results of the deflections used as input for the diagrams can also be found in the Appendix in section D.2. For the cases of the beams with openings, the value for the midspan deflection was taken as the DOFs that were the closest to the mid-point of the span, since in these cases, no DOF is placed exactly at the mid-point due to the layout of the stringer-panel model.

As observed in Figure 4.7, the deflection increased with increasing span-to-depth ratio. The same was true for the deflection above the opening that increased with increasing opening size as found in Figure 4.9. The mid-span deflection under the opening did, on the other hand, decrease with increasing opening size as shown in Figure 4.8.

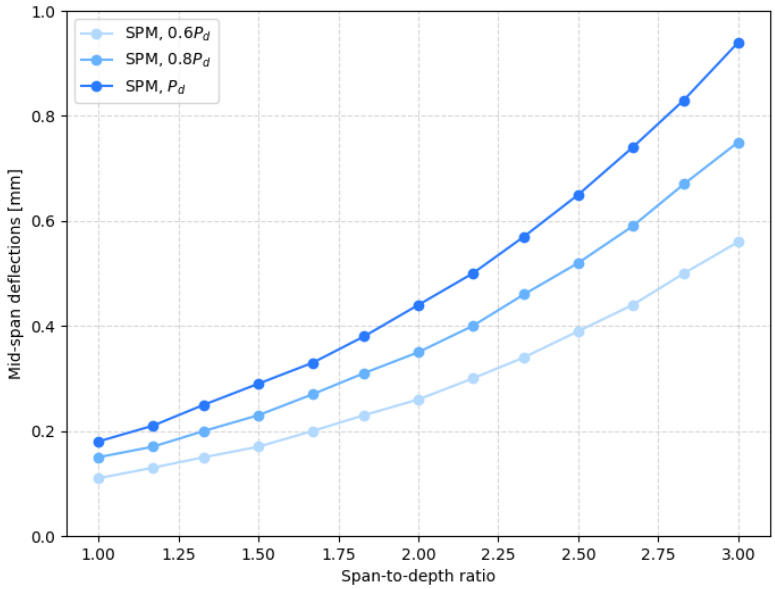

Figure 4.7: Midspan deflection for beams with varying span-to-depth ratios, designed with SPM, under different load magnitudes

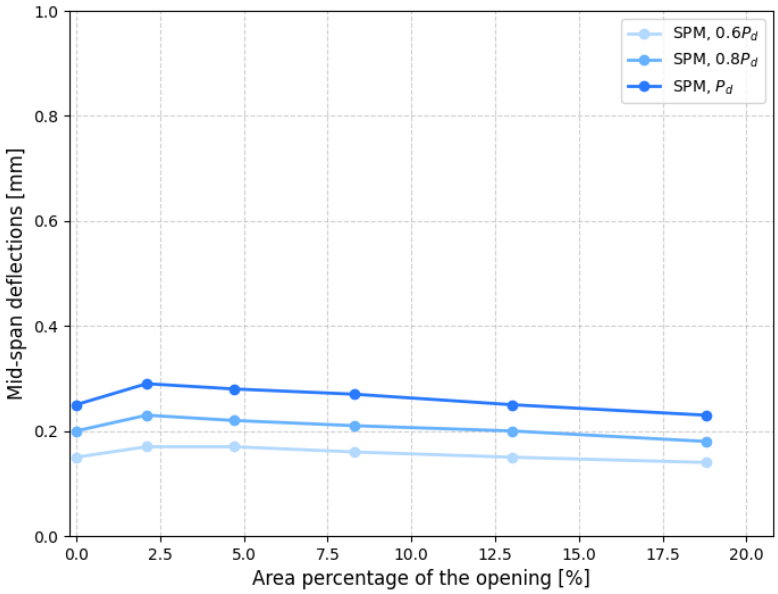

Figure 4.8: Midspan deflection for beams with varying opening sizes, designed with SPM, under different load magnitudes

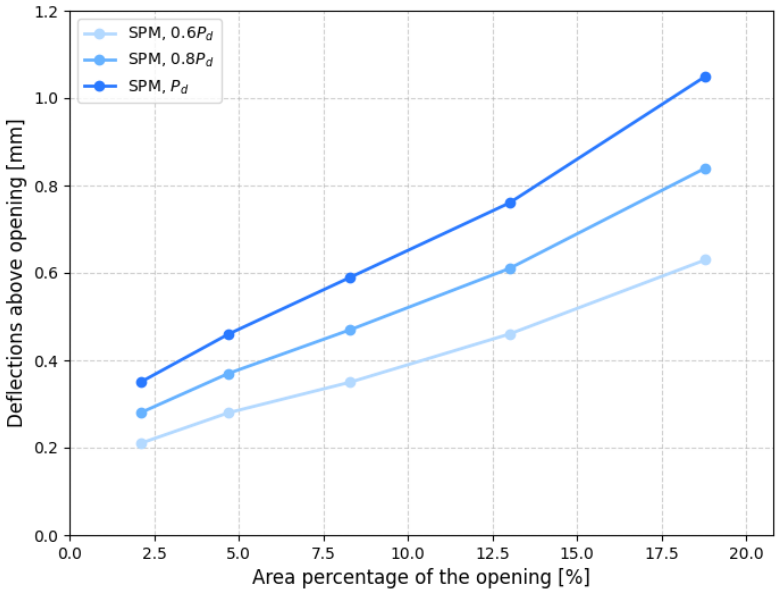

Figure 4.9: Mid deflection above the opening for beams with varying opening sizes, designed with SPM, under different load magnitudes

4.2 Results from non-linear FEA

In this section, the results of the different outputs from the non-linear FEA are presented. This includes results for beams designed with both SPM and STM, as well as all the different geometries described in section 3.1.

4.2.1 Failure load

The failure load was captured for each beam model. How the failure load was affected by the varying geometries of the beams designed with STM and SPM, respectively, is illustrated in Figure 4.10 and 4.11. The values for the different failure loads for the beams of varying sizes without openings and the results for the beams with varying opening sizes can also be found in the Appendix in section E.1.

It can be seen in Figure 4.10 that the failure loads for the beams designed with STM and SPM were similar for span-to-depth ratios below 2, and quite similar afterwards. The failure load for the more slender beams was higher for SPM than for STM. The slope of the curves changed for both STM and SPM at the span-to-depth ratio of 2, which indicates a change in structural behaviour or failure mode. The difference between STM and SPM was, as shown in Figure 4.11, larger for beams with openings where the STM beams tended to reach a higher failure load. However, for the beam with the highest area percentage of the opening, SPM had a higher failure load. For all beams, the failure load was higher than the design load of $3000\,\mathrm{kN}$.

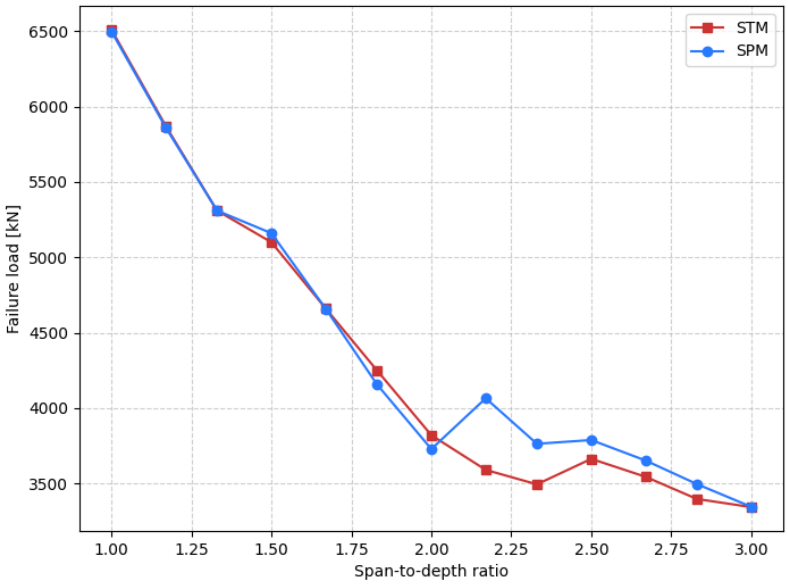

Figure 4.10: Failure load for beams with varying span-to-depth ratios, designed with STM and SPM

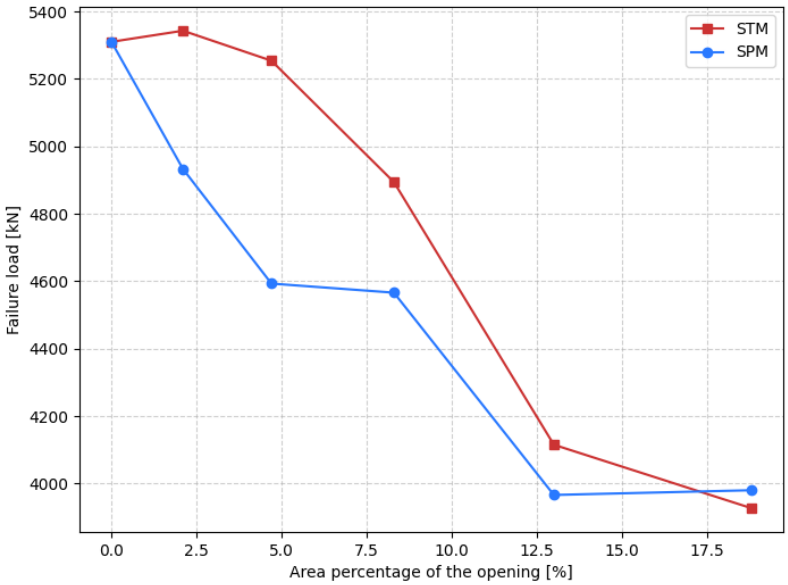

Figure 4.11: Failure load for beams with varying opening sizes, designed with STM and SPM

4.2.2 Stresses in reinforcement

The stresses in the bottom tensile reinforcement at the midpoints of the spans are presented in Figure 4.12, 4.13, 4.14, and 4.15, as a function of the magnitude of the applied load. At this point, the maximum stress for the tensile reinforcement was found. The different plots are divided between STM and SPM, and between beams with and without openings. These load-stress curves illustrate the stress at the given point in the reinforcement in the normal direction, up to the ultimate applied load. As can be seen for both STM and SPM, the yield stress was only reached for beams with a shorter span length, which were also the beams with the highest failure load. Beams longer than $4.5\,\mathrm{m}$ failed before the tensile reinforcement yielded. This indicates a change in structural behaviour and possibly failure mode, since the tension reinforcement is not fully utilised at failure for the longer spans. For the beams with openings, reinforcement of the two beams with the largest openings did not yield at the mid-point of the tensile reinforcement along the bottom. These beams were also failing at a smaller load.

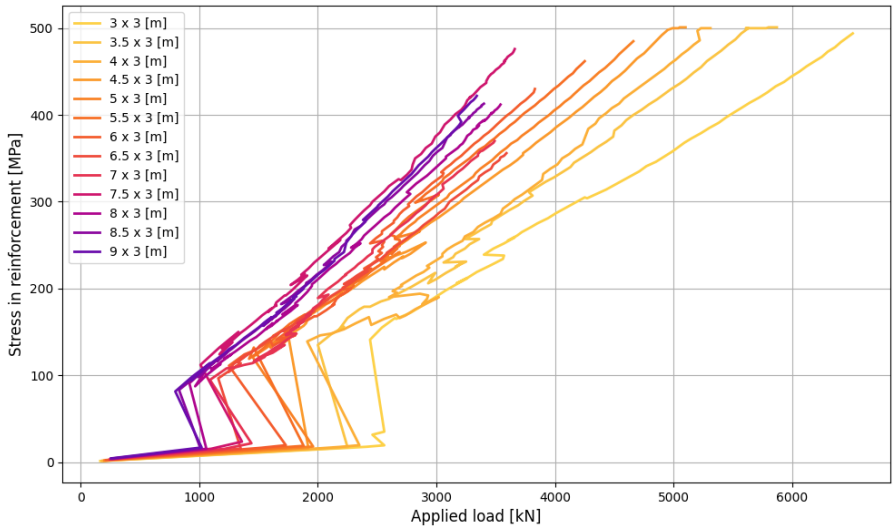

Figure 4.12: Load-stress curve for the midpoint of the tensile reinforcement for beams with varying span-to-depth ratios, designed with STM

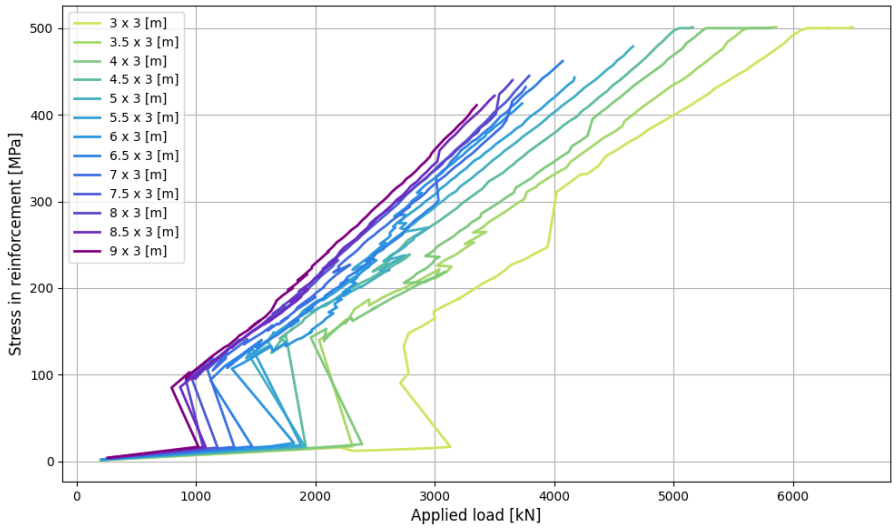

Figure 4.13: Load-stress curve for the midpoint of the tensile reinforcement for beams with varying span-to-depth ratios, designed with SPM

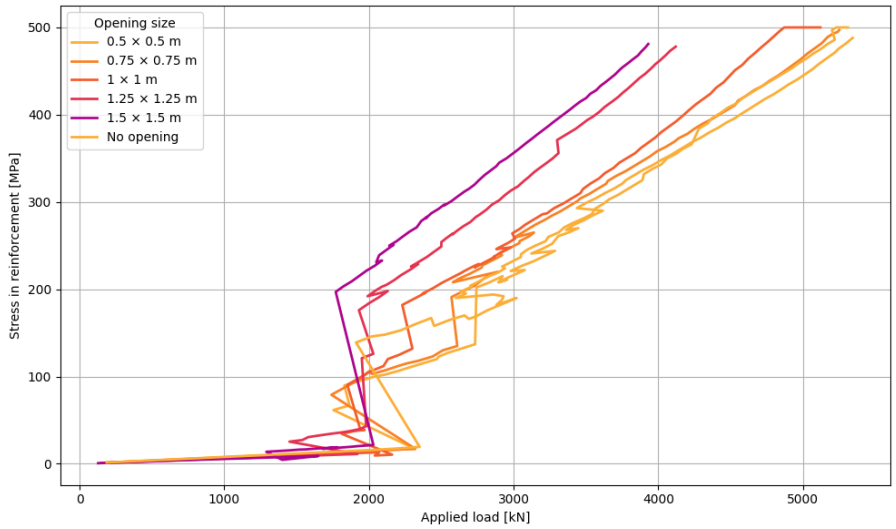

Figure 4.14: Load-stress curve for the midpoint of the tensile reinforcement for beams with varying opening sizes, designed with STM

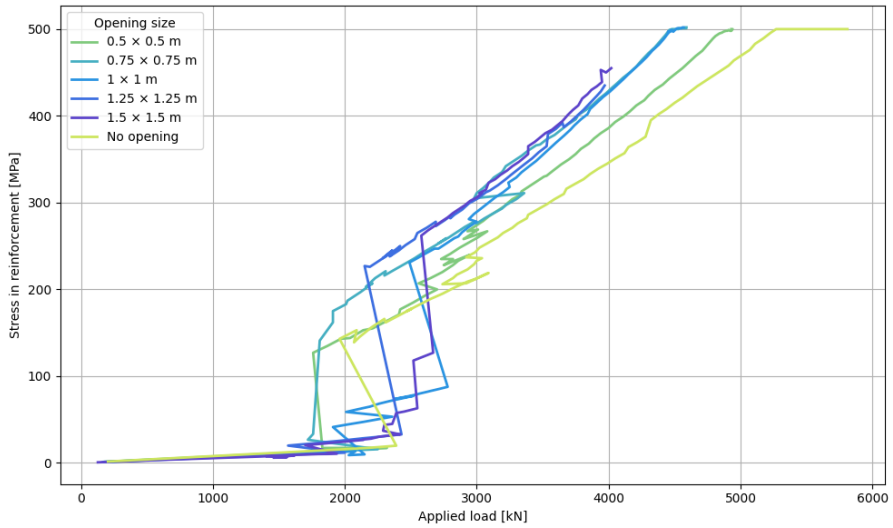

Figure 4.15: Load-stress curve for the midpoint of the tensile reinforcement for beams with varying opening sizes, designed with SPM

4.2.3 Crack pattern

The crack patterns for some beams with varying span lengths designed with STM are shown in Figure 4.16 and for some beams designed with SPM in Figure 4.17. The beams displayed are the smallest beam ($3\,\mathrm{m} \times 3\,\mathrm{m}$), the largest beam ($3\,\mathrm{m} \times 9\,\mathrm{m}$) and the mid-range beam ($3\,\mathrm{m} \times 6\,\mathrm{m}$). The crack pattern was illustrated for the loads $2400\,\mathrm{kN}$, $3000\,\mathrm{kN}$, and $3500\,\mathrm{kN}$, from left to right on each row of the figures. However, for both STM and SPM, the ultimate load for the largest span widths did not reach $3500\,\mathrm{kN}$, which is why the crack patterns at their ultimate loads are presented instead. As described in

subsection 3.3.2, no cracks below $w_k = 0.11875$ mm were visualised, and cracks of $1\,\mathrm{mm}$ were the upper limit of the colour bar in the figures. It can be observed that the crack patterns were similar between the beams designed with STM and SPM, especially for the beam of $3\,\mathrm{m} \times 6\,\mathrm{m}$. For the $3\,\mathrm{m} \times 3\,\mathrm{m}$ m beam, SPM gave larger crack widths for all load steps, while for the $3\,\mathrm{m} \times 9\,\mathrm{m}$ m beam, STM gave larger crack widths. The colour scale is shown at the bottom of each figure and is valid for all beams and stages within the figure.

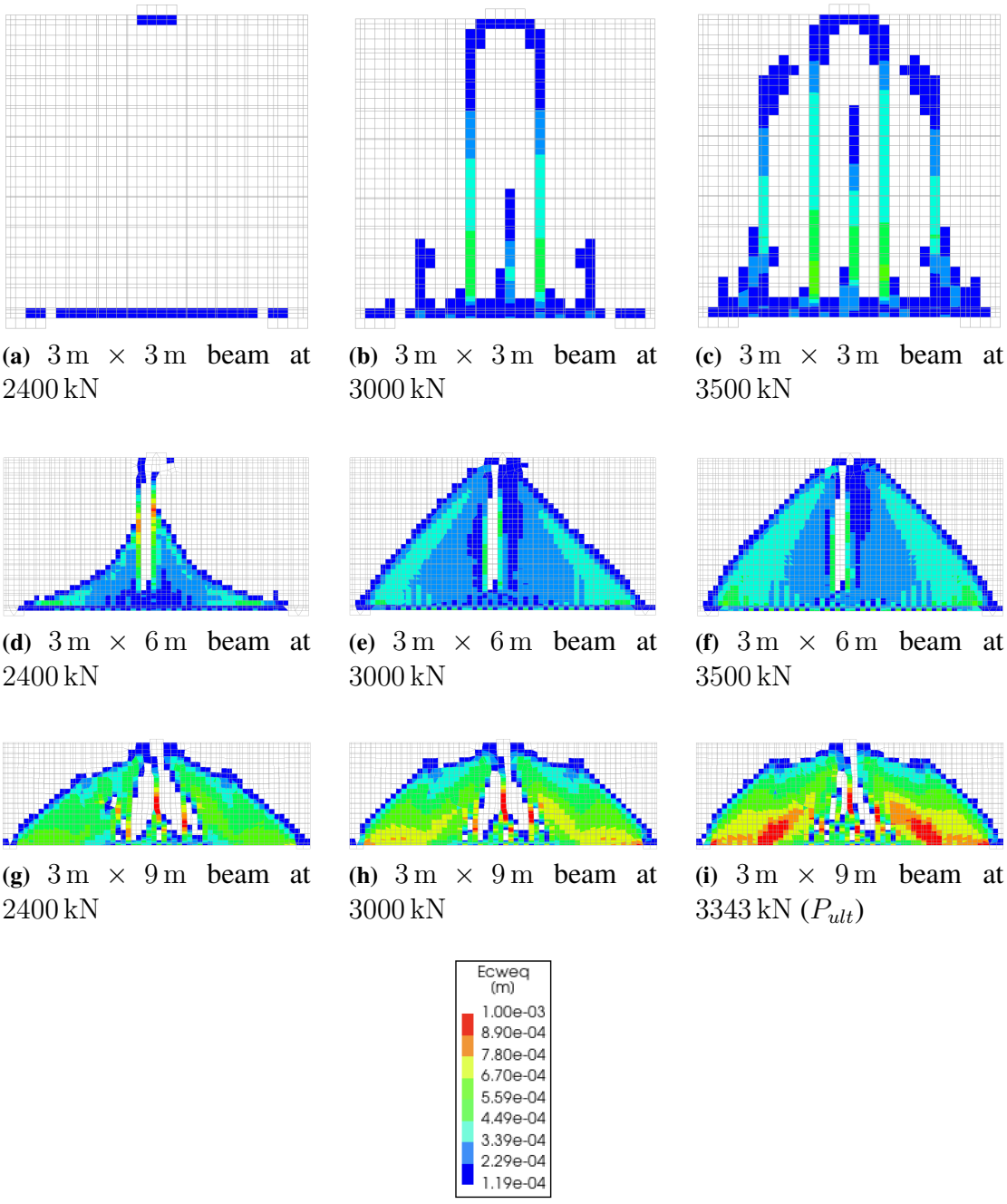

(a) $3\,\mathrm{m} \times 3\,\mathrm{m}$ beam at $2400\,\mathrm{kN}$ **(b)** $3\,\mathrm{m} \times 3\,\mathrm{m}$ beam at $3000\,\mathrm{kN}$ **(c)** $3\,\mathrm{m} \times 3\,\mathrm{m}$ beam at $3500\,\mathrm{kN}$

(d) $3\,\mathrm{m} \times 6\,\mathrm{m}$ beam at $2400\,\mathrm{kN}$ **(e)** $3\,\mathrm{m} \times 6\,\mathrm{m}$ beam at $3000\,\mathrm{kN}$ **(f)** $3\,\mathrm{m} \times 6\,\mathrm{m}$ beam at $3500\,\mathrm{kN}$

(g) $3\,\mathrm{m} \times 9\,\mathrm{m}$ beam at $2400\,\mathrm{kN}$ **(h)** $3\,\mathrm{m} \times 9\,\mathrm{m}$ beam at $3000\,\mathrm{kN}$ **(i)** $3\,\mathrm{m} \times 9\,\mathrm{m}$ beam at $3343\,\mathrm{kN}$ (P_{ult})

Figure 4.16: Crack pattern propagation for three beams with varying span-to-depth ratios, designed with STM, at increasing levels of applied load

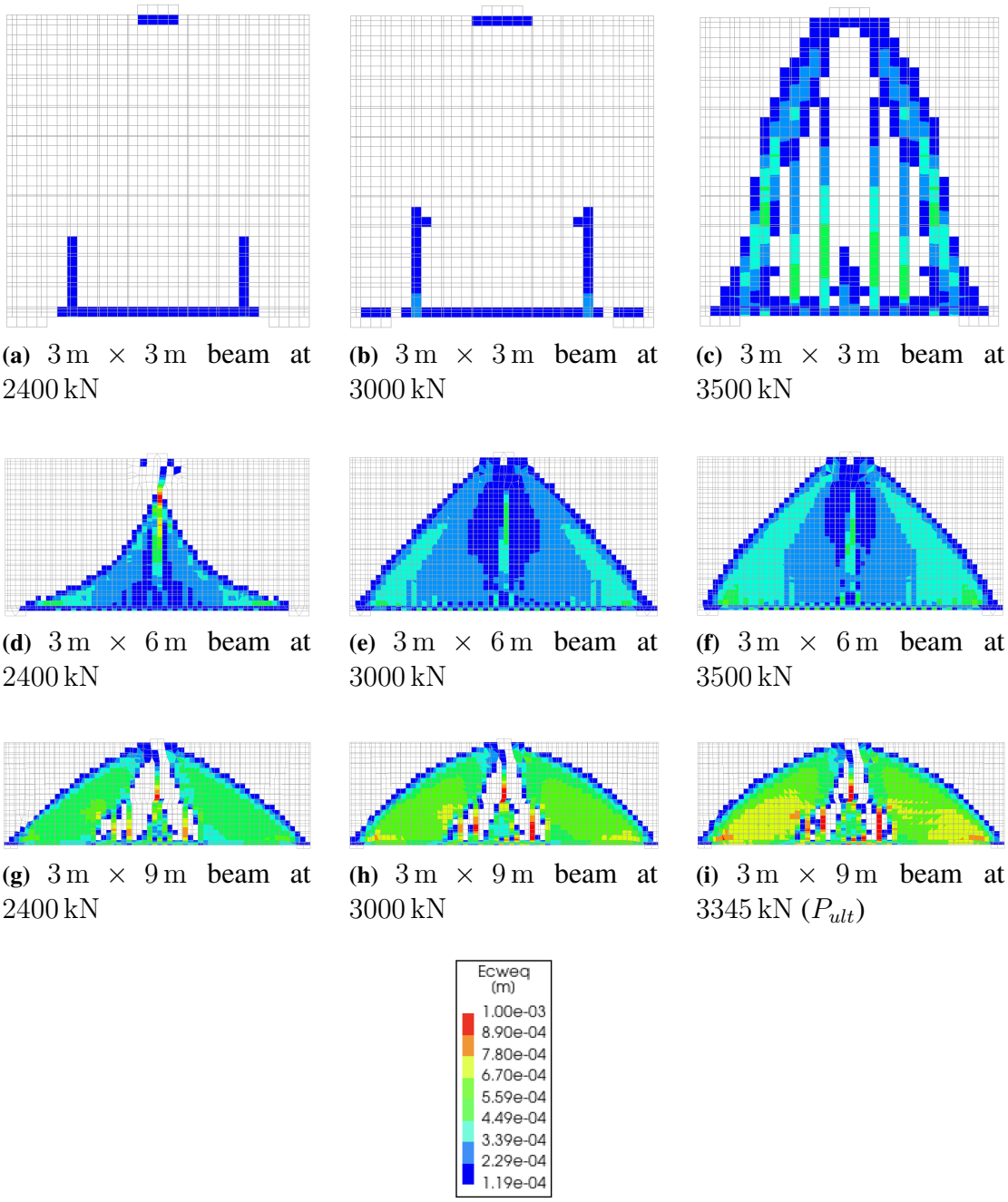

(a) 3 m × 3 m beam at 2400 kN

(b) 3 m × 3 m beam at 3000 kN

(c) 3 m × 3 m beam at 3500 kN

(d) 3 m × 6 m beam at 2400 kN

(e) 3 m × 6 m beam at 3000 kN

(f) 3 m × 6 m beam at 3500 kN

(g) 3 m × 9 m beam at 2400 kN

(h) 3 m × 9 m beam at 3000 kN

(i) 3 m × 9 m beam at 3345 kN (P_{ult})

Figure 4.17: Crack pattern propagation for three beams with varying span-to-depth ratios, designed with SPM, at increasing levels of applied load

The crack patterns for the beams with openings are shown in Figure 4.18 and 4.19, where the beams with the largest, smallest, and mid-range size of the opening are shown for both STM and SPM. As for the beams with varying span length, not all beams with openings needed to be shown, since they behaved similarly in-between the shown figures. The same ranges were used for the crack pattern plots as for the varying span lengths for the same reasons as mentioned above. For the beams with openings, it was harder to distinguish which design, STM or SPM, resulted in more cracks. For the beam with the

largest opening, STM showed some tendencies of more cracks below the opening than SPM did.

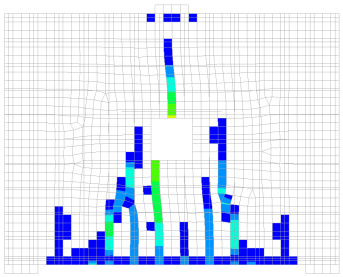

(a) 0.5 m × 0.5 m opening at 2400 kN

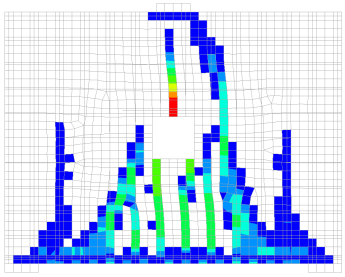

(b) 0.5 m × 0.5 m opening at 3000 kN

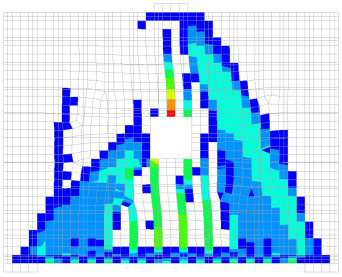

(c) 0.5 m × 0.5 m opening at 3500 kN

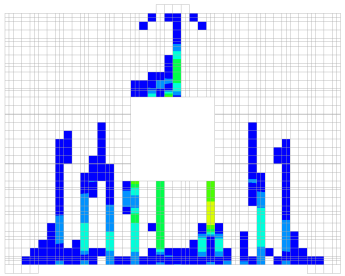

(d) 1 m × 1 m opening at 2400 kN

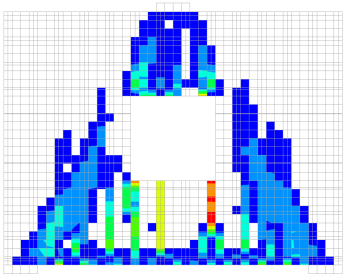

(e) 1 m × 1 m opening at 3000 kN

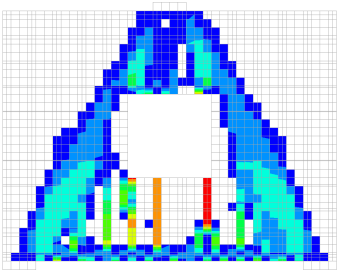

(f) 1 m × 1 m opening at 3500 kN

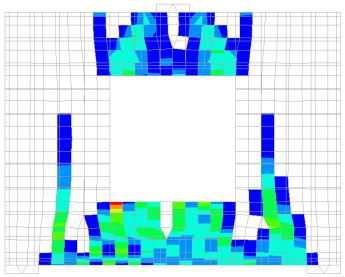

(g) 1.5 m × 1.5 m opening at 2400 kN

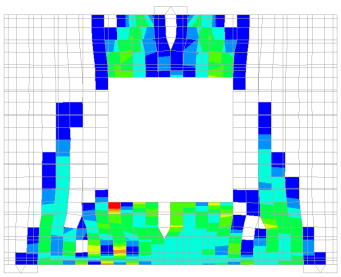

(h) 1.5 m × 1.5 m opening at 3000 kN

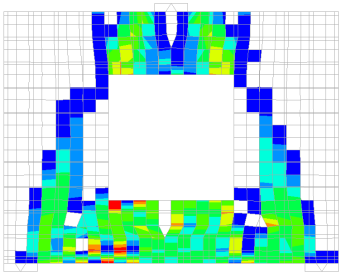

(i) 1.5 m × 1.5 m opening at 3500 kN

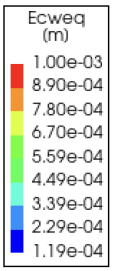

Figure 4.18: Crack pattern propagation for three beams with varying opening sizes, designed with STM, at increasing levels of applied load

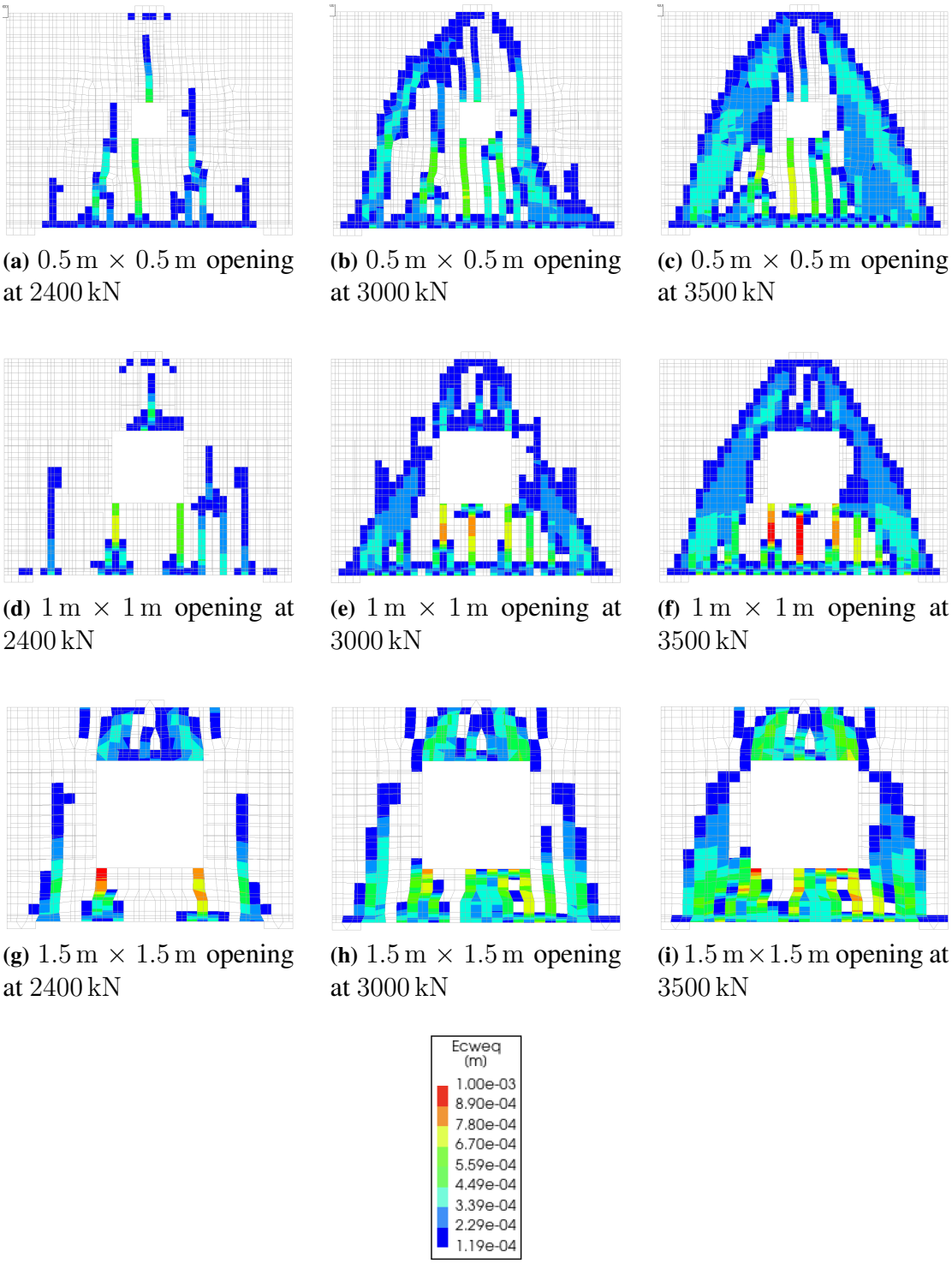

(a) 0.5 m × 0.5 m opening at 2400 kN

(b) 0.5 m × 0.5 m opening at 3000 kN

(c) 0.5 m × 0.5 m opening at 3500 kN

(d) 1 m × 1 m opening at 2400 kN

(e) 1 m × 1 m opening at 3000 kN

(f) 1 m × 1 m opening at 3500 kN

(g) 1.5 m × 1.5 m opening at 2400 kN

(h) 1.5 m × 1.5 m opening at 3000 kN

(i) 1.5 m × 1.5 m opening at 3500 kN

Figure 4.19: Crack pattern propagation for three beams with varying opening sizes, designed with SPM, at increasing levels of applied load

The crack pattern at the ultimate load for the beams of varying lengths is shown in Figure 4.20 for the beams designed with STM and Figure 4.21 for the beams designed with SPM. The crack pattern is shown for all beams with an integer span length, and the same

colour gradient was used as in previous crack plots. As can be seen, the SPM beam of the size $3\,\mathrm{m} \times 3\,\mathrm{m}$ obtained larger crack widths than STM for the ultimate load, even if the crack patterns were similar. However, the beams with lengths from $4\,\mathrm{m}$ to $7\,\mathrm{m}$ had very similar sizes and patterns of the cracks for both STM and SPM, while the beams with lengths $8\,\mathrm{m}$ and $9\,\mathrm{m}$ seemed to result in more cracks for the STM beams. Another observation is that the beams with shorter span lengths generally had flexure cracks as the most prominent cracks at failure, while the longest spans had more prominent diagonal shear cracks.

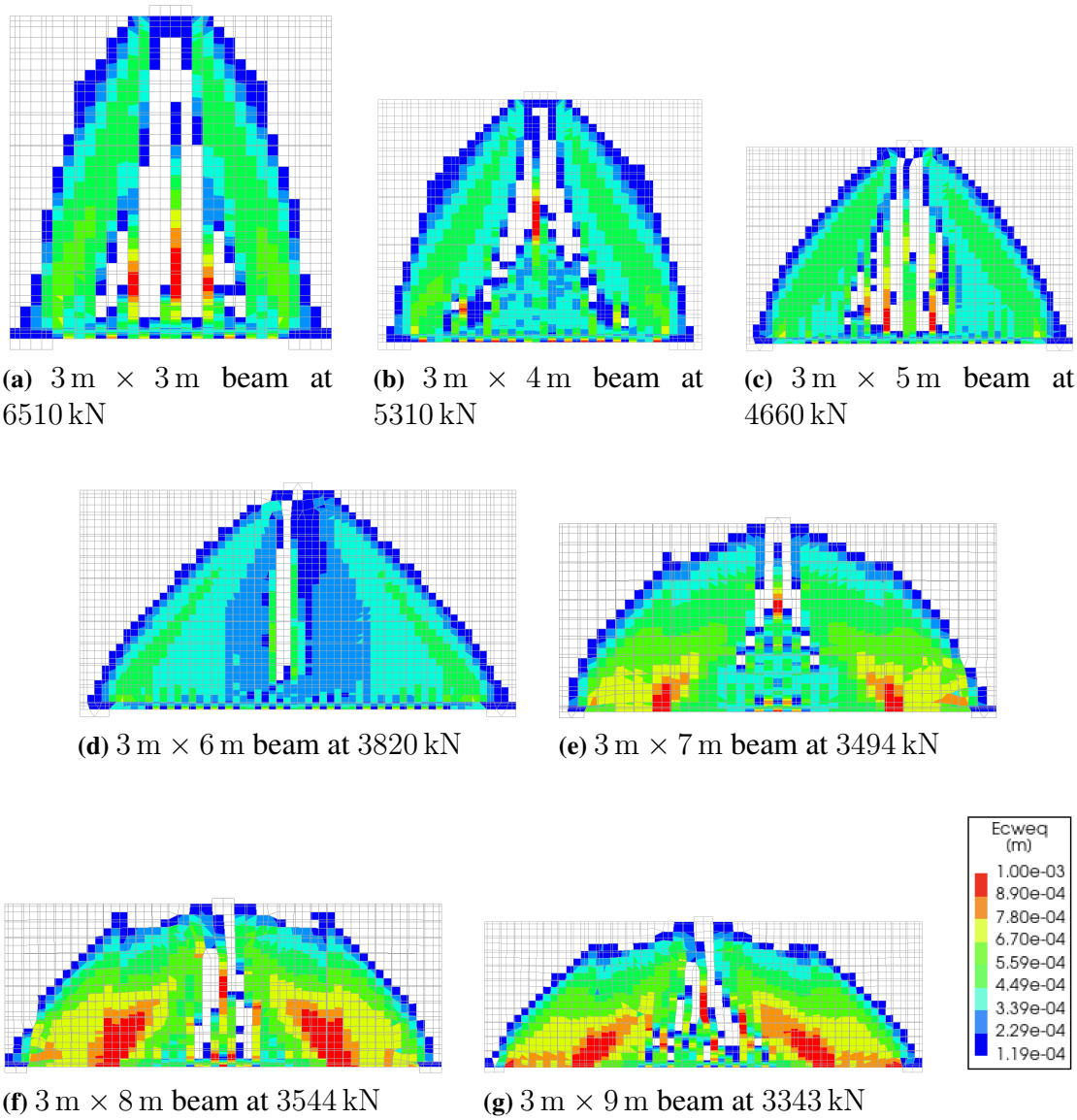

(a) $3\,\mathrm{m} \times 3\,\mathrm{m}$ beam at $6510\,\mathrm{kN}$

(b) $3\,\mathrm{m} \times 4\,\mathrm{m}$ beam at $5310\,\mathrm{kN}$

(c) $3\,\mathrm{m} \times 5\,\mathrm{m}$ beam at $4660\,\mathrm{kN}$

(d) $3\,\mathrm{m} \times 6\,\mathrm{m}$ beam at $3820\,\mathrm{kN}$

(e) $3\,\mathrm{m} \times 7\,\mathrm{m}$ beam at $3494\,\mathrm{kN}$

(f) $3\,\mathrm{m} \times 8\,\mathrm{m}$ beam at $3544\,\mathrm{kN}$

(g) $3\,\mathrm{m} \times 9\,\mathrm{m}$ beam at $3343\,\mathrm{kN}$

Figure 4.20: Crack pattern at the ultimate load step for each beam with varying span-to-depth ratios, designed with STM

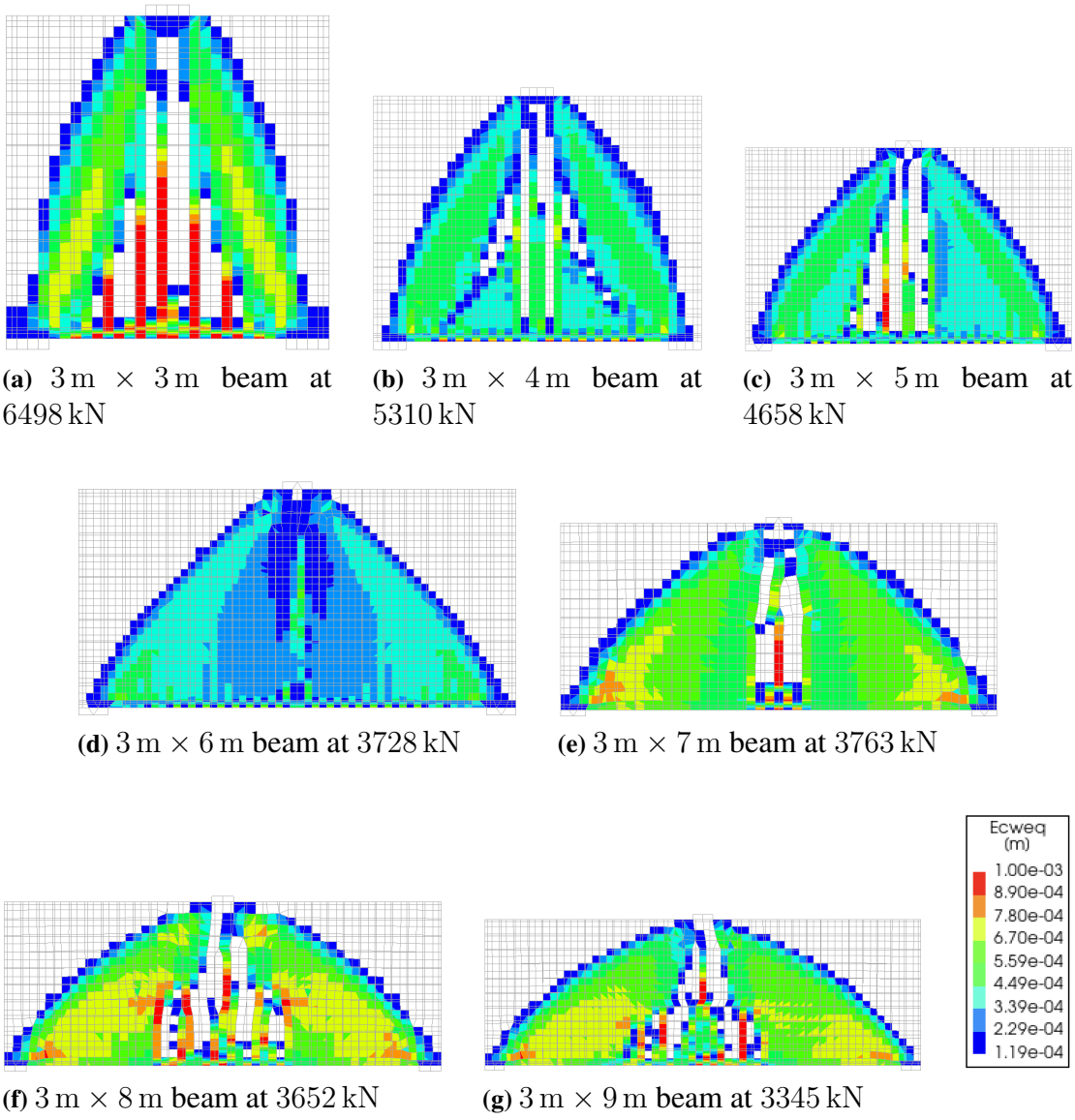

(a) $3\,\mathrm{m} \times 3\,\mathrm{m}$ beam at $6498\,\mathrm{kN}$

(b) $3\,\mathrm{m} \times 4\,\mathrm{m}$ beam at $5310\,\mathrm{kN}$

(c) $3\,\mathrm{m} \times 5\,\mathrm{m}$ beam at $4658\,\mathrm{kN}$

(d) $3\,\mathrm{m} \times 6\,\mathrm{m}$ beam at $3728\,\mathrm{kN}$

(e) $3\,\mathrm{m} \times 7\,\mathrm{m}$ beam at $3763\,\mathrm{kN}$

(f) $3\,\mathrm{m} \times 8\,\mathrm{m}$ beam at $3652\,\mathrm{kN}$

(g) $3\,\mathrm{m} \times 9\,\mathrm{m}$ beam at $3345\,\mathrm{kN}$

Figure 4.21: Crack pattern at the ultimate load step for each beam with varying span-to-depth ratios, designed with SPM

The crack patterns at the ultimate load for the beams with openings are shown in Figure 4.22 for the beams designed with STM and Figure 4.23 for the beams designed with SPM. The colour scale is different for the upper limit in these figures than for the figures showing the crack propagation. This was to better show the variations of the crack widths when they become larger than $1\,\mathrm{mm}$. For all beams, the crack pattern was very similar at the ultimate load between the STM and SPM designs. However, for the three smallest openings, SPM gave slightly larger cracks underneath the opening than STM did, while for the beam with the $1.25\,\mathrm{m} \times 1.25\,\mathrm{m}$ opening, it was the opposite. For the beam with the largest opening, both the crack pattern and width were very similar.

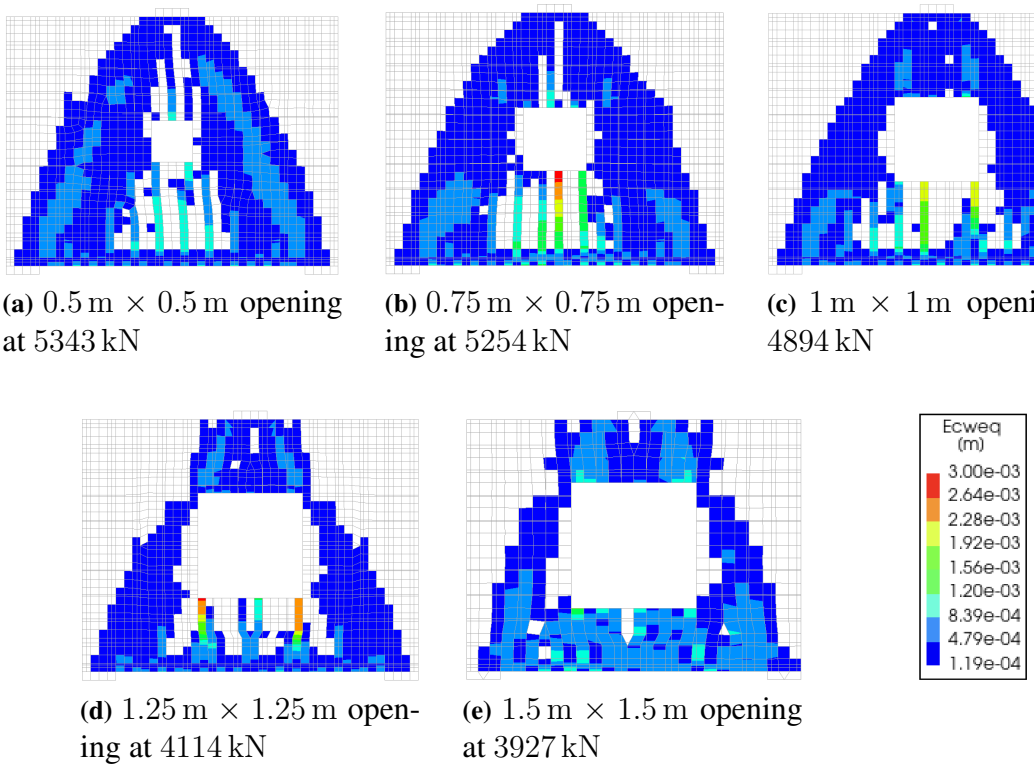

(a) 0.5 m × 0.5 m opening at 5343 kN

(b) 0.75 m × 0.75 m opening at 5254 kN

(c) 1 m × 1 m opening at 4894 kN

(d) 1.25 m × 1.25 m opening at 4114 kN

(e) 1.5 m × 1.5 m opening at 3927 kN

Figure 4.22: Crack pattern at the ultimate load step for each beam for varying opening sizes, designed with STM

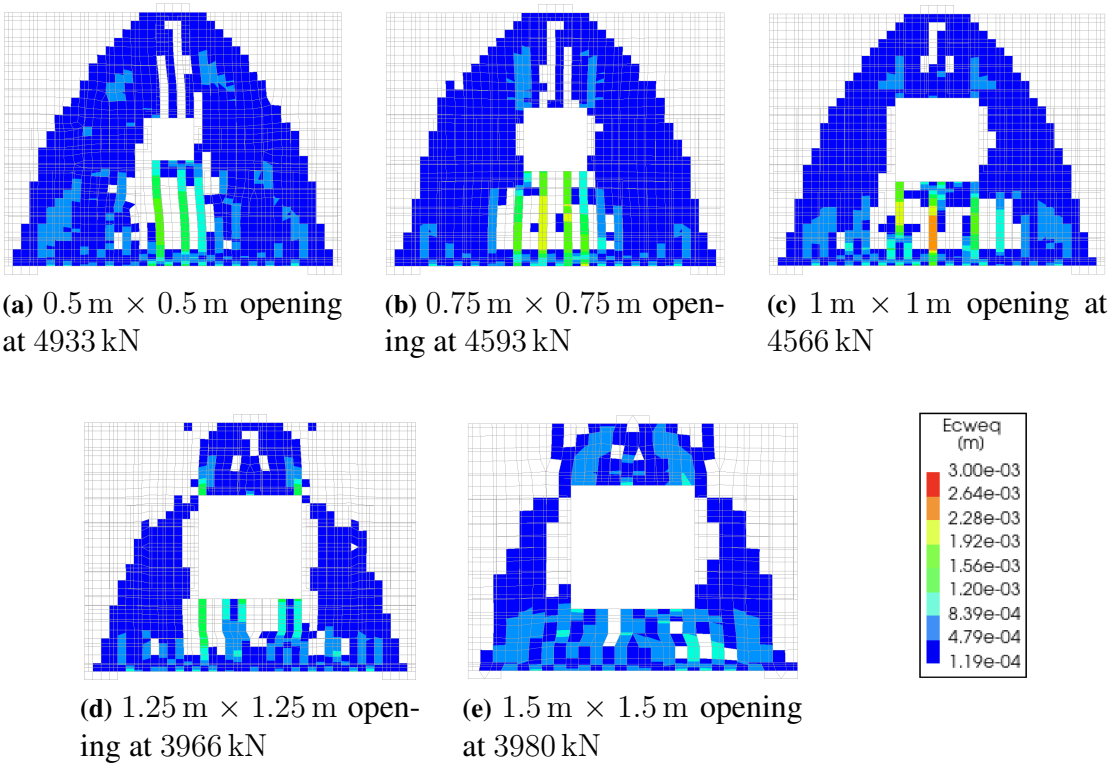

(a) $0.5\,\mathrm{m} \times 0.5\,\mathrm{m}$ opening at $4933\,\mathrm{kN}$

(b) $0.75\,\mathrm{m} \times 0.75\,\mathrm{m}$ opening at $4593\,\mathrm{kN}$

(c) $1\,\mathrm{m} \times 1\,\mathrm{m}$ opening at $4566\,\mathrm{kN}$

(d) $1.25\,\mathrm{m} \times 1.25\,\mathrm{m}$ opening at $3966\,\mathrm{kN}$

(e) $1.5\,\mathrm{m} \times 1.5\,\mathrm{m}$ opening at $3980\,\mathrm{kN}$

Figure 4.23: Crack pattern at the ultimate load step for each beam for varying opening sizes, designed with SPM

4.2.4 Crack widths

Maximum bottom crack widths across load steps for beams with varying span-to-depth ratios are presented in Figure 4.24, and for beams with varying opening sizes in Figure 4.25. Corresponding numerical values are listed in the Appendix in section E.2. At $0.6P_d$, only the beam with the largest opening exhibited cracking, while beams with the lowest span-to-depth ratios remained uncracked. At $0.8P_d$ and P_d, crack widths increased slightly with the span-to-depth ratio for both STM and SPM. A modest increase was also observed with larger opening sizes. However, no clear correlation was found between design method and crack width, suggesting that geometry was the dominant factor.

At the failure load, this trend was less evident. Crack widths showed significant variation across beam lengths for both STM and SPM, with no consistent link to geometry, as seen in Figure 4.24. For beams with openings at failure, STM produced similar crack widths across all opening sizes (Figure 4.25), while SPM showed no clear correlation between opening area and crack width.

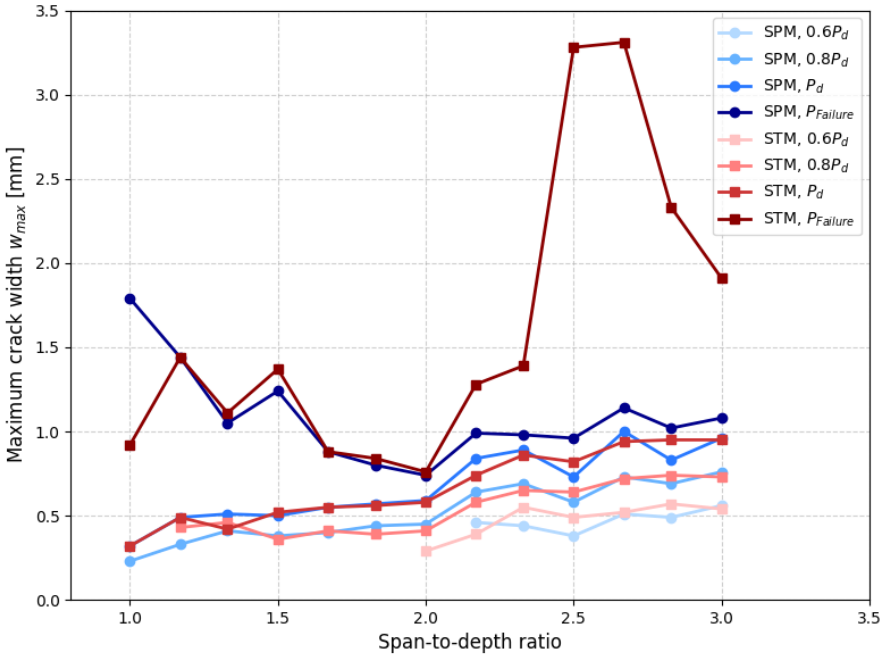

Figure 4.24: Maximum crack width along the bottom of the beams, for beams with varying span-to-depth ratios, designed with STM and SPM, under different load magnitudes

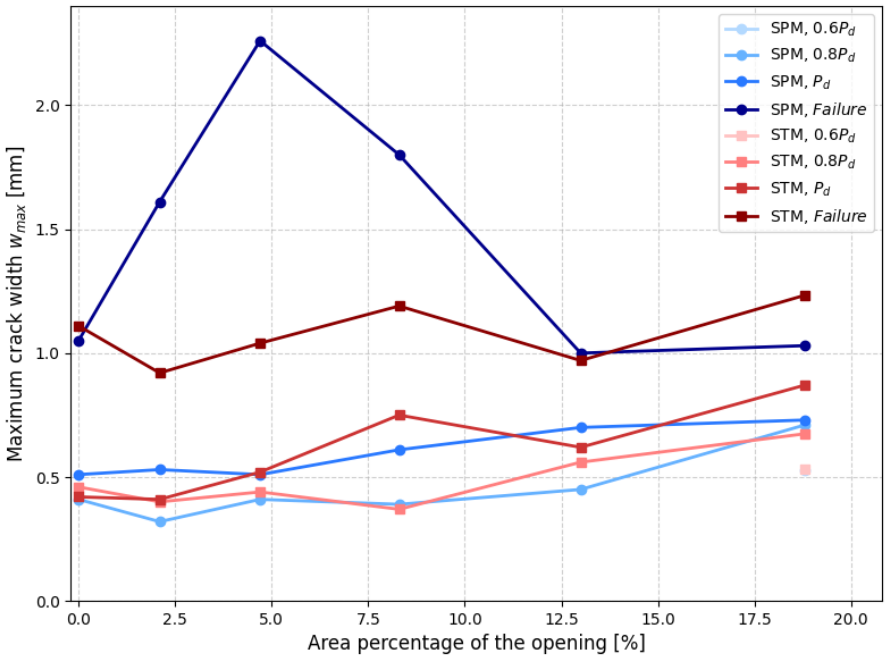

Figure 4.25: Maximum crack width along the bottom of the beams, for beams with varying opening sizes, designed with STM and SPM, under different load magnitudes

Table 4.4 and 4.5 present the maximum overall crack widths, regardless of location, for beams with and without openings across the analysed load steps. These were generally

larger than the maximum bottom cracks, except in cases where the largest crack occurred along the bottom. This was observed for SPM-designed beams of lengths $3.5\,\mathrm{m}$, $4\,\mathrm{m}$, $6\,\mathrm{m}$, and $8\,\mathrm{m}$, and STM-designed beams from $6\,\mathrm{m}$ to $9\,\mathrm{m}$. For beams with openings, the largest crack typically occurred elsewhere, except for the SPM-designed beam with a $0.75\,\mathrm{m} \times 0.75\,\mathrm{m}$ opening.

Table 4.4: Maximum crack width overall for beams with varying span-to-depth ratios, designed with STM and SPM, under different load magnitudes

Beam size [m]	w_{max} overall [mm]							
	STM				SPM			
	$0.6P_d$	$0.8P_d$	P_d	P_{ult}	$0.6P_d$	$0.8P_d$	P_d	P_{ult}
3×3	-	-	0.52	1.12	-	0.23	0.32	1.89
3×3.5	-	0.49	0.73	1.54	-	0.78	0.69	1.44
3×4	-	0.56	1.03	0.99	-	0.59	0.80	1.05
3×4.5	-	0.68	0.62	1.51	-	0.69	0.70	1.47
3×5	-	0.71	0.64	0.98	-	0.82	0.68	1.11
3×5.5	-	0.80	0.56	0.84	-	0.69	0.76	0.82
3×6	0.69	0.90	0.58	0.76	-	1.02	0.59	0.74
3×6.5	0.65	0.85	1.03	1.28	0.94	0.99	1.20	1.34
3×7	1.30	1.07	1.07	1.39	0.83	0.76	0.97	1.22
3×7.5	0.64	0.78	0.82	3.28	0.67	0.85	0.94	0.99
3×8	0.83	0.98	1.25	3.31	0.85	1.00	1.22	1.14
3×8.5	0.96	1.06	1.11	2.33	0.88	1.02	1.21	1.33
3×9	0.95	1.20	1.41	1.91	0.83	1.00	1.25	2.33

Table 4.5: Maximum crack width overall for beams with varying opening sizes, designed with STM and SPM, under different load magnitudes

Opening size [m]	w_{max} overall [mm]							
	STM				SPM			
	$0.6P_d$	$0.8P_d$	P_d	P_{ult}	$0.6P_d$	$0.8P_d$	P_d	P_{ult}
0.5×0.5	-	0.70	1.22	0.98	-	0.58	0.67	1.91
0.75×0.75	-	0.73	0.64	1.07	-	0.61	0.77	2.26
1×1	-	0.73	0.90	2.06	-	0.78	0.87	2.56
1.25×1.25	0.27	1.18	1.87	2.67	0.25	0.80	0.92	1.47
1.5×1.5	1.03	0.97	1.14	1.61	0.63	0.93	0.90	1.12

4.2.5 Deflections

Mid-span deflections at the bottom of the beam for each load step are shown in Figure 4.26 and 4.27 for beams of varying length designed with STM and SPM, respectively. Corresponding results for beams with different opening sizes, as well as the $4\,\mathrm{m}$ beam without an opening, are presented in Figure 4.28 and 4.29. For both STM and SPM, and across all beam configurations, the load–deflection curves appear jagged, particularly in

the range of approximately 1000 to 3000 kN. This irregularity includes instances of deflection increase during load decrease, despite the overall trend of increasing deflection with increasing load.

From Figure 4.26 and 4.27, beams without openings show similar behaviour regardless of the design method. Shorter beams exhibited lower deflections under the same load and smaller ultimate deflections. However, STM-designed beams generally reached higher mid-span deflections before failure than their SPM counterparts, particularly in longer spans. This distinction was less apparent for shorter spans. For beams with openings, STM and SPM yielded similar deflection patterns (Figure 4.28, 4.29). Beams with larger openings reached lower failure loads and smaller deflections, while smaller openings allowed for greater deflections.

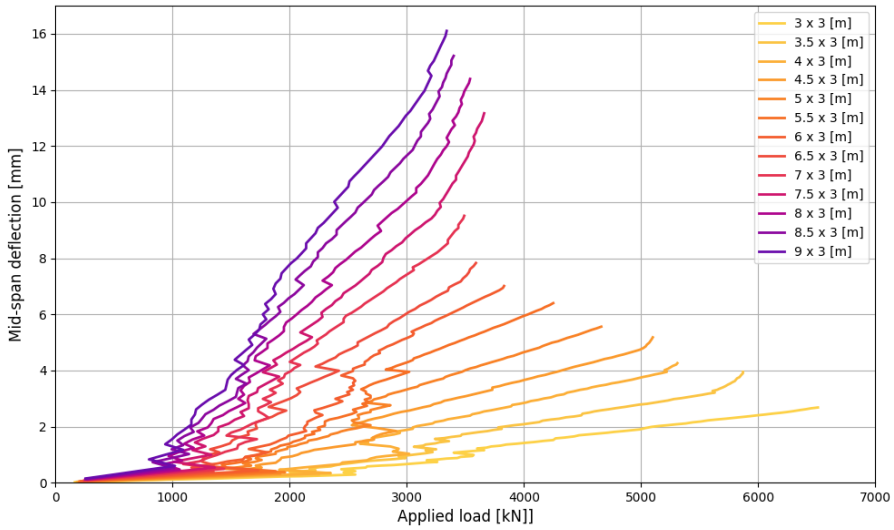

Figure 4.26: Mid-span deflection-load curve for beams with varying span-to-depth ratios, designed with STM

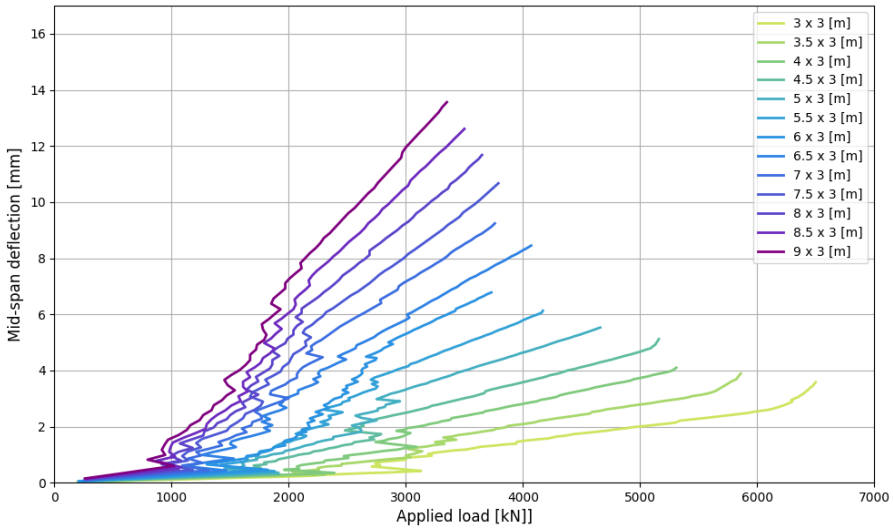

Figure 4.27: Mid-span deflection-load curve for beams with varying span-to-depth ratios, designed with SPM

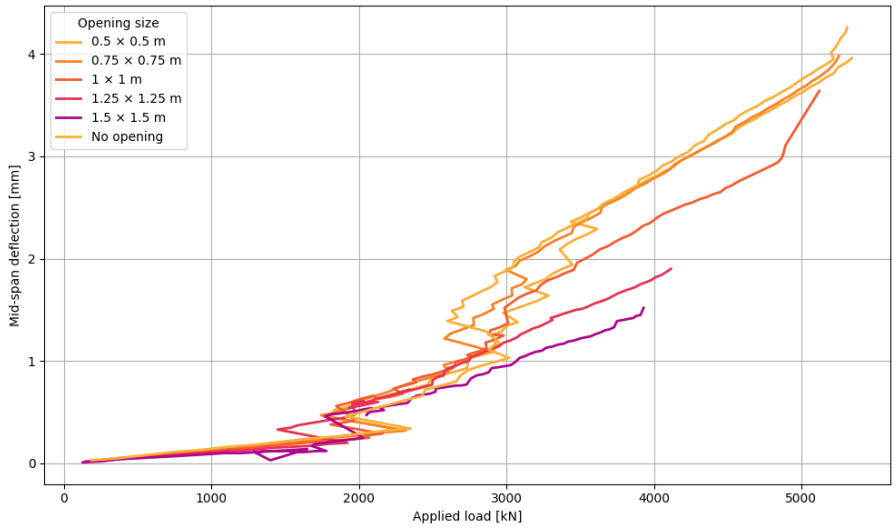

Figure 4.28: Mid-span deflection-load curve for beams with varying opening sizes, designed with STM

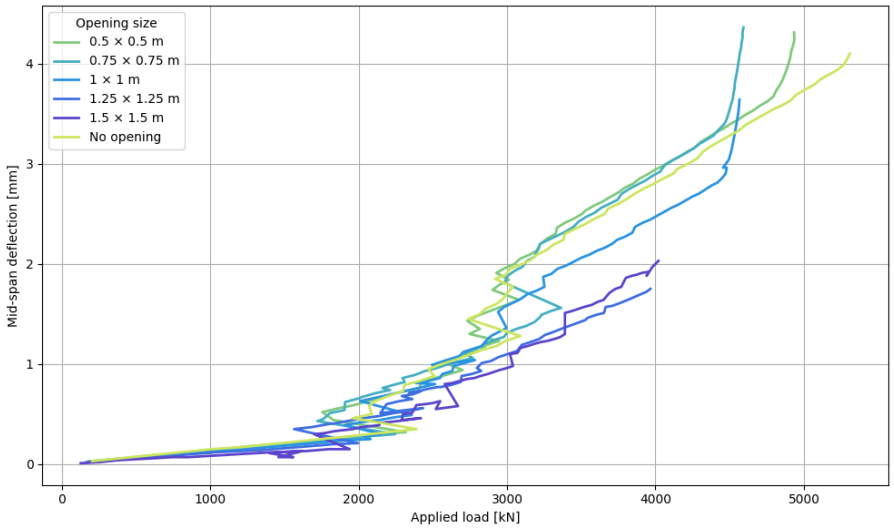

Figure 4.29: Mid-span deflection-load curve for beams with varying opening sizes, designed with SPM

Maximum mid-span deflections at each load step from the FEA are presented in Figure 4.30 and 4.31, with numerical values summarised in the Appendix in section E.3. No significant difference was observed between STM- and SPM-designed beams across varying spans, although STM beams generally showed slightly higher deflections for the longest spans at all load levels. For load steps $0.6P_d$, $0.8P_d$, and P_d, mid-span deflections were similar across opening sizes and between STM and SPM, with no consistent pattern indicating which method produced greater deflections. At $0.6P_d$, deflections were nearly identical for all opening sizes, except for the beam with the largest opening. At failure load, SPM beams typically exhibited larger deflections than STM. Additionally, the influence of opening size became more pronounced at failure, with smaller openings leading to greater mid-span deflections.

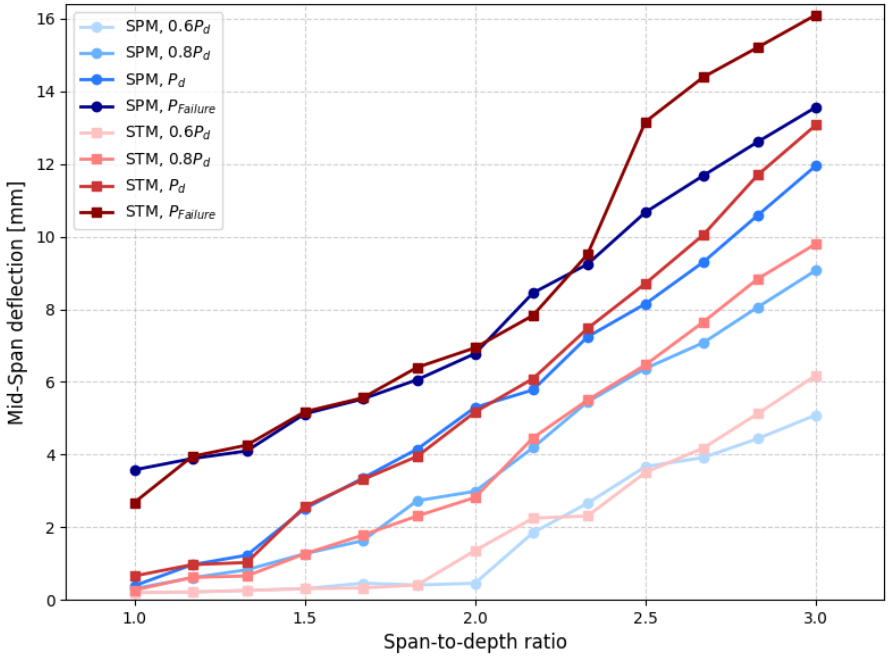

Figure 4.30: Mid-span deflection for beams with varying span-to-depth ratios, designed with STM and SPM, under different load magnitudes

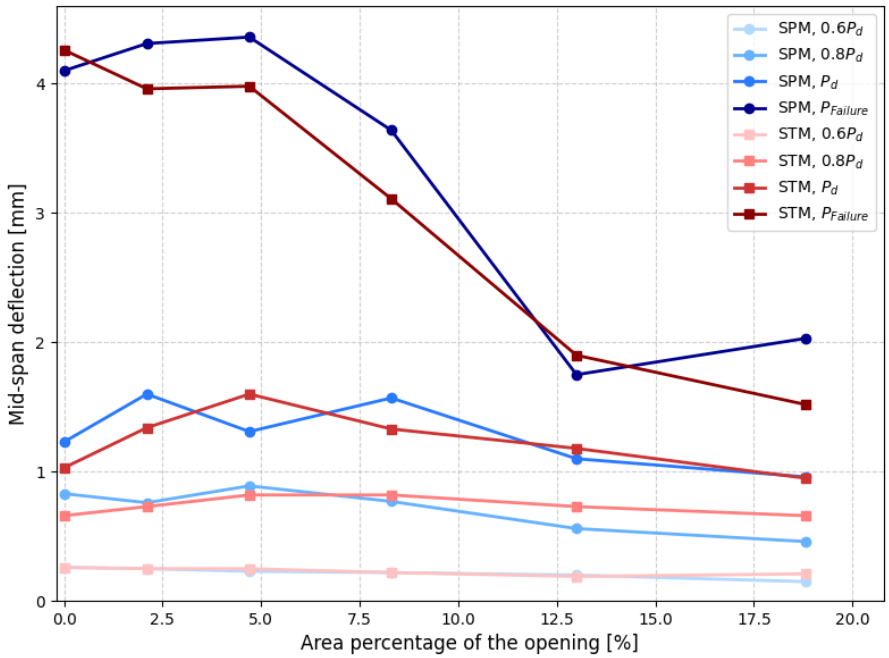

Figure 4.31: Mid-span deflection for beams with varying opening sizes, designed with STM and SPM, under different load magnitudes

Maximum deflections above the opening for each load step are shown in Figure 4.32, with corresponding values in the Appendix in section E.3. For larger openings, STM-designed

beams exhibited greater deflections than those designed with SPM, whereas the opposite was true for smaller openings. For load levels $0.6P_d$, $0.8P_d$, and P_d, deflections increased slightly with the opening area for both methods. At failure load, deflections in SPM beams decreased with increasing opening size, while those in STM beams continued to increase.

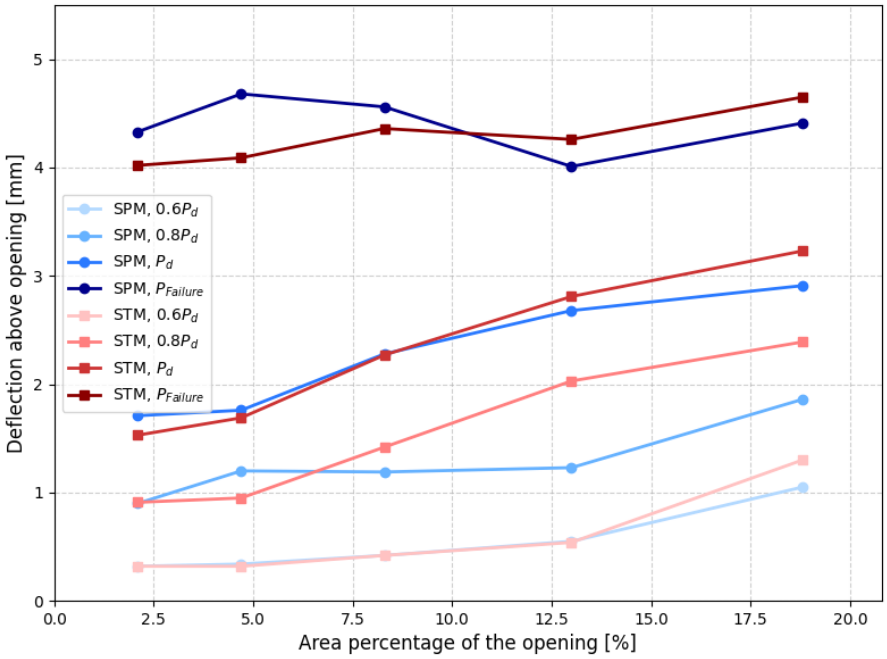

Figure 4.32: Deflection above the opening for beams with varying opening sizes, designed with STM and SPM, under different load magnitudes

4.3 Comparison between analytical and numerical results

In this section, the results obtained from the analytical calculations and the results from the FEA are compared with each other. In each figure in this section, stresses derived from analytical calculations at various load levels were depicted using dashed lines, while stresses obtained from FEA were shown with solid lines.

4.3.1 Stresses in reinforcement

Representative examples of reinforcement stress distributions are presented in this section. In Figure 4.33 and 4.34, the tensile reinforcement stresses were illustrated for a beam without openings, designed using STM and SPM, respectively. Corresponding results for a beam with an opening are shown in Figure 4.35 and 4.36. The data presented has been limited to two beam geometries, the $3\,\mathrm{m} \times 6\,\mathrm{m}$ beam and the $3\,\mathrm{m} \times 4\,\mathrm{m}$ beam with a $1\,\mathrm{m} \times 1\,\mathrm{m}$ opening.

The analytically derived stress distribution remained consistent across all beam configurations; therefore, the beams presented in Figure 4.33, 4.34, 4.35, and 4.36 were considered

representative. Similarly, the stress distributions obtained from FEA for beams with varying opening sizes exhibited comparable trends, although with differences in maximum stress magnitudes. These peak stress values for different opening sizes are provided in Figure 4.14 and 4.15. If these maximum values are scaled and applied to the distributions in Figure 4.35 and 4.36, the resulting stress profiles can be deemed as representative for all beams with openings.

Beams of varying lengths also exhibited similar stress distribution patterns across almost all load levels, although the maximum stress values varied by length. These maxima are detailed in Figure 4.12 and 4.13. For the shortest beams designed using SPM, the stress distribution diverged slightly from that shown in Figure 4.34, particularly at load levels of $0.8P_d$ and P_d, where stresses in the central region of the tensile reinforcement were reduced and stresses near the ends were elevated. Nonetheless, the beams shown in Figure 4.33 and 4.34 remain broadly representative of beams with varying lengths.

Across all cases, the tensile stresses obtained by FEA were significantly lower than those assumed in the analytical design. Notably, the yield stress was not reached at the design load in any configuration. For many beams without openings, yielding was not reached even at the failure load. As previously discussed, stress levels vary with beam geometry, as illustrated in Figure 4.12, 4.13, 4.14, and 4.15, and yielding was reached for some beams. In beams with openings, tensile reinforcement is employed at multiple locations, which differ between STM and SPM designs. However, when comparing regions where reinforcement placement was consistent across both methods, the stress levels and distributions showed similar characteristics. Overall, the actual stress distribution obtained from FEA was between the analytically predicted distributions from STM and SPM, but with lower maximum levels.

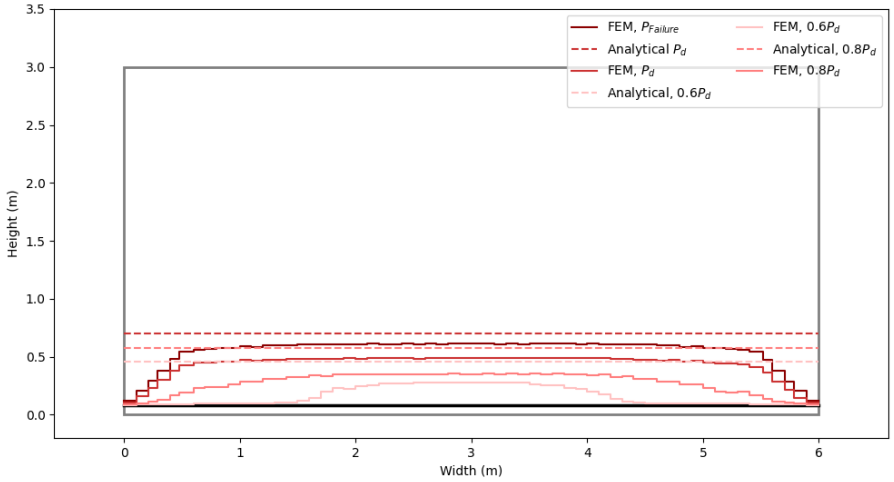

Figure 4.33: Stress distribution in the tensile reinforcement for a beam without opening, designed with STM

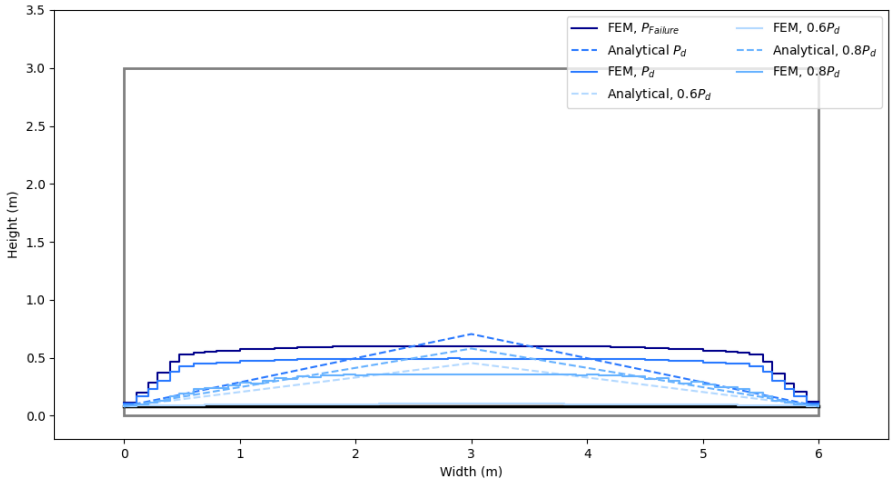

Figure 4.34: Stress distribution in the tensile reinforcement for a beam without opening, designed with SPM

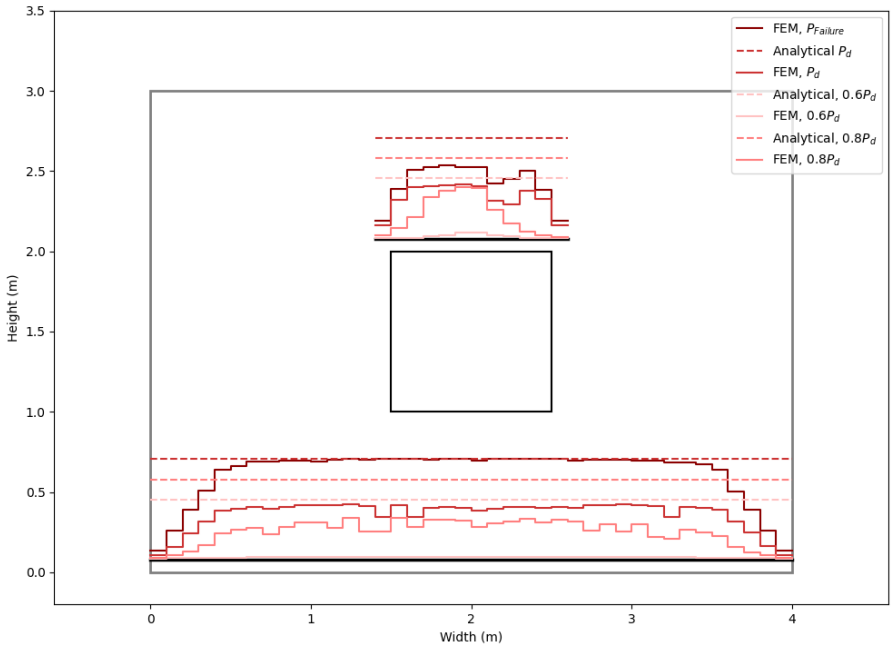

Figure 4.35: Stress distribution in the tensile reinforcement for a beam with an opening, designed with STM

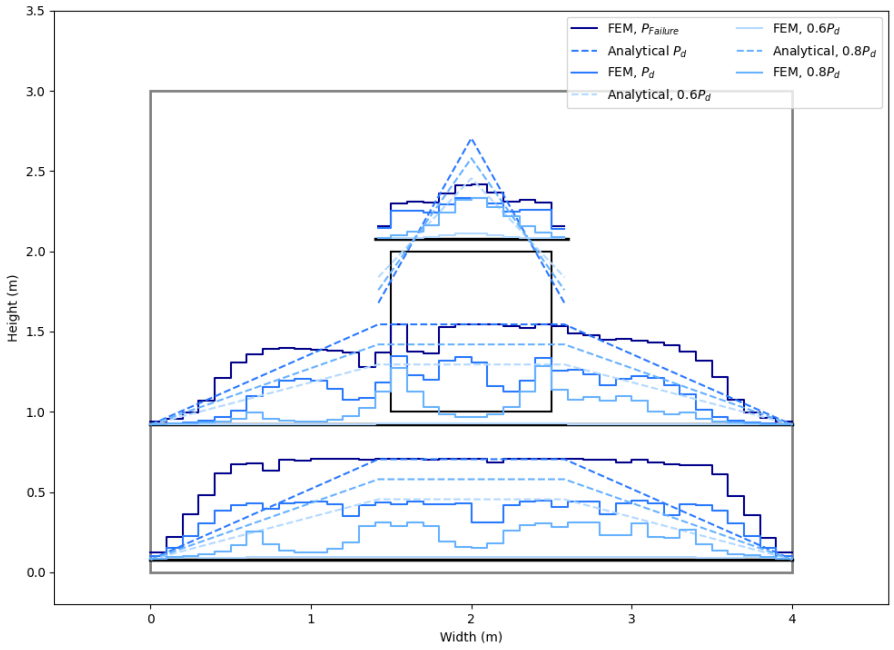

Figure 4.36: Stress distribution in the tensile reinforcement for a beam with an opening, designed with SPM

4.3.2 Crack widths

The characteristic crack widths obtained from the analytical calculations were compared to the maximum crack width along the bottom of the beams at different load steps. In Figure 4.37, the crack widths for varying span lengths are shown and compared, and in Figure 4.38, the same is done but for varying opening sizes.

The crack widths obtained from the FEA increased with increased span-to-depth ratio, while the opposite can be observed from the analytical calculations. The crack widths of the STM and SPM beams do, on a general level, not differ much from each other. For the beams with varying opening sizes, the results of the analytical calculations and the FEA aligned more than for the cases without openings, both in the sizes of the cracks and also in the trend of the curves.

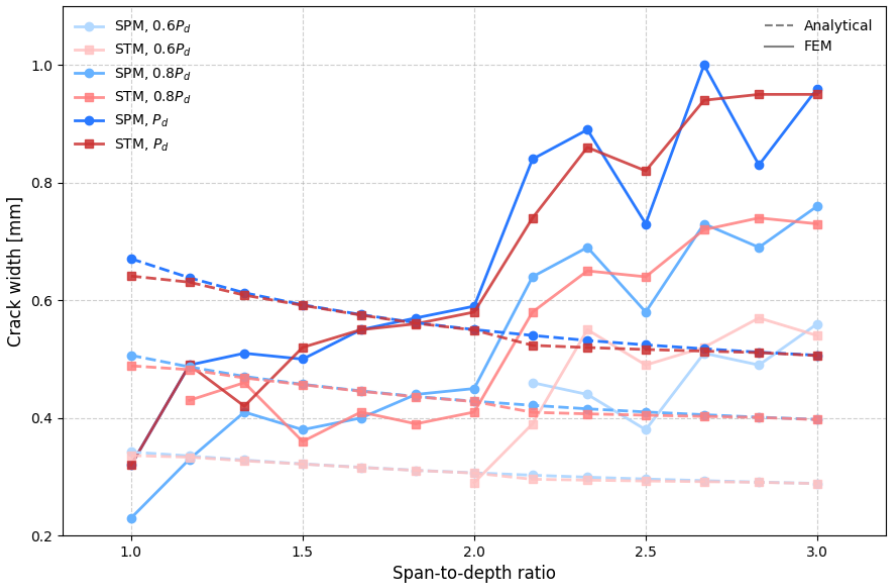

Figure 4.37: Comparison between the crack widths obtained from the FEA (w_{max}) and the analytical calculations (w_k) for beams with varying span-to-depth ratios

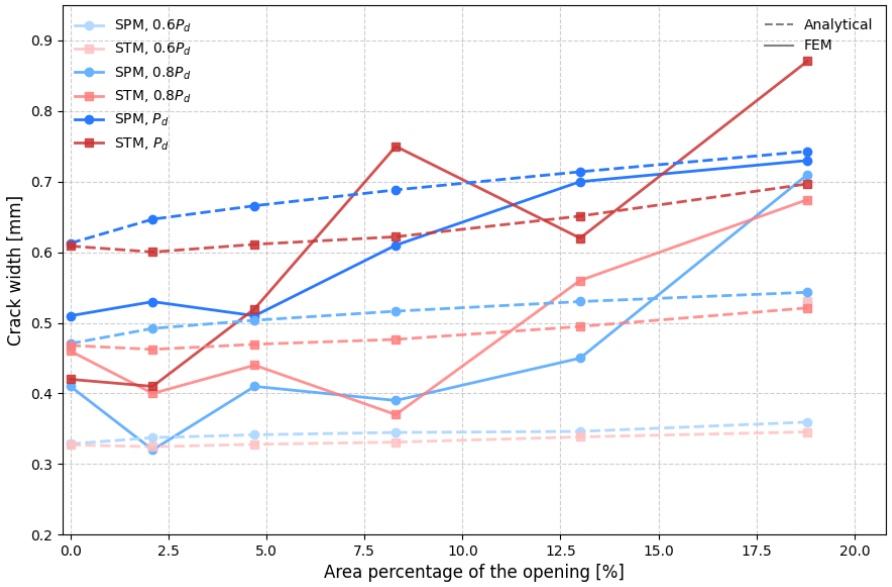

Figure 4.38: Comparison between the crack widths obtained from the FEA (w_{max}) and the analytical calculations (w_k) for beams with varying opening sizes

4.3.3 Deflections

Figure 4.39 and 4.40 show the comparison between the deflection at mid-span at the bottom of the beams at different load levels, for varying span length and varying opening size separately. Figure 4.41 shows the deflection above the openings, at the mid-point of the upper edge of the opening. In this case, analytical calculations have only been carried out for SPM, since no similar simplified method is available for STM, as previously explained.

For the varying span lengths, the deflections got larger with longer spans and higher loads for both the analytical results and the FEA results. The magnitude of the deflections did, however, only correspond relatively well between the FEA and analytical results for the smallest span when the load $0.8P_d$ was applied, and to the span-to-depth ratio of 2 for the load $0.6P_d$. At these load steps and span lengths, the beam had not yet cracked. For all other span lengths and load steps, the results from the analytical calculations were significantly lower than the FEA results. For the beams with openings of varying sizes, the analytical results resembled mostly to the FEA results when the load $0.6P_d$ was applied. For the other loads, the FEA results were significantly larger than the analytical results. This was true for both the deflection at mid-span at the bottom of the beams and at the top of the openings.

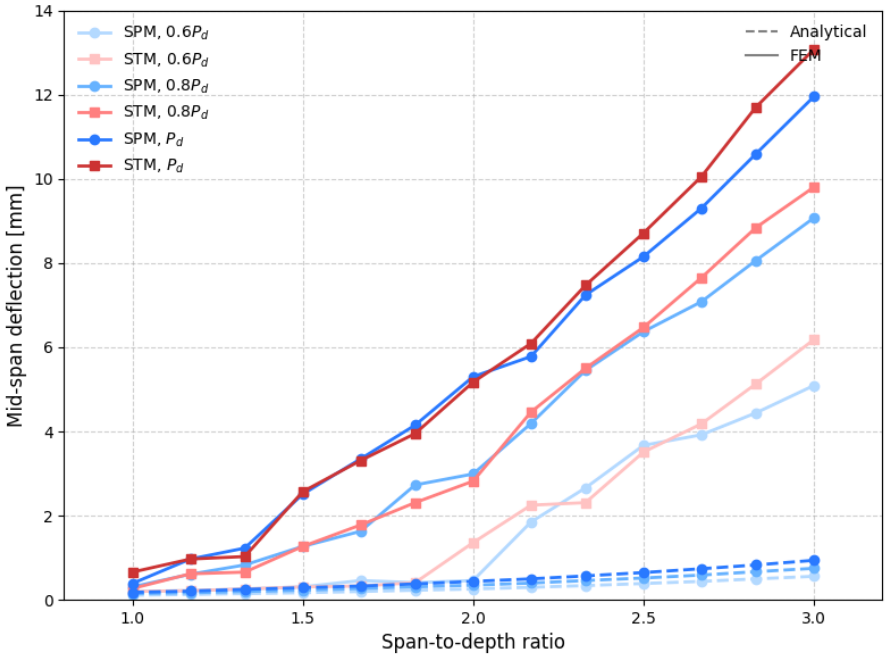

Figure 4.39: Comparison between the mid-span deflection obtained from the FEA and the analytical calculations for beams with varying span-to-depth ratios

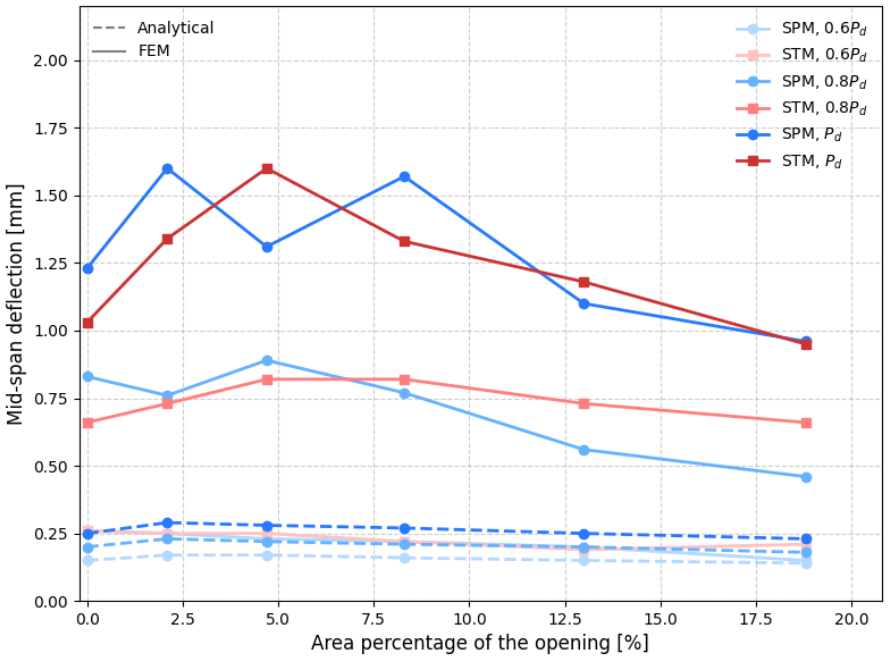

Figure 4.40: Comparison between the mid-span deflection obtained from the FEA and the analytical calculations for beams with varying opening sizes

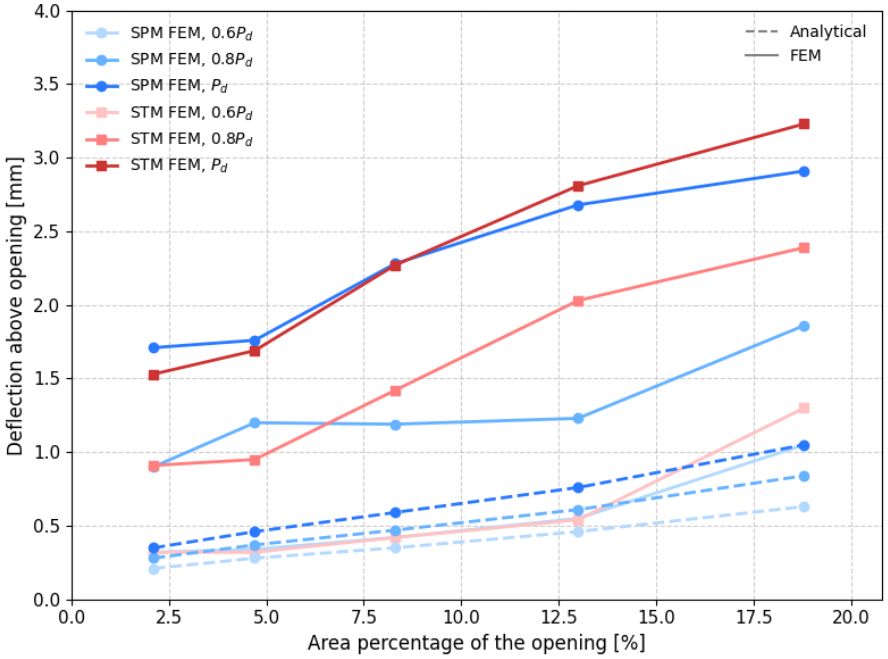

Figure 4.41: Comparison between the deflection above the opening obtained from the FEA and the analytical calculations for beams with varying opening sizes

4.4 SPM calculations, comparison with linear analysis and reduction of stiffness

In this section, the results obtained from the FEA are compared to analytical calculations done with the stiffness of the stringers and panels reduced by a factor of 0.1 and 0.2. A comparison between the analytical calculations without stiffness reduction and linear FEA is also presented here.

4.4.1 Comparison to linear analysis

As mentioned in subsection 3.3.3, the analytical results regarding the deflections were only applicable to linear analysis. A comparison of the analytical results, without any reduction of the stiffness, and the results from a linear FEA was therefore performed for the beams designed with SPM. The comparison for beams with varying span-to-depth ratios can be found in Figure 4.42. Both the analytical results and the linear FEA results followed similar trends, both with increasing span length and load. The FEA results were approximately larger by a factor of two compared to the analytical results. The differences were, however, never larger than $1\,\mathrm{mm}$ even for the longest span, and in most cases not larger than $0.5\,\mathrm{mm}$ for the beams with varying span-to-depth ratio as well as varying opening sizes.

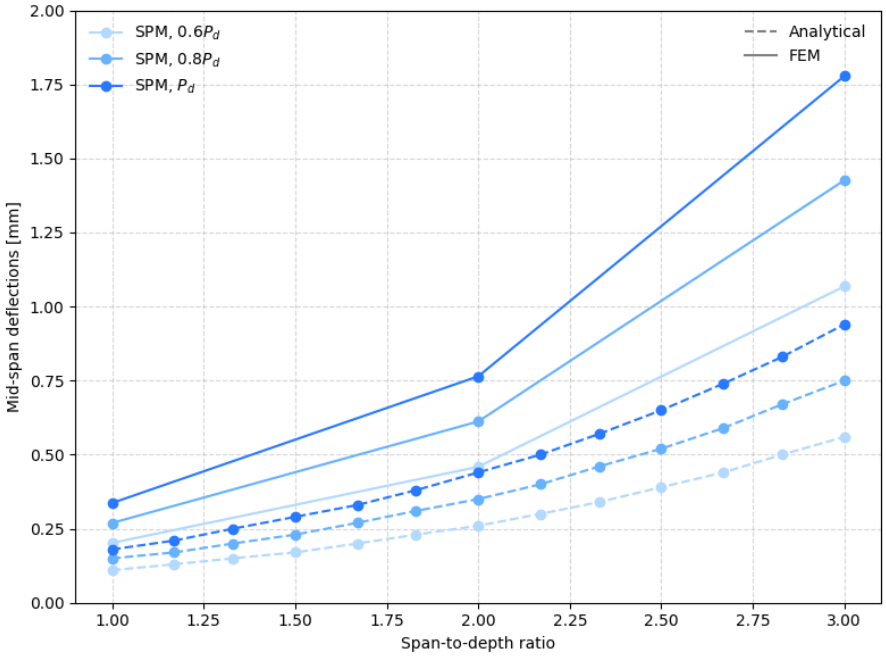

Figure 4.42: Comparison between the mid-span deflection obtained from the linear FEA and the analytical calculations for beams with varying span-to-depth ratios

The comparisons of the analytical and numerical results for the beams with varying opening sizes can be found in Figure 4.43 and 4.44 for the deflections at the bottom of the beam and the top of the opening. The linear FEA results were larger than the analytical results for these cases as well. The differences between them were, however, slightly smaller than for the varying span lengths. The trends of the graphs corresponded well with the analytical and FEA results.

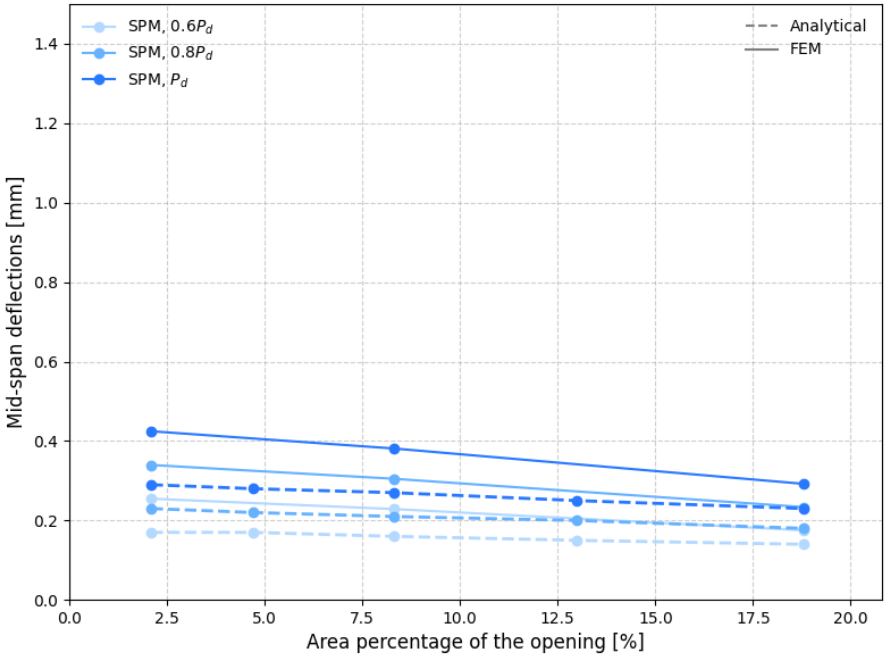

Figure 4.43: Comparison between the mid-span deflection obtained from the linear FEA and the analytical calculations for beams with varying opening sizes

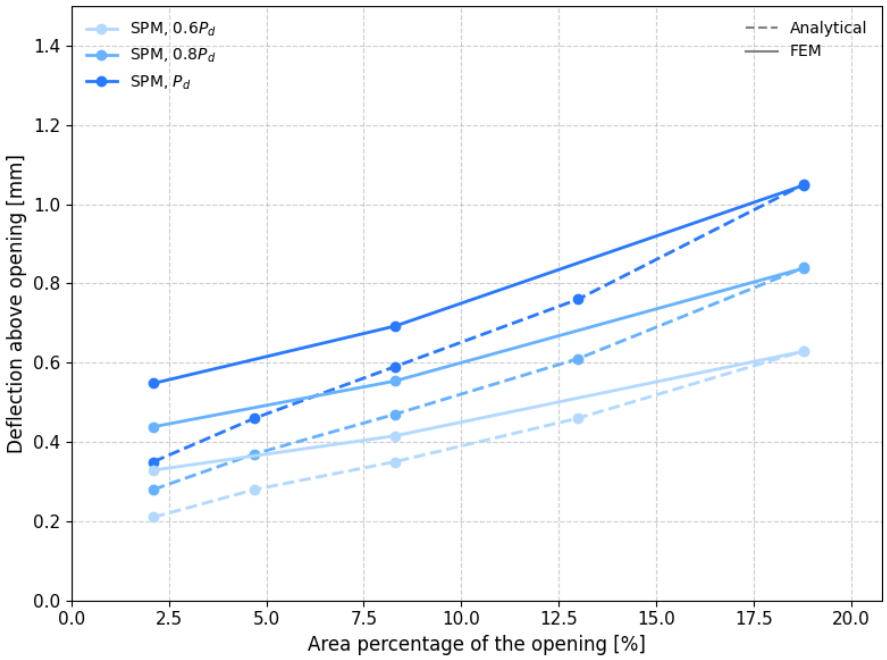

Figure 4.44: Comparison between the deflection above the opening obtained from the linear FEA and the analytical calculations for beams with varying opening sizes

4.4.2 Reduction of stiffness

In Figure 4.45, 4.46, and 4.47, the deflections for the different beams with varying span-to-depth ratios or opening sizes were plotted alongside the deflections obtained with the modified stiffness for the analytical calculations of the deflections for the beams designed with SPM.

For the beams with varying span-to-depth ratios, the stiffness reduction factor of 0.1 was a bit conservative for smaller spans, but on the low side for longer spans compared to the FEA results. For the longer spans with the factor 0.1 and the load $0.6P_d$, the FEA results and the analytical results were relatively similar. For the larger loads, the analytical graph and the FEA graphs crossed somewhere around the mid-range of the span lengths. The analytical results with the stiffness reduction factor 0.2 were generally much lower compared to the FEA results, except for the smallest spans at the loads $0.6P_d$ and P_d, but larger than the FEA results for the load $0.6P_d$ up until the mid-range ratio.

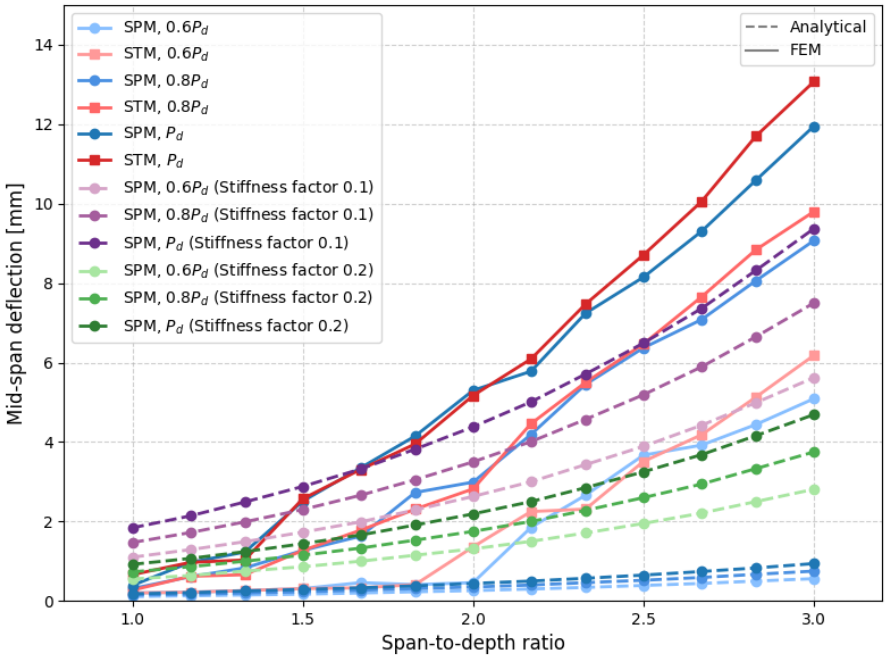

Figure 4.45: Comparison between the mid-span deflection obtained from the FEA and the analytical calculations with lower stiffness, for beams with varying span-to-depth ratios

For the deflection of the bottom of the beams as well as the top of the opening for the beams with varying opening sizes, the analytical results using the factor 0.1 were significantly larger for all load cases and opening sizes. For the deflection at the bottom, the analytical results using the factor 0.2 did, however, correspond relatively well with the FEA results for the load P_d. For all other load cases, the analytical results using the factor 0.2 were larger than the FEA results for most opening sizes and load steps.

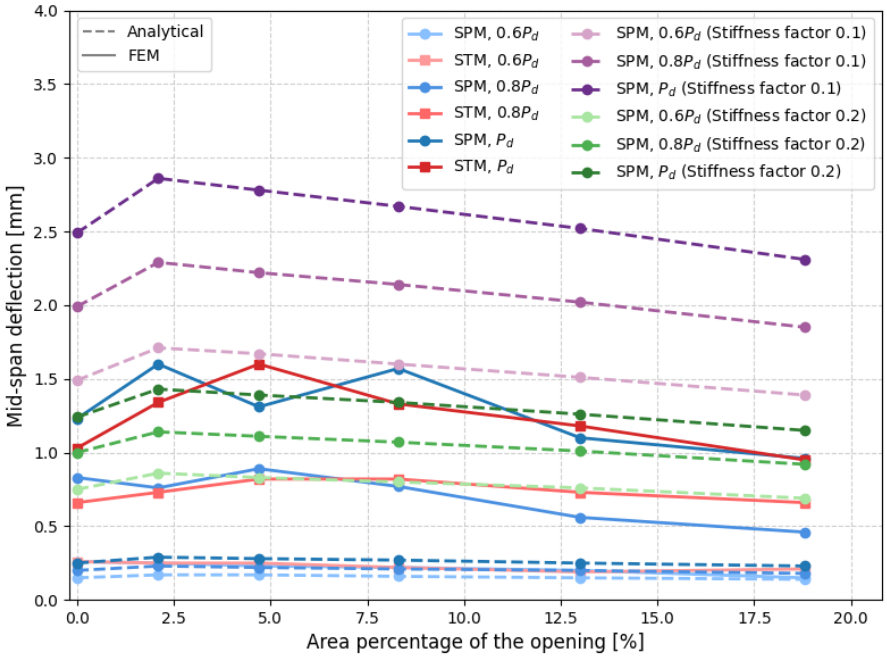

Figure 4.46: Comparison between the mid-span deflection obtained from the FEA and the analytical calculations with lower stiffness, for beams with varying opening sizes

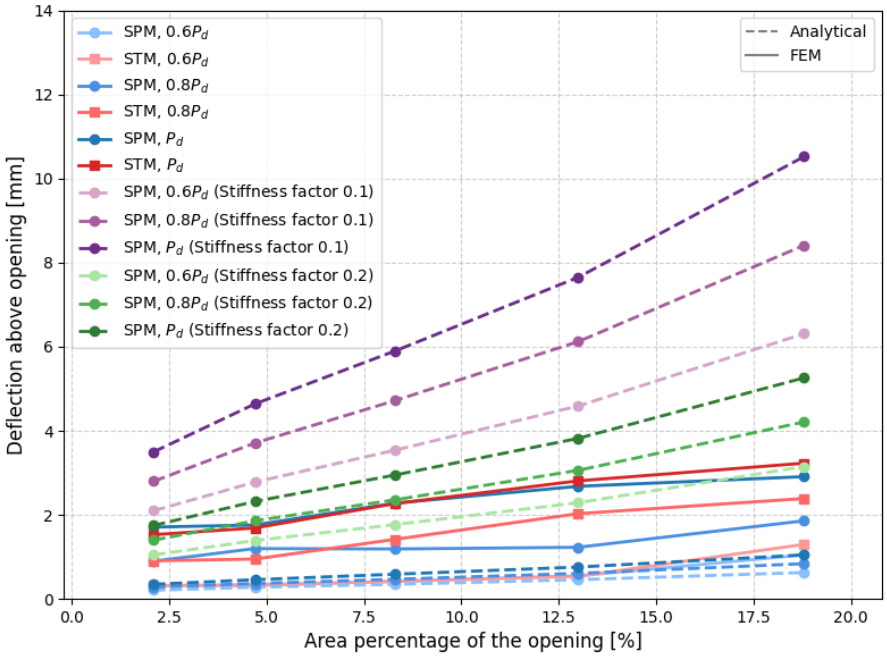

Figure 4.47: Comparison between the deflection above the opening obtained from the FEA and the analytical calculations with lower stiffness, for beams with varying opening sizes

5

Discussion

In this chapter, the influence of the geometry, the chosen reinforcement design method, and the choices and assumptions made during design are discussed. The Strut-and-Tie Method (STM) and Stringer-Panel Method (SPM) are compared and evaluated against each other, and analytical calculations are compared against finite element analysis (FEA). It is also discussed whether any of the methods is superior in any aspect.

5.1 Effect of displacement control

Displacement control was used to capture the non-linear behaviour, for which the load does not increase proportionally with the applied deformation (DIANA FEA BV, 2024b). Due to the fluctuating nature of the reaction force, there can be substantial variation in the deformation and corresponding load step at which a particular force level is reached. This aspect is critical when comparing STM and SPM, but especially when comparing FEA against analytical calculations, as it highlights the structural mechanisms that govern behaviour under realistic loading conditions.

This phenomenon is evident in the figures plotting the applied load along the x-axis, like in Figure 4.26 to 4.29. Between approximately $1000\,\mathrm{kN}$ and $3000\,\mathrm{kN}$, the graphs show pronounced irregularities in load progression. These irregularities occur primarily because this is the range during which most cracks initiate. After $3000\,\mathrm{kN}$, the behaviour is dominated by crack propagation rather than initiation, resulting in fewer abrupt drops in load.

The specific fluctuation of the load path at which a given force level is reached can significantly influence the results, especially since it varies between beam geometries. This can lead to greater differences in deformation, stress, and crack width than could otherwise be expected. However, this variability also contributes to a more realistic representation of structural behaviour. The initiation and propagation of cracks, which cause these load fluctuations, are fundamental to understanding the true non-linear response. Since different beam geometries crack at different load levels, this influences the deformation and stress distribution across various stages of loading.

5.2 FEA and the DIANA model

This section discusses the impact of the mesh size on the results and the verification of the DIANA model.

5.2.1 Verification of DIANA model

As noted in subsection 3.4.6, the DIANA model shows some deviations from experimental beam tests, particularly in deflection, which is often underestimated. This may be due to the model not accounting for support settlements or apparatus deformations, whereas some experimental tests may have included these effects, inflating measured deflections. Despite this, the DIANA deflection results in this study align well with those from similar DIANA simulations and match experimental data in two cases, indicating a fundamentally sound modelling approach.

Crack width data was only available for two of the analysed beams and showed that DIANA slightly underestimates those values. These estimates were made at failure, a stage where numerical instability is common, and experimental methods for measuring crack widths were not clearly defined. Predictions of initial cracking loads varied, sometimes higher, sometimes lower, suggesting inconsistencies in how cracking was identified experimentally, and since in reality, material properties are not homogeneous and crack initiation may be triggered by the presence of local defects. Nevertheless, DIANA's predictions fell within a reasonable range, and failure load estimates differed by just a few percent across three beams, further supporting the model's reliability, at least to determine the ultimate load capacity.

While explainable, the observed discrepancies may affect comparisons with analytical calculations and should be investigated in future research. However, since both STM and SPM were modelled under identical conditions, these differences do not compromise the fairness or validity of their comparison within the FEA framework.

5.2.2 Impact of Mesh Size

In some cases, the obtained crack width from the FEA for both STM and SPM seemed a bit random, especially at failure load, as can be seen in subsection 4.2.4. This could be an effect of the formation of cracks and the crack pattern, which is dependent on the finite element mesh. This, in turn, also has an impact on the crack width.

This mesh dependency is particularly critical near failure load, where minor changes in local stiffness due to cracking can result in a significant variation in predicted response (Modéer, 1979). As Alañón et al. (2018) found, a too coarse mesh might underestimate cracks while a too fine mesh overestimate them. Consequently, the size and shape of elements directly influence the distribution and magnitude of cracks. A too fine mesh is therefore likely the reason why, for some beams, the cracks get substantially larger than for other geometries, since there is no structural explanation for this. Hence, the variability in crack width for the beams at failure may not only reflect the structural behaviour, but also numerical issues due to mesh sensitivity.

5.3 Impact of SPM design

For the deep beams designed with SPM within this thesis, the coarsest possible grid of stringers and panels was chosen according to the method described in subsubsection 2.3.2.1. This creates relatively simple and manageable layouts of the stringer-panel grid and is described by, for example, Blaauwendraad (2018) as desirable. However, the engineer can choose another layout by, for example, dividing the structure into smaller panels, which could affect the reinforcement and the structural behaviour. There could be advantages to further subdividing the grid, especially in areas with high stress gradients, as noted by Blaauwendraad (2018). A grid with more, smaller panels might enable a more optimised reinforcement layout in some cases. On the other hand, this often results in complex and highly specific reinforcement arrangements that may be difficult to implement practically. This underlines how the design of the stringer-panel grid can significantly affect the final design and performance. Moreover, the engineer's choices when using STM also impact the results, especially when multiple valid STM options exist. For both STM and SPM, the range of possible design choices, particularly for complex structural geometries, can have a greater influence on the outcome than the choice of method itself.

An advantage of SPM is the increased possibility for standardisation. By using consistent layouts and simplifications, designs may become easier to replicate and verify. In contrast, STM often allows for greater optimisation of the internal force flow, but this also demands more experience from the designer and often leads to complex reinforcement layouts. More investigations are needed to establish guidelines for design strategies that balance optimisation of the structure and constructability for different cases, which could be beneficial for designing complex structures.

5.4 Impact of beam geometry

The geometry of the deep beam has a significant impact on the structural behaviour and on how forces are distributed. For instance, when the opening is large, the structure tends to behave more like a beam on two columns. The force paths are then more direct, where the force paths are redirected more vertically above the supports, reducing stress concentrations and deformations beneath the opening. This reduces the demand and leads to reduced bending in this zone. This behaviour contrasts with shorter beams, where the structure exhibits more of a column-like response due to the more limited horizontal span for force redistribution. When the span-to-depth ratio exceeds approximately 3, the structural behaviour generally transitions towards that of a conventional Euler-Bernoulli beam, as stated by Engström (2015). In such cases, internal force redistribution follows classical beam theory, and the use of strut-and-tie models or stringer-panel models is typically not required.

The geometry of the beam has a fundamental impact on the outcome of all the analyses performed. Variations in geometry affect load paths, stress distribution, deformation patterns, and ultimately the suitability and accuracy of the modelling approach. From this

study, it can be observed that changing the geometry parameters does, in most cases, affect the results to a larger extent than the choice of method for reinforcement design. This can be observed in the graphs with varying span-to-depth ratio or opening area percentage on the x-axis, where the value of the result tends to differ more between each point on the x-axis than between the different results for the two methods at the same geometry. This dependency will be discussed in detail in the evaluation of each result presented below. However, to draw general conclusions about how geometric parameters influence structural behaviour, and to determine under which conditions STM or SPM provides more accurate or efficient representations, additional analyses covering a wider range of geometries are necessary. Such studies would enable a more comprehensive understanding of the interaction between geometry and modelling strategy.

5.5 Reinforcement amount

For STM, changes in geometry, such as changes in opening size or increased beam length, can lead to sharp increases in required reinforcement when the STM layout is forced to change shape. In contrast, SPM generally produces a more uniformly distributed reinforcement pattern and, in most cases, requires less main reinforcement. Exceptions include geometries like the $1\,\mathrm{m} \times 1\,\mathrm{m}$ and $1.25\,\mathrm{m} \times 1.25\,\mathrm{m}$ openings, where SPM occasionally requires more, possibly indicating a more optimised STM layout in those cases.

STM offers greater flexibility, with reinforcement quantities heavily influenced by the designer's modelling decisions. SPM follows a more systematic approach but can be harder to apply practically, especially due to its varying reinforcement grids. There is room for optimisation in SPM, since the amount of reinforcement of the entire stringer is based on its peak force, potentially leading to over-dimensioning. Using a finer SPM mesh, as mentioned, could allow for more localised reinforcement and reduced total volume, though this may be challenging to implement in practice. It is also worth noting that the theoretical reinforcement differences observed in this study may be less relevant in real projects. Standard practices, such as rounding to the nearest available bar size, for example, to meet a minimum of $400\,\mathrm{mm}^2/\mathrm{m}$, can make small differences negligible. When the theoretically calculated differences between the models are small, they would likely be even less significant in practical applications. This is because factors such as rounding to standard bar sizes and other standard detailing constraints could have a greater influence on the final reinforcement layout than the choice of design method itself.

In agreement with previous research by Sgambi and Tarquini (2003), the results of this investigation show that the reinforcement requirements between STM and SPM are, overall, comparable. For some geometries, STM required up to 20% more reinforcement, while SPM exceeded STM by up to 2.6% just before the 6-meter beam. For beams with openings, SPM needed up to 32% more reinforcement in the most extreme case. Differences were generally more pronounced with openings, but no consistent trend emerged. Ultimately, beam geometry and modelling choices had a greater impact on the results than the chosen method itself.

5.6 Failure load and yielding of reinforcement

The evaluation of failure load and yielding behaviour offers insights into the performance and potential over-dimensioning associated with both STM and SPM. In all cases, failure loads exceed the design load of $3000\,\mathrm{kN}$, often significantly, indicating a substantial reserve capacity. This could be a result of STM and SPM both being based on the theory of lower bound plasticity, and would therefore provide models on the safe side, as described by Blaauwendraad (2018).

The failure loads range from approximately $6500\,\mathrm{kN}$ for the shortest beams to $3500\,\mathrm{kN}$ for the longest. For spans up to $6\,\mathrm{m}$, the failure load decreases linearly with length for both methods, showing a strong correlation. Beyond $6\,\mathrm{m}$, when the span-to-depth ratio is above 2, this trend weakens. It can also be found that shorter spans exhibit yielding in the bottom tensile reinforcement before failure, unlike longer beams, which fail beforehand. This suggests a changed behaviour at this point, and perhaps a different failure mode. This could also be observed in the crack pattern plots, where the shorter beams have large crack widths along the bottom, indicating bending failure, while the longer beams have a crack pattern indicating shear failure, which is in line with the observations of the cracking behaviour made by Haque et al. (1986). This could be why the tensile reinforcement does not yield for the longer beams. It could also have to do with local failures of the beam due to the beam not having sufficient material ductility, as suggested by Engström (2015). For span-to-depth ratios above 2, the differences between the two methods also become more pronounced, with SPM generally offering higher ultimate capacities. This could be because STM beams have a layout change at this point, and, unlike for shorter beams, are not as similar to the SPM layout for those beams. The SPM beams also have slightly more distributed reinforcement, which resists the shear forces.

In beams with openings, STM achieves higher failure loads, particularly for larger openings. The absence of yielding below large openings aligns with the low tensile demands at that point expected from the geometry. These differences may reflect how each method handles stress redistributions around discontinuities and openings, and how reinforcement is distributed in those areas. Yielding behaviour further supports the conclusion of over-dimensioning. At the design load, none of the beams reaches yielding in the tensile reinforcement. This could, besides the over-dimensioning, possibly be due to the reinforcement modelling in the FEA, which assumes a single-layer concentration of the reinforcement, potentially leading to local stiffness effects and altered stress distribution, which may not fully capture a realistic behaviour.

A comparison of reinforcement quantities and failure loads shows that for span-to-depth ratios below 2, the two methods exhibit similar efficiency in terms of total reinforcement volume in comparison to ultimate load capacity, as can be seen in Figure 4.1 and Figure 4.10. For ratios above this point, beams designed using SPM require less reinforcement while achieving higher ultimate load capacities, indicating a more efficient design. In contrast, for beams with varying opening sizes, STM consistently results in lower total reinforcement volumes and higher failure loads in all cases except for the beam with the largest opening, as shown in Figure 4.2 and Figure 4.11.

Since all beams are designed for the same load, the differences in failure load suggest that the geometry has a greater influence than reinforcement layout when it comes to ultimate load capacity. One reason for the higher failure loads in shorter beams may be the uniform application of minimum grid reinforcement across all beam lengths. In STM, this is constant regardless of size, and in SPM, it remains unchanged in panels without higher local demands. As a result, shorter beams, with relatively low tensile reinforcement needs, receive disproportionately high reinforcement amounts. This surplus may enhance tensile resistance, reducing stress in the main tensile reinforcement and preventing it from reaching yielding, even under high loads. Accounting for neighbouring grid reinforcement in regions with tensile reinforcement may allow for reduced reinforcement without compromising performance.

Lastly, while higher failure loads may imply robustness, they may also imply inefficiency if achieved through excessive material use. If a design approach systematically has higher failure capacities than needed, there could be a case for revisiting the applied safety factors or partial factors associated with that method. However, such conclusions would require broader validation across more cases.

5.7 Deflection and cracking behaviour

From the point at which cracking initiates in the beam, the mid-span deflection increases significantly with increased span-to-depth ratio. For the largest spans, the beams designed with STM experience a slightly larger deflection for all load steps. This difference is for all cases smaller than $10\,\%$, except for at the ultimate load, where the difference is larger. The trend points towards a continuation of this difference also for even longer spans. The fact that the beams designed with STM experience larger deflections for the longest spans is in line with the crack pattern observations, where those beams developed more cracks than their SPM counterparts. However, no clear correlation between method and maximum crack width at failure could be established.

The maximum crack width along the bottom of the beams increases as the span length increases, but no clear trend of whether either of the two methods gives larger crack widths than the other can be identified. This is reasonable since the reinforcement design obtained from both methods is relatively similar, especially up to $6.5\,\mathrm{m}$ span length. Both methods demonstrated scattered results in terms of crack widths, especially at failure load, likely due to local effects and, as mentioned, modelling assumptions. The maximum crack width for the beams is not always that of a crack proceeding from the bottom of the beam, but can also be found in the compressive diagonal struts, for beams designed with both STM and SPM. The crack patterns in the beams without openings, designed using both STM and SPM, generally follow the trajectories of the principal stresses, aligning with the statements made by Haque et al. (1986). A similar trend is observed in the beams with openings, though the correspondence is somewhat less distinct.

When observing the results of the beams with openings, the mid-span deflections tend to decrease as the size of the opening increases, which can be explained by the behaviour going towards a more beam-column-like behaviour. These observations regarding

the deflections are found in beams designed with both STM and SPM, with just a small difference in deflection. For both the mid-span deflection as well as for the deflection above the opening, the beams designed with STM experience slightly larger deflections for most cases, especially for the larger openings. This may be due to its more distributed reinforcement and stress field, which could lead to smaller and more widely spaced cracks. The mid-span deflections are, however, relatively similar regardless of opening size at the load $0.6P_d$ for both methods, which is before the cracks have formed. This confirms the statements made by Yang et al. (2006). The maximum crack width along the bottom of the beams with openings shows a slight increase as the opening size increases, but with no clear trend of which method gives larger crack widths. The maximum crack width can, just as for the beams without openings, also be found in the compressive diagonal struts. This is the case for beams designed with both STM and SPM, but mostly in the beams with smaller openings. The maximum crack width can also be found adjacent to the opening, where stress concentrations tend to occur.

While deflections and crack widths are primarily relevant for serviceability states, their values at both the design load and the ultimate load were also analysed in this study to gain a deeper understanding of the structural behaviour associated with the two design methods. The general trends that can be observed in this study are that for short beams and beams with small openings, both STM and SPM perform comparably in terms of crack development and deflection. For long beams, SPM shows a slight advantage in controlling deflections and reducing crack widths near failure, which can be due to the amount of distributed reinforcement. For beams with large openings, SPM results in smaller deflections both above and below the openings. However, despite these observations, it is difficult to establish a definitive preference for one method over the other across all geometries and load cases, as discussed in section 5.4.

5.8 Applicability of analytical calculations

The comparison between analytical calculations and FEA highlights both the strengths and limitations of simplified methods used for analytical calculations. The findings indicate that the assumptions made in analytical calculations may not always reflect a realistic behaviour.

As previously mentioned, FEA results show that tensile reinforcement does not reach yielding at the design load in any configuration, and in some cases, not even at failure. One explanation for this may be the simplifications made in the analytical calculations when designing the reinforcement, leading to conservative estimates and potential overdimensioning. No regard is taken to the tension carried by the concrete or grid reinforcement, and in SPM, the entire reinforcement area is designed from the largest normal force, meaning most of the reinforcement area is larger than needed.

Analytical stress distributions, especially in the tensile reinforcement, remain consistent across all configurations, as shown in STM and SPM results. However, FEA results suggest a more nuanced reality with a stress distribution that lies between the ones assumed by STM and SPM, with local variations dependent on geometry, span length, load level,

and the presence of openings. This suggests that analytical assumptions, though useful, oversimplify real behaviour. Although analytical assumptions provide a reasonable approximation in the linear elastic range, they become increasingly inaccurate as non-linear effects such as cracking and redistribution occur.

When the beam enters the non-linear range and cracking initiates, the analytical models tend to underestimate the deflections, since they rely on linear elastic assumptions and neglect stiffness degradation. For shorter spans and lower loads, the agreement is generally acceptable since no extensive cracking has yet taken place in those cases, but differences grow with increasing span-to-depth ratio or structural discontinuities like openings. The analytically calculated crack widths for the SPM and STM designed beams are equally close to the FEA results, there is no notable difference depending on the method used. The best correlation between the analytical and the FEA results is around the span-to-depth ratio of 2. For the beams with openings, the correlation is somewhat better overall.

In almost all cases, the analytical predictions underestimate deflections relative to non-linear FEA results as well as to linear-elastic FEA. This may be due to simplifications in how stiffness is modelled in analytical approaches, particularly concerning reinforcement positioning and boundary conditions. These findings emphasise the need to consider stiffness degradation explicitly when evaluating serviceability limits such as deflection. Overall, analytical calculations remain useful for estimating structural response under service conditions. However, their applicability diminishes when non-linear behaviour dominates.

5.8.1 Change of stiffness

The results indicate that analytical displacement calculations using SPM are valid only in the linear, uncracked range. To better approximate deflections in the non-linear state, the panel and stringer stiffnesses were reduced using factors of 0.1 and 0.2 to simulate the effects of cracking.

As shown in section 4.4, applying these reduction factors led to varying accuracy. For short-span beams, both factors tended to overestimate deflections compared to non-linear FEA. In contrast, for beams longer than approximately $6\,\mathrm{m}$, even the 0.1 factor underestimated deflections. At a load level of $0.6P_d$, the match improved notably for longer beams when using a 0.1 factor. For the shortest spans, a factor slightly above 0.2 might be more appropriate. However, additional investigations are required to confirm and refine these preliminary trends, particularly for other beam depths and cross-sectional properties.

These findings suggest that a constant stiffness reduction factor is insufficient across all beam configurations. A more accurate approach might involve a stiffness factor dependent on span-to-depth ratio, span length, or other parameters such as load level, crack initiation, or tensile reinforcement stress. Since cracking evolves differently across load steps, the effective stiffness and thus deflection vary accordingly. For uncracked states, a factor of

1.0 may be valid, while cracked sections exposed to high loads require substantially lower values.

For beams with openings, a 0.2 stiffness factor approximated mid-span deflection reasonably well at $3000\,\mathrm{kN}$. However, for other load levels and deflections above the opening, especially at lower loads, this factor consistently overestimated the deflection. The 0.1 factor was consistently too conservative. These results suggest that a uniform stiffness reduction is insufficient in the presence of openings. Nevertheless, a simplified reduction factor may still be useful for practical design because the critical deflection typically occurs at mid-span. A more comprehensive solution would involve developing an empirical stiffness factor that also accounts for opening size as a percentage of cross-sectional area. However, to establish such a factor with sufficient reliability, further investigations are necessary. This includes studying beams with different heights, opening sizes, and placements.

6

Conclusion

This study compares two reinforcement design methods for D-regions in concrete structures, the Strut-and-Tie Method (STM) and the Stringer-Panel Method (SPM). These were applied to deep beams with varying span-to-depth ratios and central openings of different sizes. The goal of the study was to assess the applicability and accuracy of analytical calculations and reinforcement design made with SPM, particularly in comparison to the more established STM. The results indicate that although SPM is less commonly used in practice, it performs on a comparable level to STM and can be considered a fully viable alternative for design.

6.1 General conclusions

In the ultimate limit state (ULS), both methods showed substantial reserve capacity, particularly in shorter spans, indicating a trend toward over-dimensioning. The results indicate that SPM exhibits certain tendencies to better prevent shear failure compared to STM, due to more distributed reinforcement. For larger span-to-depth ratios, SPM results in lower reinforcement requirements and higher failure loads compared to STM. Conversely, for beams with openings, STM generally yields lower reinforcement quantities while still achieving higher failure loads. The parametric analysis showed that variations in span-to-depth ratio and opening size led to comparable crack widths and deflections for beams designed with both methods. However, for longer spans, SPM exhibited slightly lower deflections. Overall, it can be concluded that SPM is generally more robust to geometric variations, whereas STM is more sensitive to modelling assumptions.

Analytical calculations using SPM showed acceptable approximations of structural behaviour under service loads and for configurations within the linear elastic range. However, its accuracy in predicting crack widths, deflections, and stress distributions in the non-linear range remains limited. The findings suggest that such analytical models are best suited as preliminary design tools or as complements to finite element analysis (FEA). However, a key advantage of SPM is its ability to directly estimate the deflections by analytical calculations. The findings also suggest that introducing an appropriate stiffness reduction factor could enable SPM to better estimate deflections in the post-cracking stage, expanding its design potential.

Both methods are valid for design purposes. SPM reduces the risk of significant modelling errors by the designer by being easier to automate and standardise, although it may also

limit some opportunities for optimisation. STM remains reliable for conservative ULS design and offers much freedom to the designer. No definitive conclusion can be drawn regarding the overall superiority of one method, and hence, no recommendations can be made at this stage.

6.2 Further research

While this study provides insight into the behaviour of reinforced concrete beams designed using STM and SPM, several aspects remain open for further investigation. Additional research is needed to draw more general conclusions about the limitations and differences between the two methods, as well as the applicability of the analytical calculations. This is also needed for the calibration of a stiffness reduction factor for estimating deflections of SPM beams. Further research should include a broader range of D-regions and load cases. This could involve variations such as the placement and number of openings, dapped ends, and different cross-sectional dimensions. Exploring how the methods perform under different loading conditions would also help assess their robustness and adaptability in practical applications.

Further verification of the DIANA model is necessary to ensure the validity of the comparisons with FEA results. This includes calibrating the model against more comprehensive experimental results to confirm that it reliably represents the real structural behaviour of deep beams. Conducting physical beam tests under controlled laboratory conditions would be particularly valuable in validating both the numerical simulations and the analytical predictions. Additionally, the stiffness reduction factor applied in the analytical model could be refined by calibrating against experimental data, helping to identify appropriate reduction factors for practical use.

Another promising area of further research is the exploration of different SPM layouts for identical beam geometries. It would be of interest to assess how sensitive the results are to variations in mesh size, panel arrangement, or the degree of discretisation. For example, dividing the beam into smaller panels might lead to more efficient reinforcement distributions, but this effect needs to be quantified through systematic studies.

Bibliography

Abdulmajed, D. A. A., Daud, S. A., & Alrshoudi, F. (2024). Numerical Validation of Long-term Behaviour of Reinforced Recycled Aggregate Concrete Beam. *Sciendo*, *20*(2), 1129–1139. https://doi.org/10.2478/CEE-2024-0082

Al-Ahmed, A., Khalaf, M. R., & Hussein, A. (2017). Openings effect on the performance of reinforced concrete deep beams. https://doi.org/10.13140/RG.2.2.35749.96481

Alañón, A., Cerro-Prada, E., Vázquez-Gallo, M. J., & Santos, A. P. (2018). Mesh size effect on finite-element modeling of blast-loaded reinforced concrete slab. *Engineering with Computers*, *34*(4), 649–658. https://doi.org/10.1007/s00366-017-0564-4

Amini Najafian, H., & Vollum, R. L. (2013). Design of planar reinforced concrete D regions with nonlinear finite element analysis. *Engineering Structures*, *51*, 211–225. https://doi.org/10.1016/j.engstruct.2013.01.022

Bauchau, O. A., & Craig, J. I. (2009). Euler-Bernoulli beam theory. In *Structural analysis* (pp. 173–221). Springer, Dordrecht. https://doi.org/10.1007/978-90-481-2516-6{_}5

Blaauwendraad, J., & Hoogenboom, P. C. J. (1997). Discrete elements in structural concrete design. *HERON*, *42*(3).

Blaauwendraad, J. (2018). *Stringer-Panel Models in Structural Concrete Applied to D-region Design*. Springer. https://doi.org/https://doi.org/10.1007/978-3-319-76678-2

Blaauwendraad, J., & Hoogenboom, P. C. J. (2002). Design Instrument SpanCAD for Shear Walls and D-regions. *fib Congres*.

CEB-FIP Model Code 90. (1993).

Chai, S. (2020). *Finite Element Analysis for Civil Engineering with DIANA Software*. Springer. https://doi.org/10.1007/978-981-15-2945-0

Danish Transport Construction and Housing Authority. (2020). *DS/EN 1992-1-1 DK NA:2021* (tech. rep.). Danish Transport, Construction; Housing Authority. www.eurocodes.dk.

Dashlejeh, A. A., & Arabzadeh, A. (2019). Experimental and analytical study on reinforced concrete deep beams. *International Journal of Structural Engineering*, *10*(1), 1–24. https://doi.org/10.1504/IJSTRUCTE.2019.101408

de Mello, A. F. A., & de Souza, R. A. (2016). Analysis and Design of Reinforced Concrete Deep Beams by a Manual Approach of Stringer-Panel Method. *Latin American Journal of Solids and Structures*, *13*(6), 1126–1151. https://doi.org/10.1590/1679-78252623

DIANA FEA BV. (n.d.). *Linear Elastic Analysis of a Deep Beam with Web Opening* (tech. rep.). https://dianafea.com

DIANA FEA BV. (2017). DIANA Finate Element Analysis User's Manual. https://manuals.dianafea.com/d102/GetStart/GetStart.html

DIANA FEA BV. (2024a). DIANA User's Manuals. https://manuals.dianafea.com/d108/en/index-en.html

DIANA FEA BV. (2024b). Theory Manual. https://manuals.dianafea.com/d108/en/1219784-1219784-theory-108.html

Dolan, C. W., & Trey Hamilton, H. R. (2019). *Prestressed Concrete: Building, Design, and Construction*. Springer. https://doi.org/10.1007/978-3-319-97882-6

Engström, B. (2015). *Design and analysis of deep beams, plates and other discontinuity regions* (tech. rep.). CHALMERS UNIVERSITY OF TECHNOLOGY. Göteborg.

fib. (2010). fib Bulletin no 55. Model Code 2010 - First complete draft (G. L. Balázs, Ed.). *International Federation for Structural Concrete*, *1*. https://doi.org/10.35789/FIB.BULL.0055

Godínez, S. E., & Restrepo, J. I. (2023). Stringer-panel model to support the seismic design and response verification of building diaphragms. *Resilient Cities and Structures*, *2*(1), 46–67. https://doi.org/10.1016/J.RCNS.2023.02.003

Hamoda, A., Yehia, S. A., Ahmed, M., Abadel, A. A., Baktheer, A., & Shahin, R. I. (2024). Experimental and numerical analysis of deep beams with openings strengthened with galvanized corrugated and flat steel sheets. *Case Studies in Construction Materials*, *21*. https://doi.org/10.1016/j.cscm.2024.e03522

Haque, M., Rasheeduzzafar & Al-Tayyib, A. H. J. (1986). Stress Distribution in Deep Beams with Web Openings. *Journal of Structural Engineering*, *112*(5), 1147–1165. https://doi.org/10.1061/(ASCE)0733-9445(1986)112:5(1147)

Hoogenboom, P. (2017, November). *Stringer-Panel Method Element and verification manual* (tech. rep.). Delft. http://homepage.tudelft.nl/p3r3s/panelpaper.pdf

Jensen, B. C. (2012). *Beton-konstruktioner efter DS/EN1992-1-1* (2nd ed.). Nyt Teknisk Forlag.

Modéer, M. (1979). A Fracture Mechanics Approach to Failure Analyses of Concrete Materials. (3).

Mohamed, A. R., Shoukry, M. S., & Saeed, J. M. (2014). Prediction of the behavior of reinforced concrete deep beams with web openings using the finite ele ment method. *Alexandria Engineering Journal*, *53*(2), 329–339. https://doi.org/10.1016/j.aej.2014.03.001

Mohammedali, T. K., Mustafa Jalil, A., Saleem Abdul-Razzaq, K., & Mohammed, A. H. (2019). STM Experimental Verification For Reinforced Concrete Continuous Deep Beams. *International Journal of Civil Engineering and Technology (IJCIET)*, *10*(2), 2227–2239. http://www.iaeme.com/ijciet/issues.asp?JType=IJCIET&VType=10&IType=2http://www.iaeme.com/IJCIET/index.asp2228http://www.iaeme.com/ijciet/issues.asp?JType=IJCIET&VType=10&IType=2

Plos, M. (1996). *Finite element analyses of reinforced concrete structures*. CHALMERS UNIVERSITY OF TECHNOLOGY.

Schlaich, J., Schaefer, K., & Jennewein, M. (1987). Toward a Consisten Design of Structural Concrete. *PCI Journal*, *32*(3), 74–150. https://doi.org/10.15554/pcij.05011987.74.150

Sgambi, L., & Tarquini, G. (2003). Stringer Panel Method: a discrete model to project structural reinforced concrete elements. https://www.researchgate.net/publication/258847788

Swedish Standards Institute. (2008). *SS-EN 1992-1-1:2005, Eurocode 2: Design of concrete structures - Part 1-1: General rules and rules for buildings* (tech. rep.). www.sis.se

Swedish Standards Institute. (2010). *Standard - Eurokod - Grundläggande dimensioneringsregler för bärverk SS-EN 1990 - Svenska institutet för standarder, SIS* (tech. rep.). https://www.sis.se/produkter/byggnadsmaterial-och-byggnader/byggnadsindustrin/tekniska-aspekter/ssen1990/

Szczecina, M., & Winnicki, A. (2018). Analysis of "D" Regions of RC Structures Based on Example of Frame Corners. *AIP Conference Proceedings*, *1922*. https://doi.org/10.1063/1.5019132

Yang, K. H., Eun, H. C., & Chung, H. S. (2006). The influence of web openings on the structural behavior of reinforced high-strength concrete deep beams. *Engineering Structures*, *28*, 1825–1834. https://doi.org/10.1016/j.engstruct.2006.03.021

Zhang, H., Liu, X., & Yi, W. (2014). Reinforcement Layout Optimisation of RC D-regions. *17*(7). https://doi.org/https://doi.org/10.1260/1369-4332.17.7.979

A

Strut-and-Tie modelling

A.1 Python script for stress field plot

The script used in this thesis to find the elastic stress field in the software DIANA to design the deep beams with the Strut-and-Tie Method can be found on the following link: https://github.com/henryssonemma/py-SPM-STM-deep-beam.git

The script is to be pasted in the command field in the commercial software DIANA. The first part of the script is the input data for the beams. The added force, the geometry, and the material input for the concrete and plates. The second part of the script creates materials and geometries. The third part assigns the material properties to the geometries. The fourth part ad boundary conditions and loads. The last part creates a mesh, a linear analysis, and runs the analysis. The output will be a screenshot of the elastic stress field of the modelled beam.

A.2 STM data from Truss Pilot

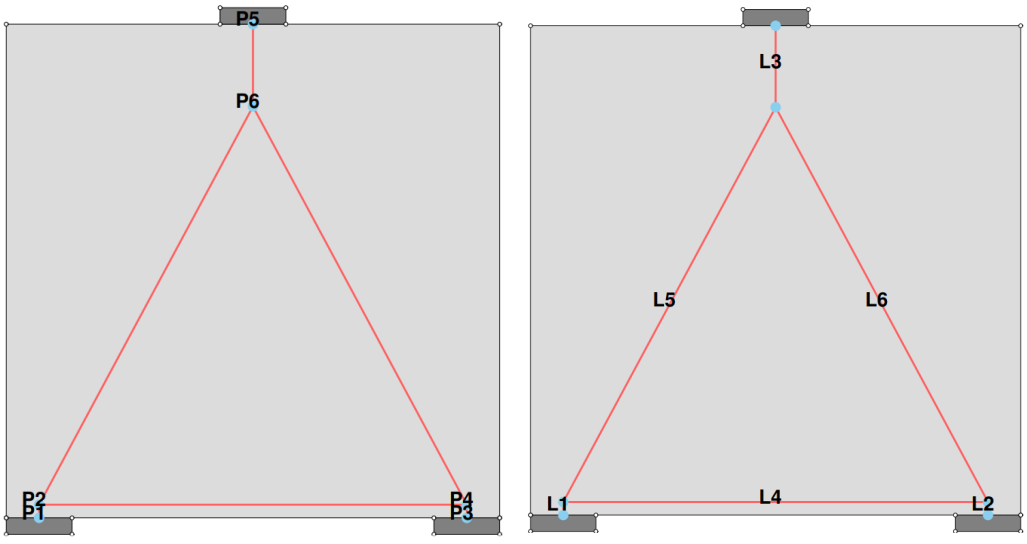

Figure A.1: Node and strut/tie numbering, beam of 3 m x 3 m

Table A.1: Node information, beam of 3 m x 3 m

	x [mm]	y [mm]	d [mm]	Node Type	$\sigma_{Rd,\max}$ [MPa]
P1	200	0	400.0	C	26.4
P2	200	80	400.0	CTC	22.4
P3	2800	0	400.0	C	26.4
P4	2800	80	400.0	CTC	22.4
P5	1500	3000	400.0	C	26.4
P6	1500	2500	400.0	CCC	26.4

Table A.2: Strut and tie information, beam of 3 m x 3 m

	P_1	P_2	L [mm]	N [kN]	A_s [mm^2]	w_1 [mm]	w_2 [mm]
L1	P1	P2	80	-1500.0	-	142	167
L2	P3	P4	80	-1500.0	-	142	167
L3	P5	P6	500	-3000.0	-	284	284
L4	P2	P4	2600	805.8	1611	-	-
L5	P2	P6	2747	-1702.7	-	189	161
L6	P6	P4	2747	-1702.7	-	161	189

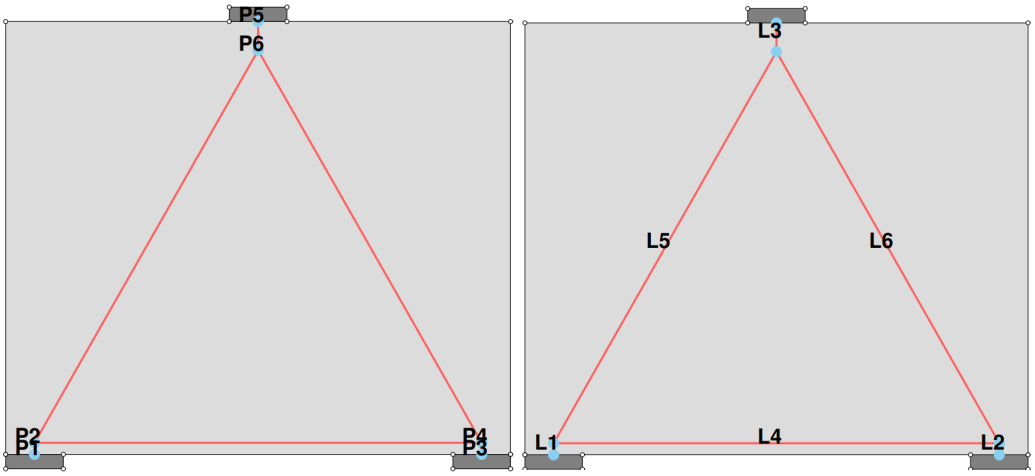

Figure A.2: Node and strut/tie numbering, beam of 3.5 m x 3 m

Table A.3: Node information, beam of 3.5 m x 3 m

	x [mm]	y [mm]	d [mm]	Node Type	$\sigma_{Rd,\max}$ [MPa]
P1	200	0	400.0	C	26.4
P2	200	80	400.0	CTC	22.4
P3	3300	0	400.0	C	26.4
P4	3300	80	400.0	CTC	22.4
P5	1750	3000	400.0	C	26.4
P6	1750	2800	400.0	CCC	26.4

Table A.4: Strut and tie information, beam of 3.5 m x 3 m

	P_1	P_2	L [mm]	N [kN]	A_s [mm^2]	w_1 [mm]	w_2 [mm]
L1	P1	P2	80	-1500.0	-	142	167
L2	P3	P4	80	-1500.0	-	142	167
L3	P5	P6	200	-3000.0	-	284	284
L4	P2	P4	3100	854.8	1709	-	-
L5	P2	P6	3130	-1726.5	-	192	163
L6	P6	P4	3130	-1726.5	-	163	192

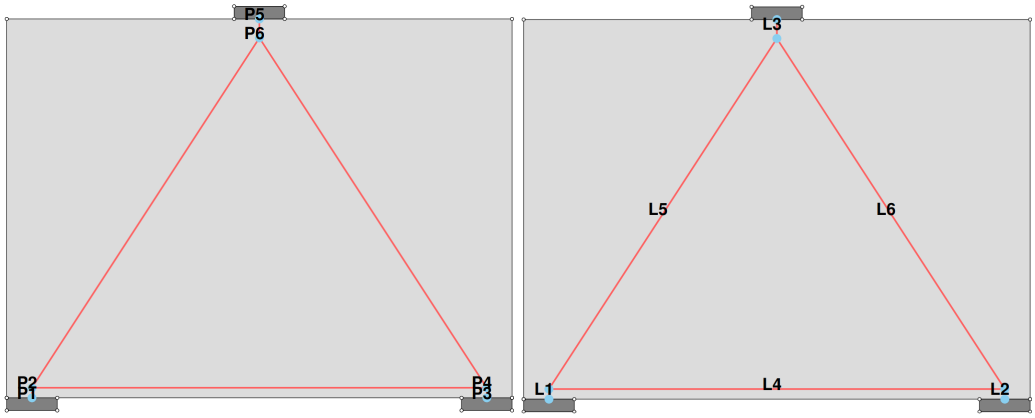

Figure A.3: Node and strut/tie numbering, beam of 4 m x 3 m

Table A.5: Node information, beam of 4 m x 3 m

	x [mm]	y [mm]	d [mm]	Node Type	$\sigma_{Rd,\max}$ [MPa]
P1	200	0	400.0	C	26.4
P2	200	80	400.0	CTC	22.4
P3	3800	0	400.0	C	26.4
P4	3800	80	400.0	CTC	22.4
P5	2000	3000	400.0	C	26.4
P6	2000	2850	400.0	CCC	26.4

Table A.6: Strut and tie information, beam of 4 m x 3 m

	P_1	P_2	L [mm]	N [kN]	A_s [mm^2]	w_1 [mm]	w_2 [mm]
L1	P1	P2	80	-1500.0	-	142	167
L2	P3	P4	80	-1500.0	-	142	167
L3	P5	P6	150	-3000.0	-	284	284
L4	P2	P4	3600	974.7	1949	-	-
L5	P2	P6	3303	-1788.9	-	199	169
L6	P6	P4	3303	-1788.9	-	169	199

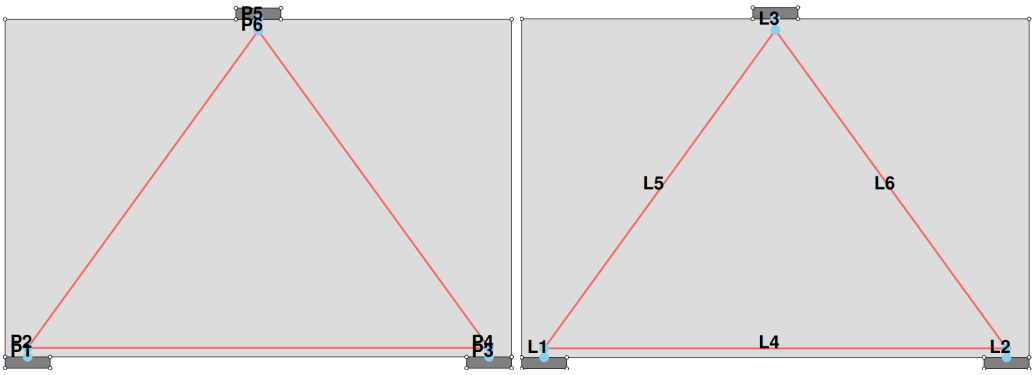

Figure A.4: Node and strut/tie numbering, beam of $4.5\,\mathrm{m}$ x $3\,\mathrm{m}$

Table A.7: Node information, beam of $4.5\,\mathrm{m}$ x $3\,\mathrm{m}$

	x [mm]	y [mm]	d [mm]	Node Type	$\sigma_{Rd,\max}$ [MPa]
P1	200	0	400.0	C	26.4
P2	200	80	400.0	CTC	22.4
P3	4300	0	400.0	C	26.4
P4	4300	80	400.0	CTC	22.4
P5	2250	3000	400.0	C	26.4
P6	2250	2900	400.0	CCC	26.4

Table A.8: Strut and tie information, beam of $4.5\,\mathrm{m}$ x $3\,\mathrm{m}$

	$\mathbf{P_1}$	$\mathbf{P_2}$	L [mm]	N [kN]	$\mathbf{A_s}$ [mm^2]	$\mathbf{w_1}$ [mm]	$\mathbf{w_2}$ [mm]
L1	P1	P2	80	-1500.0	-	142	167
L2	P3	P4	80	-1500.0	-	142	167
L3	P5	P6	100	-3000.0	-	284	284
L4	P2	P4	4100	1090.4	2180	-	-
L5	P2	P6	3486	-1854.5	-	206	175
L6	P6	P4	3486	-1854.5	-	175	206

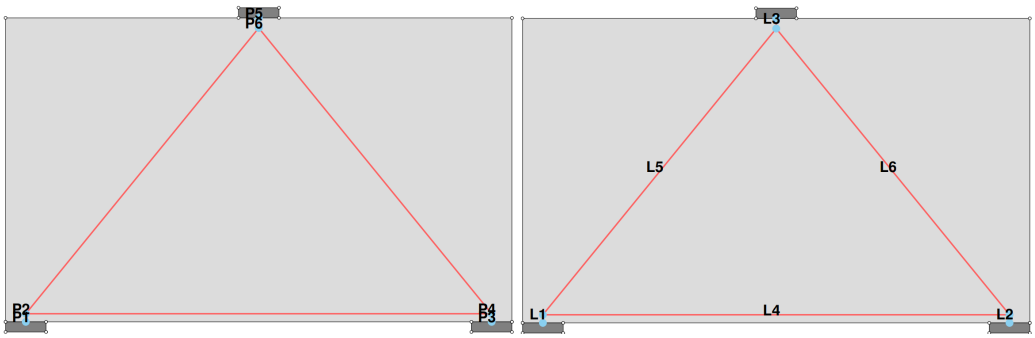

Figure A.5: Node and strut/tie numbering, beam of $5\,\mathrm{m}$ x $3\,\mathrm{m}$

Table A.9: Node information, beam of 5 m x 3 m

	x [mm]	y [mm]	d [mm]	Node Type	$\sigma_{Rd,\max}$ [MPa]
P1	200	0	400.0	C	26.4
P2	200	80	400.0	CTC	22.4
P3	4800	0	400.0	C	26.4
P4	4800	80	400.0	CTC	22.4
P5	2500	3000	400.0	C	26.4
P6	2500	2900	400.0	CCC	26.4

Table A.10: Strut and tie information, beam of 5 m x 3 m

	P_1	P_2	L [mm]	N [kN]	A_s [mm^2]	w_1 [mm]	w_2 [mm]
L1	P1	P2	80	-1500.0	-	142	167
L2	P3	P4	80	-1500.0	-	142	167
L3	P5	P6	100	-3000.0	-	284	284
L4	P2	P4	4600	1223.4	2446	-	-
L5	P2	P6	3639	-1935.6	-	215	183
L6	P6	P4	3639	-1935.6	-	183	215

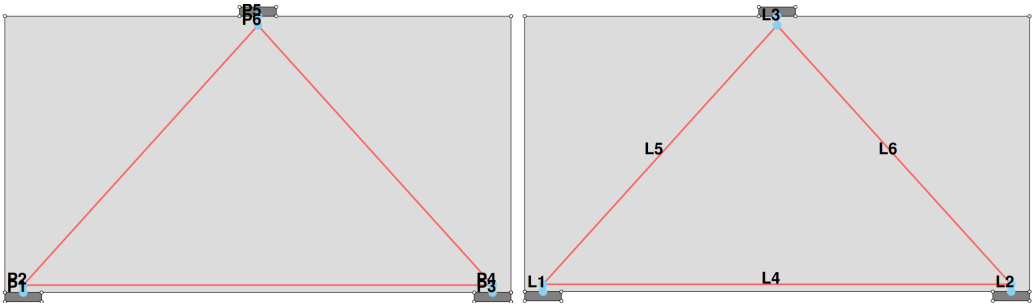

Figure A.6: Node and strut/tie numbering, beam of 5.5 m x 3 m

Table A.11: Node information, beam of 5.5 m x 3 m

	x [mm]	y [mm]	d [mm]	Node Type	$\sigma_{Rd,\max}$ [MPa]
P1	200	0	400.0	C	26.4
P2	200	80	400.0	CTC	22.4
P3	5300	0	400.0	C	26.4
P4	5300	80	400.0	CTC	22.4
P5	2750	3000	400.0	C	26.4
P6	2750	2900	400.0	CCC	26.4

Table A.12: Strut and tie information, beam of 5.5 m x 3 m

	P_1	P_2	L [mm]	N [kN]	A_s [mm^2]	w_1 [mm]	w_2 [mm]
L1	P1	P2	80	-1500.0	-	142	167
L2	P3	P4	80	-1500.0	-	142	167
L3	P5	P6	100	-3000.0	-	284	284
L4	P2	P4	5100	1356.4	2712	-	-
L5	P2	P6	3801	-2022.3	-	225	191
L6	P6	P4	3801	-2022.3	-	191	225

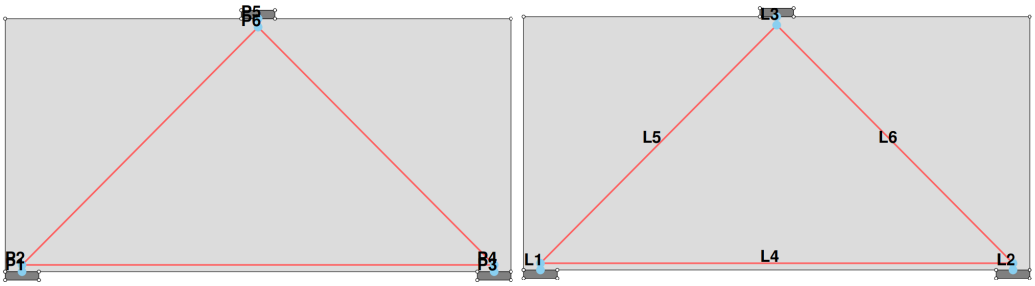

Figure A.7: Node and strut/tie numbering, beam of 6 m x 3 m

Table A.13: Node information, beam of 6 m x 3 m

	x [mm]	y [mm]	d [mm]	Node Type	$\sigma_{Rd,\max}$ [MPa]
P1	200	0	400.0	C	26.4
P2	200	80	400.0	CTC	22.4
P3	5800	0	400.0	C	26.4
P4	5800	80	400.0	CTC	22.4
P5	3000	3000	400.0	C	26.4
P6	3000	2900	400.0	CCC	26.4

Table A.14: Strut and tie information, beam of 6 m x 3 m

	P_1	P_2	L [mm]	N [kN]	A_s [mm^2]	w_1 [mm]	w_2 [mm]
L1	P1	P2	80	-1500.0	-	142	167
L2	P3	P4	80	-1500.0	-	142	167
L3	P5	P6	100	-3000.0	-	284	284
L4	P2	P4	5600	1489.4	2978	-	-
L5	P2	P6	3973	-2113.8	-	235	200
L6	P6	P4	3973	-2113.8	-	200	235

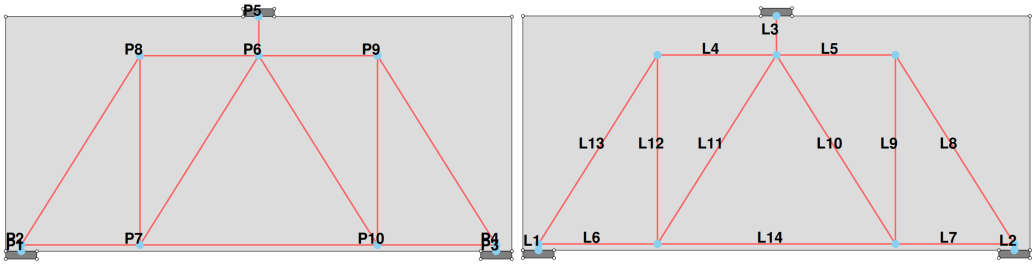

Figure A.8: Node and strut/tie numbering, beam of 6.5 m x 3 m

Table A.15: Node information, beam of 6.5 m x 3 m

	x [mm]	y [mm]	d [mm]	Node Type	$\sigma_{Rd,\max}$ [MPa]
P1	200	0	400.0	C	26.4
P2	200	80	400.0	CTC	22.4
P3	6300	0	400.0	C	26.4
P4	6300	80	400.0	CTC	22.4
P5	3250	3000	400.0	C	26.4
P6	3250	2500	400.0	CCCCC	26.4
P7	1725	80	400.0	TCTT	19.8
P8	1725	2500	400.0	CTC	22.4
P9	4775	2500	400.0	CCT	22.4
P10	4775	80	400.0	TTCT	19.8

Table A.16: Strut and tie information, beam of 6.5 m x 3 m

	P_1	**P_2**	**L [mm]**	**N [kN]**	**A_s [mm^2]**	**w_1 [mm]**	**w_2 [mm]**
L1	P1	P2	80	-1500.0	-	142	167
L2	P3	P4	80	-1500.0	-	142	167
L3	P5	P6	500	-3000.0	-	284	284
L4	P8	P6	1525	-945.2	-	105	89
L5	P6	P9	1525	-945.2	-	89	105
L6	P2	P7	1525	945.2	1890	-	-
L7	P10	P4	1525	945.2	1890	-	-
L8	P4	P9	2860	-1773.0	-	197	197
L9	P9	P10	2420	1500.0	3000	-	-
L10	P10	P6	2860	-1773.0	-	223	167
L11	P6	P7	2860	-1773.0	-	167	223
L12	P7	P8	2420	1500.0	3000	-	-
L13	P8	P2	2860	-1773.0	-	197	197
L14	P7	P10	3050	1890.5	3781	-	-

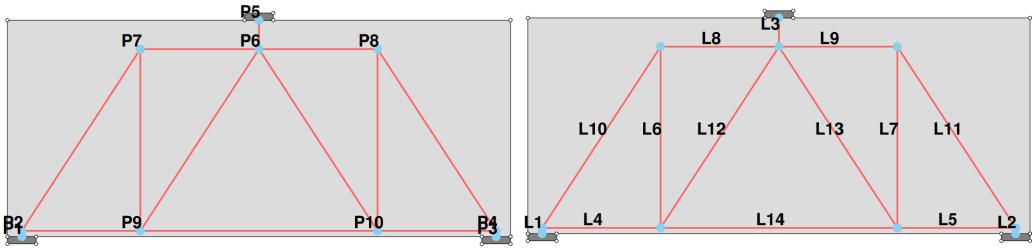

Figure A.9: Node and strut/tie numbering, beam of 7 m x 3 m

Table A.17: Node information, beam of 7 m x 3 m

	x [mm]	y [mm]	d [mm]	Node Type	$\sigma_{Rd,\max}$ [MPa]
P1	200	0	400.0	C	26.4
P2	200	80	400.0	CTC	22.4
P3	6800	0	400.0	C	26.4
P4	6800	80	400.0	CTC	22.4
P5	3500	3000	400.0	C	26.4
P6	3500	2600	400.0	CCCCC	26.4
P7	1850	2600	400.0	TCC	22.4
P8	5150	2600	400.0	TCC	22.4
P9	1850	80	400.0	TTCT	19.8
P10	5150	80	400.0	TTCT	19.8

Table A.18: Strut and tie information, beam of 7 m x 3 m

	P_1	**P_2**	**L [mm]**	**N [kN]**	**A_s [mm^2]**	**w_1 [mm]**	**w_2 [mm]**
L1	P1	P2	80	-1500.0	-	142	167
L2	P3	P4	80	-1500.0	-	142	167
L3	P5	P6	400	-3000.0	-	284	284
L4	P2	P9	1650	982.1	1964	-	-
L5	P10	P4	1650	982.1	1964	-	-
L6	P9	P7	2520	1500.0	3000	-	-
L7	P10	P8	2520	1500.0	3000	-	-
L8	P7	P6	1650	-982.1	-	109	93
L9	P6	P8	1650	-982.1	-	93	109
L10	P7	P2	3012	-1792.9	-	199	199
L11	P8	P4	3012	-1792.9	-	199	199
L12	P6	P9	3012	-1792.9	-	169	226
L13	P6	P10	3012	-1792.9	-	169	226
L14	P9	P10	3300	1964.3	3928	-	-

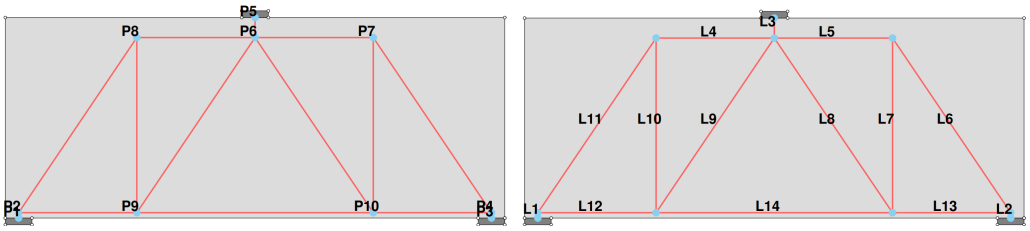

Figure A.10: Node and strut/tie numbering, beam of 7.5 m x 3 m

Table A.19: Node information, beam of 7.5 m x 3 m

	x [mm]	y [mm]	d [mm]	Node Type	$\sigma_{Rd,\max}$ [MPa]
P1	200	0	400.0	C	26.4
P2	200	80	400.0	CCT	22.4
P3	7300	0	400.0	C	26.4
P4	7300	80	400.0	CCT	22.4
P5	3750	3000	400.0	C	26.4
P6	3750	2700	400.0	CCCCC	26.4
P7	5525	2700	400.0	CCT	22.4
P8	1975	2700	400.0	CTC	22.4
P9	1975	80	400.0	CTTT	19.8
P10	5525	80	400.0	TCTT	19.8

Table A.20: Strut and tie information, beam of 7.5 m x 3 m

	P_1	**P_2**	**L [mm]**	**N [kN]**	**A_s [mm^2]**	**w_1 [mm]**	**w_2 [mm]**
L1	P1	P2	80	-1500.0	-	142	167
L2	P3	P4	80	-1500.0	-	142	167
L3	P5	P6	300	-3000.0	-	284	284
L4	P8	P6	1775	-1016.2	-	113	96
L5	P6	P7	1775	-1016.2	-	96	113
L6	P7	P4	3164	-1811.8	-	201	201
L7	P7	P10	2620	1500.0	3000	-	-
L8	P6	P10	3164	-1811.8	-	171	228
L9	P6	P9	3164	-1811.8	-	171	228
L10	P8	P9	2620	1500.0	3000	-	-
L11	P8	P2	3164	-1811.8	-	201	201
L12	P2	P9	1775	1016.2	2032	-	-
L13	P10	P4	1775	1016.2	2032	-	-
L14	P9	P10	3550	2032.4	4064	-	-

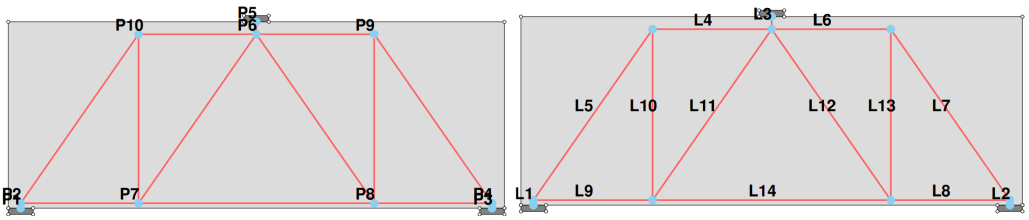

Figure A.11: Node and strut/tie numbering, beam of 8 m x 3 m

Table A.21: Node information, beam of 8 m x 3 m

	x [mm]	y [mm]	d [mm]	Node Type	$\sigma_{Rd,\max}$ [MPa]
P1	200	0	400.0	C	26.4
P2	200	80	400.0	CCT	22.4
P3	7800	0	400.0	C	26.4
P4	7800	80	400.0	CCT	22.4
P5	4000	3000	400.0	C	26.4
P6	4000	2800	400.0	CCCCC	26.4
P7	2100	80	400.0	TTCT	19.8
P8	5900	80	400.0	TCTT	19.8
P9	5900	2800	400.0	CCT	22.4
P10	2100	2800	400.0	CCT	22.4

Table A.22: Strut and tie information, beam of 8 m x 3 m

	$\mathbf{P_1}$	$\mathbf{P_2}$	L [mm]	N [kN]	$\mathbf{A_s}$ [mm^2]	$\mathbf{w_1}$ [mm]	$\mathbf{w_2}$ [mm]
L1	P1	P2	80	-1500.0	-	142	167
L2	P3	P4	80	-1500.0	-	142	167
L3	P5	P6	200	-3000.0	-	284	284
L4	P6	P10	1900	-1047.8	-	99	116
L5	P10	P2	3317	-1829.7	-	203	203
L6	P6	P9	1900	-1047.8	-	99	116
L7	P9	P4	3317	-1829.7	-	203	203
L8	P4	P8	1900	1047.8	2095	-	-
L9	P7	P2	1900	1047.8	2095	-	-
L10	P7	P10	2720	1500.0	3000	-	-
L11	P6	P7	3317	-1829.7	-	173	231
L12	P6	P8	3317	-1829.7	-	173	231
L13	P8	P9	2720	1500.0	3000	-	-
L14	P7	P8	3800	2095.6	4191	-	-

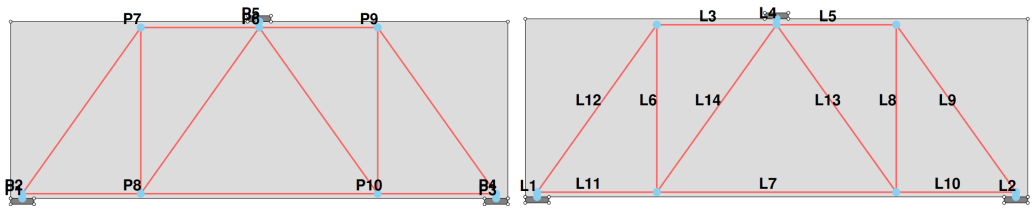

Figure A.12: Node and strut/tie numbering, beam of 8.5 m x 3 m

Table A.23: Node information, beam of 8.5 m x 3 m

	x [mm]	y [mm]	d [mm]	Node Type	$\sigma_{Rd,\max}$ [MPa]
P1	200	0	400.0	C	26.4
P2	200	80	400.0	CTC	22.4
P3	8300	0	400.0	C	26.4
P4	8300	80	400.0	CCT	22.4
P5	4250	3000	400.0	C	26.4
P6	4250	2900	400.0	CCCCC	26.4
P7	2225	2900	400.0	CTC	22.4
P8	2225	80	400.0	TTTC	19.8
P9	6275	2900	400.0	CTC	22.4
P10	6275	80	400.0	TTTC	19.8

Table A.24: Strut and tie information, beam of 8.5 m x 3 m

	P_1	**P_2**	**L [mm]**	**N [kN]**	**A_s [mm^2]**	**w_1 [mm]**	**w_2 [mm]**
L1	P1	P2	80	-1500.0	-	142	167
L2	P3	P4	80	-1500.0	-	142	167
L3	P7	P6	2025	-1077.1	-	119	101
L4	P5	P6	100	-3000.0	-	284	284
L5	P6	P9	2025	-1077.1	-	101	119
L6	P8	P7	2820	1500.0	3000	-	-
L7	P8	P10	4050	2154.3	4308	-	-
L8	P10	P9	2820	1500.0	3000	-	-
L9	P9	P4	3471	-1846.7	-	205	205
L10	P4	P10	2025	1077.1	2154	-	-
L11	P2	P8	2025	1077.1	2154	-	-
L12	P2	P7	3471	-1846.7	-	205	205
L13	P6	P10	3471	-1846.7	-	174	233
L14	P8	P6	3471	-1846.7	-	233	174

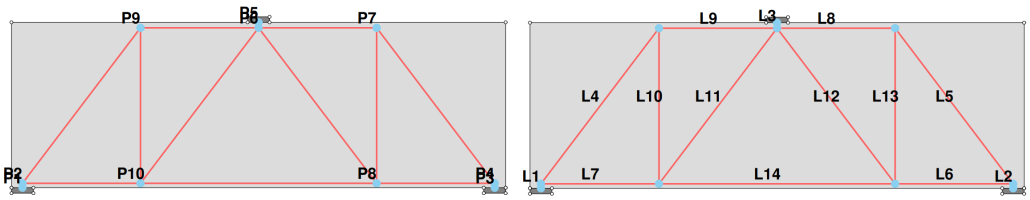

Figure A.13: Node and strut/tie numbering, beam of 9 m x 3 m

Table A.25: Node information, beam of 9 m x 3 m

	x [mm]	y [mm]	d [mm]	Node Type	$\sigma_{Rd,\max}$ [MPa]
P1	200	0	400.0	C	26.4
P2	200	80	400.0	CCT	22.4
P3	8800	0	400.0	C	26.4
P4	8800	80	400.0	CCT	22.4
P5	4500	3000	400.0	C	26.4
P6	4500	2900	400.0	CCCCC	26.4
P7	6650	2900	400.0	CCT	22.4
P8	6650	80	400.0	TCTT	19.8
P9	2350	2900	400.0	CCT	22.4
P10	2350	80	400.0	TTCT	19.8

Table A.26: Strut and tie information, beam of 9 m x 3 m

	P_1	**P_2**	**L [mm]**	**N [kN]**	**A_s [mm^2]**	**w_1 [mm]**	**w_2 [mm]**
L1	P1	P2	80	-1500.0	-	142	167
L2	P3	P4	80	-1500.0	-	142	167
L3	P5	P6	100	-3000.0	-	284	284
L4	P2	P9	3546	-1886.2	-	210	210
L5	P4	P7	3546	-1886.2	-	210	210
L6	P4	P8	2150	1143.6	2287	-	-
L7	P2	P10	2150	1143.6	2287	-	-
L8	P7	P6	2150	-1143.6	-	127	108
L9	P9	P6	2150	-1143.6	-	127	108
L10	P10	P9	2820	1500.0	3000	-	-
L11	P6	P10	3546	-1886.2	-	178	238
L12	P6	P8	3546	-1886.2	-	178	238
L13	P7	P8	2820	1500.0	3000	-	-
L14	P8	P10	4300	2287.2	4574	-	-

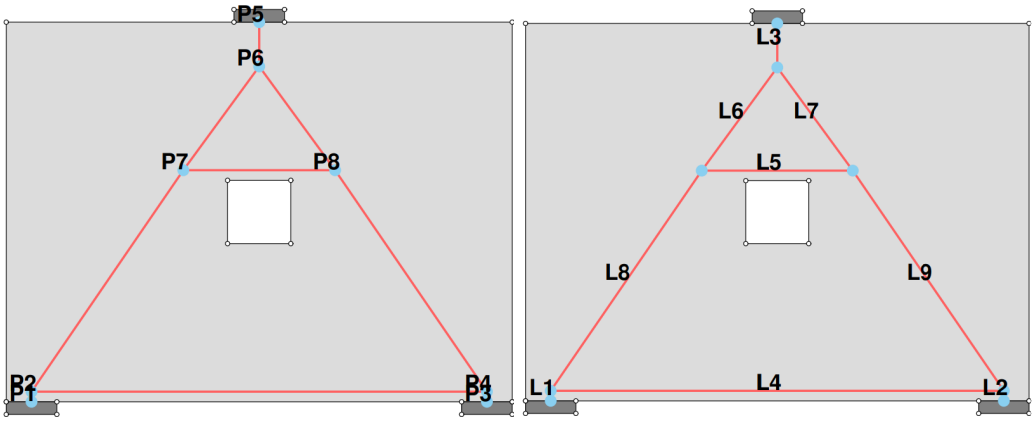

Figure A.14: Node and strut/tie numbering, beam of 4 m x 3 m with opening of 0.5 m x 0.5 m

Table A.27: Node information, beam of 4 m x 3 m with opening of 0.5 m x 0.5 m

	x [mm]	y [mm]	d [mm]	Node Type	$\sigma_{Rd,\max}$ [MPa]
P1	200	0	400.0	C	26.4
P2	200	80	400.0	CTC	22.4
P3	3800	0	400.0	C	26.4
P4	3800	80	400.0	CTC	22.4
P5	2000	3000	400.0	C	26.4
P6	2000	2650	400.0	CCC	26.4
P7	1400	1830	400.0	TCC	22.4
P8	2600	1830	400.0	TCC	22.4

Table A.28: Strut and tie information, beam of 4 m x 3 m with opening of 0.5 m x 0.5 m

	P_1	**P_2**	**L [mm]**	**N [kN]**	**A_s [mm^2]**	**w_1 [mm]**	**w_2 [mm]**
L1	P1	P2	80	-1500.0	-	142	167
L2	P3	P4	80	-1500.0	-	142	167
L3	P5	P6	350	-3000.0	-	284	284
L4	P2	P4	3600	1028.6	2057	-	-
L5	P7	P8	1200	69.0	138	-	-
L6	P7	P6	1016	-1858.7	-	207	176
L7	P6	P8	1016	-1858.7	-	176	207
L8	P7	P2	2121	-1818.8	-	202	202
L9	P8	P4	2121	-1818.8	-	202	202

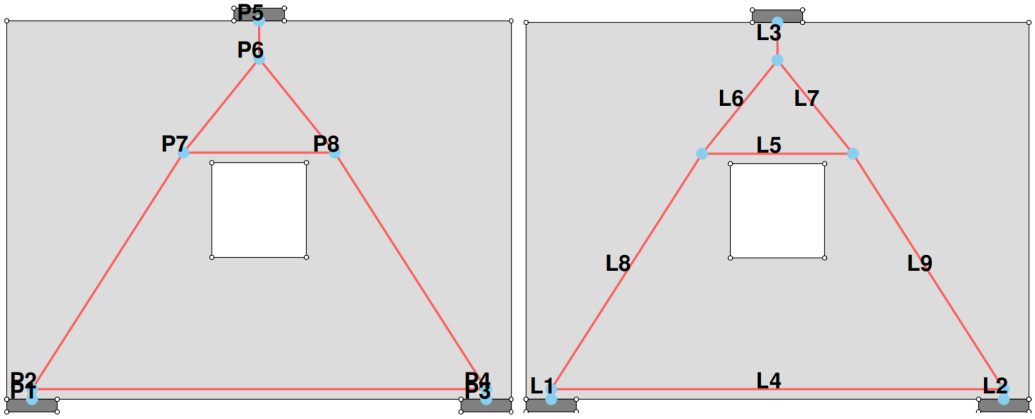

Figure A.15: Node and strut/tie numbering, beam of 4 m x 3 m with opening of 0.75 m x 0.75 m

Table A.29: Node information, beam of 4 m x 3 m with opening of 0.75 m x 0.75 m

	x [mm]	y [mm]	d [mm]	Node Type	$\sigma_{Rd,\max}$ [MPa]
P1	200	0	400.0	C	26.4
P2	200	80	400.0	CTC	22.4
P3	3800	0	400.0	C	26.4
P4	3800	80	400.0	CTC	22.4
P5	2000	3000	400.0	C	26.4
P6	2000	2700	400.0	CCC	26.4
P7	1400	1955	400.0	TCC	22.4
P8	2600	1955	400.0	TCC	22.4

Table A.30: Strut and tie information, beam of 4 m x 3 m with opening of 0.75 m x 0.75 m

	P_1	**P_2**	**L [mm]**	**N [kN]**	**A_s [mm²]**	**w_1 [mm]**	**w_2 [mm]**
L1	P1	P2	80	-1500.0	-	142	167
L2	P3	P4	80	-1500.0	-	142	167
L3	P5	P6	300	-3000.0	-	284	284
L4	P2	P4	3600	960.0	1920	-	-
L5	P7	P8	1200	248.1	496	-	-
L6	P7	P6	956	-1926.0	-	214	182
L7	P6	P8	956	-1926.0	-	182	214
L8	P7	P2	2226	-1780.9	-	198	198
L9	P8	P4	2226	-1780.9	-	198	198

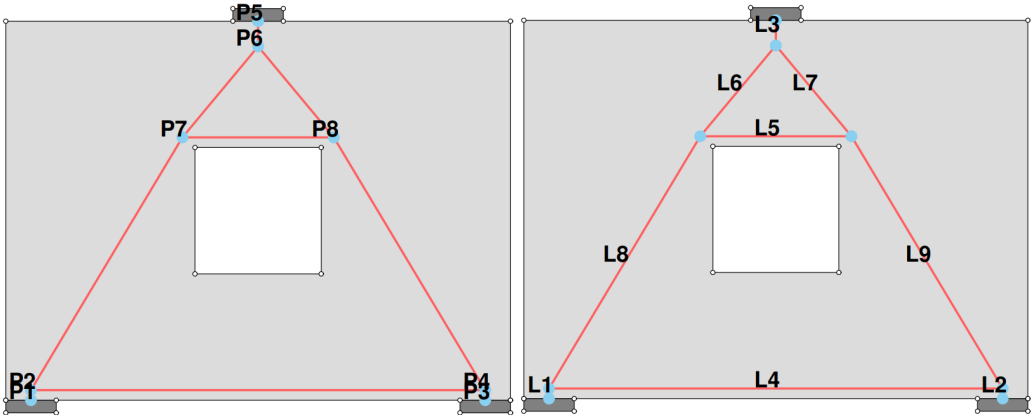

Figure A.16: Node and strut/tie numbering, beam of 4 m x 3 m with opening of 1.0 m x 1.0 m

Table A.31: Node information, beam of 4 m x 3 m with opening of 1.0 m x 1.0 m

	x [mm]	y [mm]	d [mm]	Node Type	$\sigma_{Rd,\max}$ [MPa]
P1	200	0	400.0	C	26.4
P2	200	80	400.0	CTC	22.4
P3	3800	0	400.0	C	26.4
P4	3800	80	400.0	CTC	22.4
P5	2000	3000	400.0	C	26.4
P6	2000	2800	400.0	CCC	26.4
P7	1400	2080	400.0	TCC	22.4
P8	2600	2080	400.0	TCC	22.4

Table A.32: Strut and tie information, beam of 4 m x 3 m with opening of 1.0 m x 1.0 m

	P_1	**P_2**	**L [mm]**	**N [kN]**	**A_s [mm^2]**	**w_1 [mm]**	**w_2 [mm]**
L1	P1	P2	80	-1500.0	-	142	167
L2	P3	P4	80	-1500.0	-	142	167
L3	P5	P6	200	-3000.0	-	284	284
L4	P2	P4	3600	900.0	1800	-	-
L5	P7	P8	1200	350.0	700	-	-
L6	P7	P6	937	-1952.6	-	217	184
L7	P6	P8	937	-1952.6	-	184	217
L8	P7	P2	2332	-1749.3	-	194	194
L9	P8	P4	2332	-1749.3	-	194	194

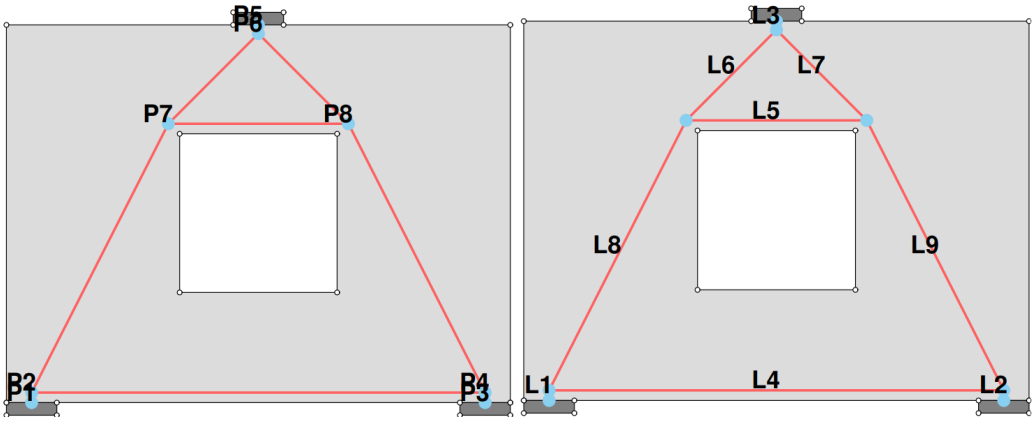

Figure A.17: Node and strut/tie numbering, beam of 4 m x 3 m with opening of 1.25 m x 1.25 m

Table A.33: Node information, beam of 4 m x 3 m with opening of 1.25 m x 1.25 m

	x [mm]	y [mm]	d [mm]	Node Type	$\sigma_{Rd,\max}$ [MPa]
P1	200	0	400.0	C	26.4
P2	200	80	400.0	CTC	22.4
P3	3800	0	400.0	C	26.4
P4	3800	80	400.0	CTC	22.4
P5	2000	3000	400.0	C	26.4
P6	2000	2931	400.0	CCC	26.4
P7	1285	2215	400.0	TCC	22.4
P8	2715	2215	400.0	TCC	22.4

Table A.34: Strut and tie information, beam of 4 m x 3 m with opening of 1.25 m x 1.25 m

	P_1	P_2	L [mm]	N [kN]	A_s [mm^2]	w_1 [mm]	w_2 [mm]
L1	P1	P2	80	-1500.0	-	142	167
L2	P3	P4	80	-1500.0	-	142	167
L3	P5	P6	69	-3000.0	-	284	284
L4	P2	P4	3600	762.3	1524	-	-
L5	P7	P8	1430	735.6	1471	-	-
L6	P7	P6	1011	-2119.8	-	236	200
L7	P6	P8	1011	-2119.8	-	200	236
L8	P7	P2	2394	-1682.6	-	187	187
L9	P8	P4	2394	-1682.6	-	187	187

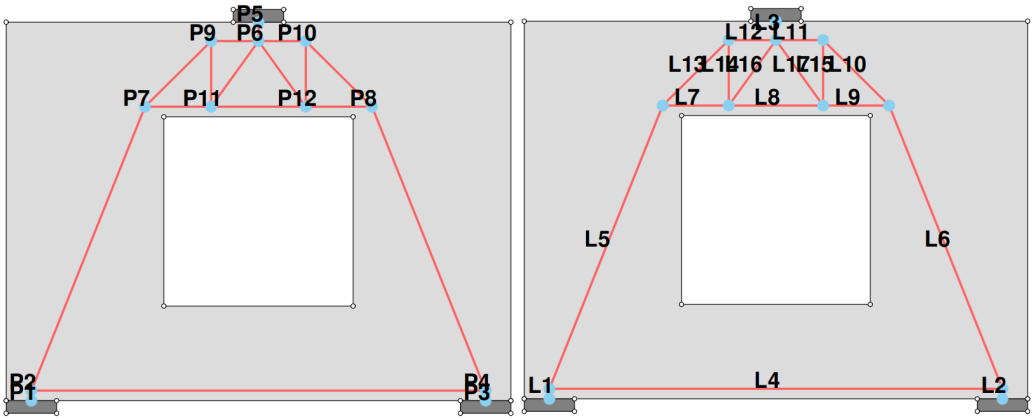

Figure A.18: Node and strut/tie numbering, beam of 4 m x 3 m with opening of 1.5 m x 1.5 m

Table A.35: Node information, beam of 4 m x 3 m with opening of 1.5 m x 1.5 m

	x [mm]	y [mm]	d [mm]	Node Type	$\sigma_{Rd,\max}$ [MPa]
P1	200	0	400.0	C	26.4
P2	200	80	400.0	CTC	22.4
P3	3800	0	400.0	C	26.4
P4	3800	80	400.0	CTC	22.4
P5	2000	3000	400.0	C	26.4
P6	2000	2850	400.0	CCCCC	26.4
P7	1100	2330	400.0	CTC	22.4
P8	2900	2330	400.0	CTC	22.4
P9	1625	2850	400.0	CCT	22.4
P10	2375	2850	400.0	CCT	22.4
P11	1625	2330	400.0	TTTC	19.8
P12	2375	2330	400.0	TTTC	19.8

Table A.36: Strut and tie information, beam of 4 m x 3 m with opening of 1.5 m x 1.5 m

	P_1	P_2	L [mm]	N [kN]	A_s [mm^2]	w_1 [mm]	w_2 [mm]
L1	P1	P2	80	-1500.0	-	142	167
L2	P3	P4	80	-1500.0	-	142	167
L3	P5	P6	150	-3000.0	-	284	284
L4	P2	P4	3600	600.0	1200	-	-
L5	P7	P2	2423	-1615.5	-	179	179
L6	P8	P4	2423	-1615.5	-	179	179
L7	P7	P11	525	914.4	1828	-	-
L8	P11	P12	750	1996.2	3992	-	-
L9	P12	P8	525	914.4	1828	-	-
L10	P8	P10	738	-2131.5	-	237	237
L11	P10	P6	375	-1514.4	-	168	143
L12	P6	P9	375	-1514.4	-	143	168
L13	P9	P7	738	-2131.5	-	237	237
L14	P9	P11	520	1500.0	3000	-	-
L15	P12	P10	520	1500.0	3000	-	-
L16	P6	P11	641	-1849.4	-	175	233
L17	P6	P12	641	-1849.4	-	175	233

A.3 Verification of truss pilot

```
%% Verification of truss pilot
clc
clear

% Geometry beam
T = 0.4; % [m]
H = 3; % [m]
L = 4; % [m]
d = 0.08; % [m]
p = 0.4; %[m]

% Concrete
f_c = 30*10^6; % [Pa] Compressive strength

% EC2 parameters and calculations
k_1 = 1;
k_2 = 0.85;
k_3 = 0.75;

v = 1-f_c/(250*10^6);

sigma_Rd_max_CCC = k_1*v*f_c; % [Pa]
sigma_Rd_max_CCT = k_2*v*f_c; % [Pa]
sigma_Rd_max_CTT = k_3*v*f_c; % [Pa]

% Steel
f_y = 500*10^6; % [Pa]

% Applied forces [N]
F = 3000*10^3;

% Reaction forces [N]
F_R = F/2;
```

```
34
35  % Tie [m]
36  x_T = L-0.4;
37  y_T = 0;
38  L_T = x_T;
39
40  % Strut 1 [m]
41  x_S_1 = 0;
42  y_S_1 = d;
43  L_S_1 = (x_S_1^2+y_S_1^2)^(1/2);
44
45  % Strut 2 [m]
46  x_S_2 = 0;
47  y_S_2 = d;
48  L_S_2 = (x_S_2^2+y_S_2^2)^(1/2);
49
50  % Strut 3 [m]
51  x_S_3 = 0;
52  y_S_3 = H-2.850;
53  L_S_3 = (x_S_3^2+y_S_3^2)^(1/2);
54
55  % Strut 4 [m]
56  x_S_4 = L/2-0.2;
57  y_S_4 = H-y_S_1-y_S_3;
58  L_S_4 = (x_S_4^2+y_S_4^2)^(1/2);
59  theta_S_4_1 = atan(y_S_4/x_S_4);
60  theta_S_4_grad_1 = theta_S_4_1*180/pi;
61  theta_S_4_2 = atan(x_S_4/y_S_4);
62  theta_S_4_grad_2 = theta_S_4_2*180/pi;
63
64  % Strut 5 [m]
65  x_S_5 = L/2-0.2;
66  y_S_5 = H-y_S_1-y_S_3;
67  L_S_5 = (x_S_5^2+y_S_5^2)^(1/2);
68  theta_S_5_1 = atan(y_S_5/x_S_5);
69  theta_S_5_grad_1 = theta_S_5_1*180/pi;
70  theta_S_5_2 = atan(x_S_5/y_S_5);
71  theta_S_5_grad_2 = theta_S_5_2*180/pi;
72
73  % Forces in strut and ties
74  F_S1 = F_R;
75  F_S2 = F_R;
76  F_S3 = F;
77
78  % Node 1 (Left bottom node)
79  F_S4 = F_R/sin(theta_S_4_1);
80  F_T= F_S4*cos(theta_S_4_1);
81
82  % Node 2 (right bottom node)
83  F_S5 = F_R/sin(theta_S_5_1);
84
85  % Node 3 (top node)
86
87  % Check Nodes
88  % Node 1 - support 1
89  F_1 = [F_S1 F_S4]; % [N] Forces in node for each face
90  s_1 = sigma_Rd_max_CCT;
91  w_1 = zeros(1,2); % Faces width [m]
92  w_1(1) = F_1(1)/(s_1*T);
93  w_1(2) = F_1(2)/(s_1*T);
94
95  if w_1(1) < p
96      display('Node 1 ok')
97  else
98      display('Node 1 not ok')
99  end
100
101 % Node 2 - support 2
102 F_2 = [F_S2 F_S5]; % [N] Forces in node for each face
103 s_2 = sigma_Rd_max_CCT;
```

```
w_2 = zeros(1,2); % Faces width [m]
w_2(1) = F_2(1)/(s_2*T);
w_2(2) = F_2(2)/(s_2*T);

if w_2(1) < p
    display('Node 2 ok')
else
    display('Node 2 not ok')
end

% Node 3
F_3 = [F_S3 F_S4 F_S5]; % [N] Forces in node for each face
s_3 = sigma_Rd_max_CCC;
w_3 = zeros(1,3); % Faces width [m]
w_3(1) = F_3(1)/(s_3*T);
w_3(2) = F_3(2)/(s_3*T);
w_3(3) = F_3(3)/(s_3*T);

if w_3(1) < p
    display('Node 3 ok')
else
    display('Node 3 not ok')
end

% Ties
A_s = F_T/f_y % [m2]
```

B

Stringer-Panel modelling

B.1 Python script for SPM

The script used in this thesis to design all different beams according to the Stringer-Panel Method can be found on the following link:
https://github.com/henryssonemma/py-SPM-STM-deep-beam.git

The first part of the script, which creates the stringer-panel grid according to the beam geometry, as well as the parts for dimensioning reinforcement and checking stresses, was written by the authors of this thesis. The part of the script that handles calculations of forces and displacements (marked in the script) was written by P.C.J. Hoogenboom and last updated on November 28, 2017. The link to Hoogenboom's original script, called SPM.py, can be found in the book written by Blaauwendraad (2018), and examples and further explanation of the script can be found in the manual by Hoogenboom (2017).

The outputs from the script used in the thesis are the reinforcement area needed in each stringer, the reinforcement area needed in each panel, total reinforcement volume, displacement for each DOF, the normal forces at the beginning and end of each stringer, the shear forces in each panel, and the support reactions.

The same script and input data were used for all beams in this thesis, except for the geometry of the beam. The input data that was the same for each beam can be found in the script found in the link above, and also in subsection 3.2.2. Below follows a specification of the input data that was changed for each beam. Table B.1 specifies the variables used for the beams with varying span-to-depth ratios, and Table B.2 specifies the variables used for the beams with varying opening sizes. The "Force" value, which in the script is interpreted as the applied force, is also changed depending on the load magnitude that was investigated.

Table B.1: Input values for the varying parameters used in the Python script for the beams with varying span lengths

	Names of variables in the script				
Beam dimensions [m]	**width**	**height**	**hole**	**width_hole**	**height_hole**
3×3	3	3	"no"	-	-
3×3.5	3.5	3	"no"	-	-
3×4	4	3	"no"	-	-
3×4.5	4.5	3	"no"	-	-
3×5	5	3	"no"	-	-
3×5.5	5.5	3	"no"	-	-
3×6	6	3	"no"	-	-
3×6.5	6.5	3	"no"	-	-
3×7	7	3	"no"	-	-
3×7.5	7.5	3	"no"	-	-
3×8	8	3	"no"	-	-
3×8.5	8.5	3	"no"	-	-
3×9	9	3	"no"	-	-

Table B.2: Input values for the varying parameters used in the Python script for the beams with varying opening sizes

	Names of variables in the script				
Opening dimensions [m]	**width**	**height**	**hole**	**width_hole**	**height_hole**
0.5×0.5	4	3	"yes"	0.5	0.5
0.75×0.75	4	3	"yes"	0.75	0.75
1×1	4	3	"yes"	1	1
1.25×1.25	4	3	"yes"	1.25	1.25
1.5×1.5	4	3	"yes"	1.5	1.5

C

FEM modelling

C.1 Python script for non-linear DIANA model

The script used in this thesis to model the reinforced concrete deep beams, created for the software DIANA, can be found on this link: https://github.com/henryssonemma/py-SPM-STM-deep-beam.git

The script is to be pasted in the command field in the commercial software DIANA. The first part of the script is the input data for the beams. The added displacement, the geometry and the reinforcement. The first part also contains the material input data. The input for the concrete, the reinforcement, and the loading and support plates. The second part creates the materials and geometries. The third part assigns properties and materials to the geometries. The fourth part adds loads and boundary conditions for the beams, and tyings between geometries when needed. The fifth and last part creates a mesh and analysis for the beam, both a linear and a non-linear analysis. The model is then run, and the results can be collected for the model in DIANA

C.2 Verification of DIANA analysis

The geometries for each of the beams used to verify the DIANA model are presented below. The input data for the reinforcement, concrete, and steel can be found in the report for each beam.

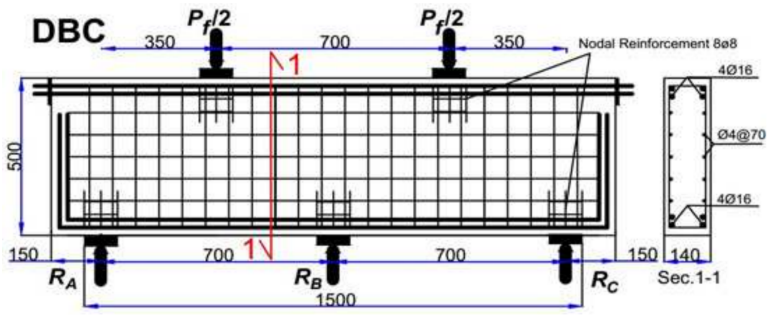

Figure C.1: Geometry of experimentally tested beam 1 (Mohammedali et al., 2019)

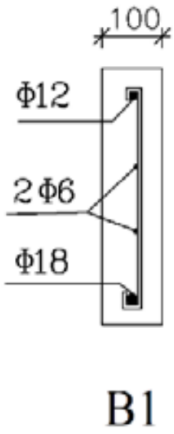

Figure C.2: Cross section of experimentally tested beam 2 with length $0.8\,\mathrm{m}$ and height $0.4\,\mathrm{m}$ (Dashlejeh and Arabzadeh, 2019)

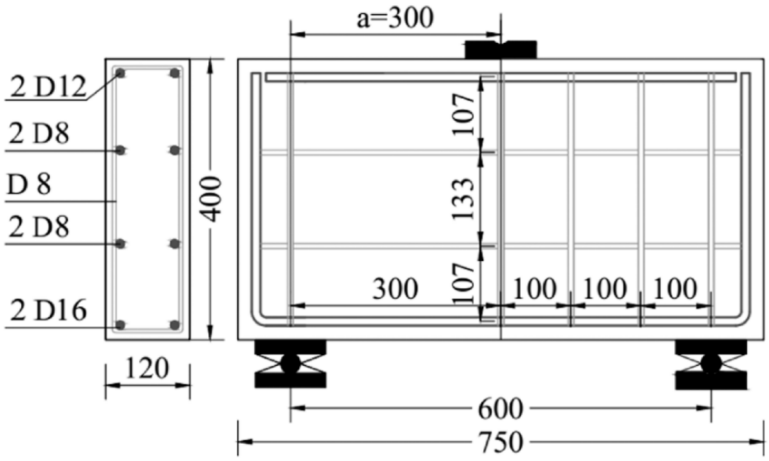

Figure C.3: Geometry of experimentally tested beam 3 (Hamoda et al., 2024)

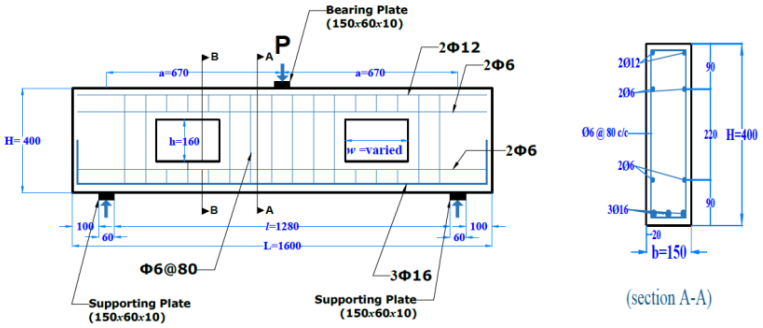

Figure C.4: Geometry of experimentally tested beam 4 (Al-Ahmed et al., 2017)

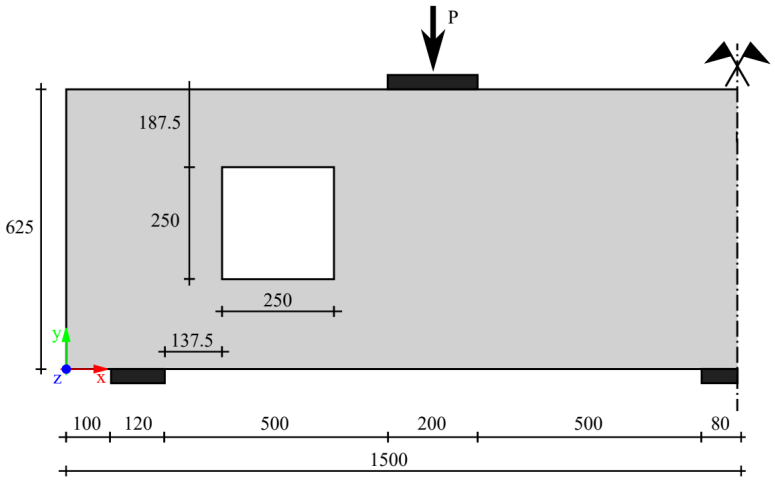

Figure C.5: Geometry of finite element model of beam 5 (DIANA FEA BV, n.d.)

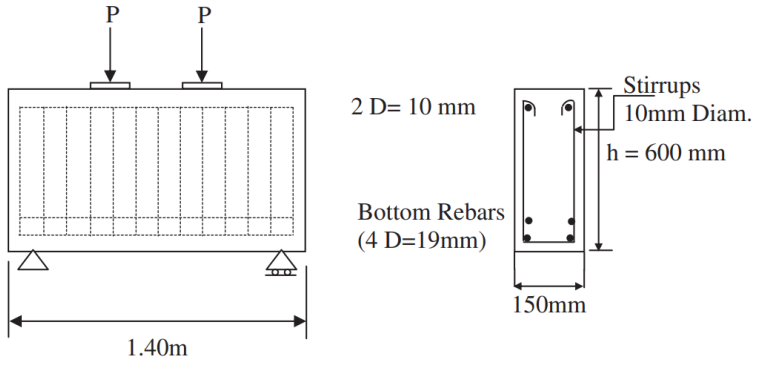

Figure C.6: Geometry of experimentally tested beam 6 (Mohamed et al., 2014)

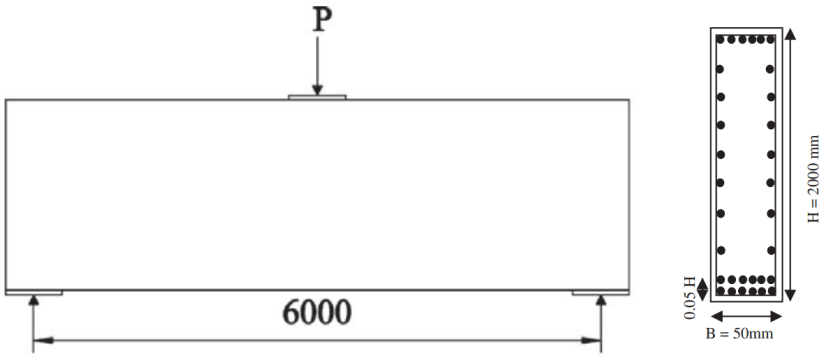

Figure C.7: Geometry of finite element model of beam 7 (Mohamed et al., 2014)

D

Results from analytical calculations

D.1 Crack widths

Table D.1: Characteristic crack widths, w_k, for the different beam geometries without openings for beams designed with STM, at different magnitudes of the applied point load. The design load used, P_d, is $3000\,\mathrm{kN}$

Beam dimensions [m]	w_k [mm]		
	$0.6P_d$	$0.8P_d$	P_d
3x3	0.3361	0.4886	0.6412
3x3.5	0.3334	0.4821	0.6308
3x4	0.3272	0.4680	0.6088
3x4.5	0.3216	0.4565	0.5914
3x5	0.3158	0.4453	0.5748
3x5.5	0.3108	0.4359	0.5610
3x6	0.3063	0.4279	0.5494
3x6.5	0.2958	0.4096	0.5234
3x7	0.2943	0.4070	0.5197
3x7.5	0.2929	0.4047	0.5164
3x8	0.2917	0.4027	0.5136
3x8.5	0.2906	0.4009	0.5111
3x9	0.2884	0.3972	0.5060

Table D.2: Characteristic crack widths for the different beam geometries without openings for beams designed with SPM, at different magnitudes of the applied point load. The design load used, P_d, is $3000\,\mathrm{kN}$

Beam dimensions [m]	w_k [mm]		
	$0.6P_d$	$0.8P_d$	P_d
3x3	0.3422	0.5064	0.6706
3x3.5	0.3354	0.4868	0.6383
3x4	0.3284	0.4706	0.6128
3x4.5	0.3219	0.4572	0.5924
3x5	0.3162	0.4460	0.5757
3x5.5	0.3111	0.4365	0.5619
3x6	0.3067	0.4284	0.5502
3x6.5	0.3027	0.4215	0.5403
3x7	0.2993	0.4155	0.5317
3x7.5	0.2962	0.4102	0.5242
3x8	0.2934	0.4055	0.5176
3x8.5	0.2909	0.4013	0.5118
3x9	0.2887	0.3976	0.5066

Table D.3: Characteristic crack widths for beams designed with STM with different opening sizes, at different magnitudes of the applied point load. The design load used, P_d, is $3000\,\mathrm{kN}$

Opening dimensions [m]	w_k [mm]		
	$0.6P_d$	$0.8P_d$	P_d
0.5x0.5	0.3245	0.4624	0.6003
0.75x0.75	0.3279	0.4696	0.6112
1x1	0.3310	0.4765	0.6219
1.25x1.25	0.3384	0.4948	0.6512
1.5x1.5	0.3455	0.5211	0.6968

Table D.4: Characteristic crack widths for beams designed with SPM with different opening sizes, at different magnitudes of the applied point load. The design load used, P_d, is $3000\,\mathrm{kN}$

Opening dimensions [m]	w_k [mm]		
	$0.6P_d$	$0.8P_d$	P_d
0.5x0.5	0.3374	0.4921	0.6468
0.75x0.75	0.3414	0.5036	0.6659
1x1	0.3447	0.5165	0.6883
1.25x1.25	0.3462	0.5301	0.7140
1.5x1.5	0.3594	0.5433	0.7429

D.2 Deflection

Table D.5: Mid-span deflection, $d_{y.mid}$, for the different beam geometries without openings for beams designed with SPM, at different magnitudes of the applied point load. The design load used, P_d, is $3000\,\mathrm{kN}$

Beam dimensions [m]	$d_{y.mid}$ [mm]		
	$0.6P_d$	$0.8P_d$	P_d
3x3	0.11	0.15	0.18
3x3.5	0.13	0.17	0.21
3x4	0.15	0.20	0.25
3x4.5	0.17	0.23	0.29
3x5	0.20	0.27	0.33
3x5.5	0.23	0.31	0.38
3x6	0.26	0.35	0.44
3x6.5	0.30	0.40	0.50
3x7	0.34	0.46	0.57
3x7.5	0.39	0.52	0.65
3x8	0.44	0.59	0.74
3x8.5	0.50	0.67	0.83
3x9	0.56	0.75	0.94

Table D.6: Mid-span deflection, $d_{y.mid}$, for beams designed with SPM with different opening sizes, at different magnitudes of the applied point load. The design load used, P_d, is $3000\,\mathrm{kN}$

Opening dimensions [m]	$d_{y.mid}$ [mm]		
	$0.6P_d$	$0.8P_d$	P_d
0.5x0.5	0.17	0.23	0.29
0.75x0.75	0.17	0.22	0.28
1x1	0.16	0.21	0.27
1.25x1.25	0.15	0.20	0.25
1.5x1.5	0.14	0.18	0.23

Table D.7: Mid deflection over the opening, $d_{y.open}$, for beams designed with SPM with different opening sizes, at different magnitudes of the applied point load. The design load used, P_d, is $3000\,\mathrm{kN}$

Opening dimensions [m]	$d_{y.open}$ [mm]		
	$0.6P_d$	$0.8P_d$	P_d
0.5x0.5	0.21	0.28	0.35
0.75x0.75	0.28	0.37	0.46
1x1	0.35	0.47	0.59
1.25x1.25	0.46	0.61	0.76
1.5x1.5	0.63	0.84	1.05

E

Results from FEM

E.1 Failure load

Table E.1: Comparison of failure loads for different beam sizes designed with STM and SPM

Beam size [m]	Failure load [kN]	
	STM	**SPM**
3×3	6510	6498
3×3.5	5870	5860
3×4	5310	5310
3×4.5	5100	5160
3×5	4660	4658
3×5.5	4250	4157
3×6	3820	3728
3×6.5	3590	4065
3×7	3494	3763
3×7.5	3663	3788
3×8	3544	3652
3×8.5	3397	3496
3×9	3343	3345

Table E.2: Comparison of failure loads for beams with different opening sizes designed with STM and SPM

Opening size [m]	Failure load [kN]	
	STM	**SPM**
0.5×0.5	5343	4933
0.75×0.75	5254	4593
1×1	4894	4566
1.25×1.25	4115	3966
1.5×1.5	3927	3980

E.2 Crack width

Table E.3: Maximum crack width along the bottom of the beams without openings for different load steps

Beam size [m]	w_{max} along bottom [mm]							
	STM				SPM			
	$0.6P_d$	$0.8P_d$	P_d	P_{ult}	$0.6P_d$	$0.8P_d$	P_d	P_{ult}
3×3	-	-	0.32	0.92	-	0.23	0.32	1.79
3×3.5	-	0.43	0.49	1.44	-	0.33	0.49	1.44
3×4	-	0.46	0.42	1.11	-	0.41	0.51	1.05
3×4.5	-	0.36	0.52	1.37	-	0.38	0.50	1.24
3×5	-	0.41	0.55	0.88	-	0.40	0.88	2.03
3×5.5	-	0.39	0.56	0.84	-	0.44	0.57	0.80
3×6	0.29	0.45	0.58	0.76	-	0.45	0.59	0.74
3×6.5	0.39	0.58	0.74	1.28	0.46	0.64	0.84	0.99
3×7	0.55	0.65	0.86	1.39	0.44	0.69	0.89	0.98
3×7.5	0.49	0.64	0.82	3.28	0.38	0.58	0.73	0.96
3×8	0.52	0.72	0.94	3.31	0.51	0.73	1.00	1.14
3×8.5	0.57	0.74	0.94	2.33	0.49	0.69	0.83	1.02
3×9	0.54	0.73	0.95	1.91	0.56	0.76	0.96	1.08

Table E.4: Maximum crack width along the bottom of the beams with openings for different load steps

Opening size [m]	w_{max} along bottom [mm]							
	STM				SPM			
	$0.6P_d$	$0.8P_d$	P_d	P_{ult}	$0.6P_d$	$0.8P_d$	P_d	P_{ult}
0.5×0.5	-	0.40	0.41	0.92	-	0.32	0.53	1.61
0.75×0.75	-	0.44	0.52	1.04	-	0.41	0.51	2.26
1×1	-	0.37	0.75	1.19	-	0.39	0.61	1.80
1.25×1.25	-	0.56	0.62	0.97	-	0.45	0.70	1.00
1.5×1.5	0.53	0.67	0.87	1.23	0.53	0.71	0.73	1.03

E.3 Deflection

Table E.5: Deflection of the mid-span of beams without openings at different load steps for STM and SPM

Beam size [m]	Deflection at mid-span, $d_{y.mid}$ [mm]							
	STM				SPM			
	$0.6P_d$	$0.8P_d$	P_d	P_{ult}	$0.6P_d$	$0.8P_d$	P_d	P_{ult}
3×3	0.20	0.27	0.66	2.68	0.20	0.31	0.39	3.58
3×3.5	0.22	0.62	0.97	3.95	0.22	0.61	0.97	3.89
3×4	0.26	0.66	1.03	4.26	0.26	0.83	1.23	4.10
3×4.5	0.31	1.27	2.57	5.18	0.31	1.27	2.51	5.12
3×5	0.33	1.78	3.31	5.56	0.46	1.63	3.35	5.53
3×5.5	0.41	2.31	3.95	6.40	0.41	2.73	4.15	6.06
3×6	1.36	2.82	5.17	6.94	0.46	2.99	5.30	6.78
3×6.5	2.25	4.46	6.09	7.83	1.85	4.19	5.78	8.45
3×7	2.31	5.50	7.47	9.51	2.66	5.45	7.24	9.24
3×7.5	3.51	6.47	8.71	13.16	3.67	6.37	8.15	10.67
3×8	4.18	7.65	10.05	14.39	3.92	7.08	9.30	11.68
3×8.5	5.13	8.84	11.70	15.21	4.44	8.06	10.59	12.61
3×9	6.18	9.80	13.07	16.10	5.09	9.07	11.95	13.56

Table E.6: Deflection of the mid-span of beams with openings at different load steps for STM and SPM

Beam size [m]	Deflection at mid-span, $d_{y.mid}$ [mm]							
	STM				SPM			
	$0.6P_d$	$0.8P_d$	P_d	P_{ult}	$0.6P_d$	$0.8P_d$	P_d	P_{ult}
0.5×0.5	0.25	0.73	1.34	3.96	0.25	0.76	1.60	4.31
0.75×0.75	0.25	0.82	1.60	3.98	0.23	0.89	1.31	4.36
1×1	0.22	0.82	1.33	3.11	0.22	0.77	1.57	3.64
1.25×1.25	0.19	0.73	1.18	1.90	0.20	0.56	1.10	1.75
1.5×1.5	0.21	0.66	0.95	1.52	0.15	0.46	0.96	2.03

Table E.7: Deflection above the opening of beams with openings at different load steps for STM and SPM

Beam size [m]	Deflection at mid-span, $d_{y.open}$ [mm]							
	STM				SPM			
	$0.6P_d$	$0.8P_d$	P_d	P_{ult}	$0.6P_d$	$0.8P_d$	P_d	P_{ult}
0.5×0.5	0.32	0.91	1.53	4.02	0.32	0.91	1.71	4.33
0.75×0.75	0.32	0.95	1.69	4.09	0.34	0.95	1.76	4.68
1×1	0.42	1.42	2.27	4.36	0.42	1.42	2.28	4.56
1.25×1.25	0.54	2.03	2.81	4.26	0.55	2.03	2.68	4.01
1.5×1.5	1.3	2.39	3.23	4.65	1.05	2.39	2.91	4.41

DEPARTMENT OF SOME SUBJECT OR TECHNOLOGY
CHALMERS UNIVERSITY OF TECHNOLOGY
Gothenburg, Sweden
www.chalmers.se

CHALMERS
UNIVERSITY OF TECHNOLOGY